L.B.Krivdin
Russ. Chem. Rev., 2021, **90** (9) 1166 – 1212

https://doi.org/10.1070/RCR4976

Computational NMR of heavy nuclei involving ^{109}Ag, ^{113}Cd, ^{119}Sn, ^{125}Te, ^{195}Pt, ^{199}Hg, ^{205}Tl, and ^{207}Pb

Leonid B. Krivdin [a, b]

[a] *A.E.Favorsky Irkutsk Institute of Chemistry, Siberian Branch of the Russian Academy of Sciences, ul. Favorskogo 1, 664033 Irkutsk, Russian Federation*
[b] *Angarsk State Technical University, ul. Tchaikovskogo 60, 665835 Angarsk, Irkutsk Region, Russian Federation*

The present review addresses the computation of the NMR parameters of ^{109}Ag, ^{113}Cd, ^{119}Sn, ^{125}Te, ^{195}Pt, ^{199}Hg, ^{205}Tl, and ^{207}Pb isotopes. The presented material is based on papers that appeared mainly in the interim period of 2000 – 2020. These calculations are rapidly developing and becoming of increasing practical interest on the cutting edge of modern computational chemistry. The review focuses on the most essential papers in this area, concentrating on the computational aspects of such calculations together with their structural and stereochemical applications in organometallic chemistry, which seems to be urgent and timely. The bibliography includes 173 references.

Dedicated to Professor Teobald Kupka (University of Opole, Institute of Chemistry, Poland), an Advisory Board Member of a leading worldwide journal, Magnetic Resonance in Chemistry, in view of his outstanding contribution to the field of computational NMR.

Contents

1. Introduction 1166
2. Computational NMR of heavy nuclei 1167
2.1. Relativistic calculations 1167
2.2. ^{109}Ag NMR 1168
2.3. ^{113}Cd NMR 1170
2.4. ^{119}Sn NMR 1173
2.5. ^{125}Te NMR 1179
2.6. ^{195}Pt NMR 1188
2.7. ^{199}Hg NMR 1191
2.8. ^{205}Tl NMR 1197
2.9. ^{207}Pb NMR 1201
2.10. Other isotopes 1204
3. Note added in proof 1205
4. Conclusion 1205
5. List of acronyms 1208

Leonid Krivdin graduated from M.V.Lomonosov Moscow State University in 1977, received his PhD in 1982 from the Irkutsk State University, which was followed by a postdoctoral fellowship at Flinders University of South Australia in the group of Professor Ernst Della (1990 – 1991). He received his DSc in 1989 and Full Professor in 1993.
His research interests focus on computation of NMR parametres being substantiated with some 400 research publications, including approximately 20 reviews and book chapters. Under his scientific supervision, 12 PhD dissertations were defended in the interim of 1989 until present. Professor Krivdin visited 50 countries invited as a visiting professor of a number of different universities involving those in Russia, the United States, Australia, Argentina, the United Kingdom, Poland, France and many others around the world. He is currently a Chief Researcher of the NMR Laboratory at A.E.Favorsky Irkutsk Institute of Chemistry and a Chair of Chemistry at Angarsk State Technical University.
E-mail: krivdin55@gmail.com

Professor Kupka *is a world class specialist in the field of nuclear magnetic resonance and molecular modeling of structural and spectroscopic parameters of molecular systems involving nanotechnology and in vivo studies. His scientific career involved research at the University of Silesia, Poland (1980 – 2003); Polimer Center of Chemistry in Zabrze, Poland (1986 – 1998, 2001); University of Waterloo, Department of Physics, Ontario, Canada (1998 – 2000); Argonne National Laboratory, Chicago, USA (2001 – 2005); Academia Sinica, Taipei, Taiwan (2005 – 2006); and finally University of Opole, Institute of Chemistry, Poland (since 2006 until present). Recently, Teobald Kupka became an Advisory Board Member of a leading NMR journal, Magnetic Resonance in Chemistry.*

1. Introduction

At present, we are witnessing an unprecedentedly fast development of theoretical and computational methods in the field of nuclear magnetic resonance (NMR) spectroscopy,[1] in parallel with marked progress in modern NMR techniques and instrumentation. In this line, NMR-oriented calculations at different levels of theory[2 – 9] involving those on relativistic grounds,[10 – 15] for the most common 1/2 spin NMR isotopes — proton,[16 – 18] carbon,[19 – 21] nitrogen,[22] fluorine,[23] silicon,[24] phosphorus,[25, 26] and selenium,[27] are in their mature period. The present review finalizes this series of reviews dealing with the computational aspects of chemical shifts and spin – spin coupling constants of heavier nuclei. In the present survey, we focus on the computation of NMR parameters of a number of most common heavy nuclei, namely, 1/2 spin isotopes of ^{109}Ag, ^{113}Cd, ^{119}Sn, ^{125}Te, ^{195}Pt, ^{199}Hg, ^{205}Tl, and ^{207}Pb, being on the cutting edge of modern computational chemistry. Presented material is based on the papers of the present century, *i.e.* those appeared in the interim of 2000 – 2020. In this period, theoretical studies in this field were rapidly developing, becoming of increasing practical interest. When this manuscript was almost ready for submission, a very interesting

Received 22 November 2020
© 2021 Uspekhi Khimii, ZIOC RAS, Russian Academy of Sciences and IOP Publishing Limited

review by Vícha *et al.*[28] on related topic but in a more theoretical fashion was just published which appears to be a marvelous theoretical foundation of the present contribution.

Traditionally, the review is oriented on NMR spectroscopists and theoreticians, utilizing modern computational methods for the calculation and interpretation of the NMR parameters of the most common 1/2 spin heavy isotopes, including those of silver, cadmium, tin, tellurium, platinum, mercury, thallium, and lead, together with a number of more exotic mainly quadruple nuclei.

2. Computational NMR of heavy nuclei

2.1. Relativistic calculations

Most of the calculations reported in the subsequent sections were performed at the relativistic level, as is common for the heavy nuclei discussed in the present review. Therefore, we start the present review with a short overview of relativistic methods used for the calculation of NMR parameters of heavy nuclei.

Nuclear magnetic resonance spectroscopy has become an efficient tool for the structural elucidation of organic and biological molecules. Theoretical prediction of NMR parameters provides a new guide into molecular structure and chemical reactivity. Recent advances in computational NMR at the relativistic level[10–15] have provided a profound impact on the calculation of chemical shifts and spin – spin coupling constants of heavy nuclei, such as those considered in the present review, two basic NMR parameters that could be derived from experimental NMR spectra.

Formally speaking, relativistic effects are pure theoretical phenomena that arise from the difference between the levels of physical theory. This means that actually there is no way to measure relativistic effects by only resorting to experiment, let it be considered in NMR measurements, or in a more general domain. Generally, relativistic effects in a particular property, including NMR parameters, can be estimated only from the difference between the property value calculated within relativistic theory and that calculated within nonrelativistic theory.

According to the Bohr model, the average speed of a 1s electron equals the nuclear charge Z. Thus, the main marker, which indicates the possible importance of relativistic effects, is that the nuclear charge Z is not much smaller than the speed of light. For example, for the first-to-third row elements, the ratios Z/c are too small to be treated on relativistic grounds, so that these elements should be referred to as 'light' elements. On the other hand, this ratio for heavy nuclei such as mercury (0.58 a.u.) indicates the 'heaviness' of the nucleus. Indeed, the most pronounced relativistic effect for mercury consists of the fact that the 1s radial orbital essentially shrinks compared to that calculated in the nonrelativistic representation. Thus, it follows that a relativistic approach to many-electron problems, including NMR spectra, is to be used when there are electrons in the system with an average orbital speed close to the speed of light.

The types of relativistic effects, resulting in the values of NMR parameters, compared to nonrelativistic calculations in the molecules containing heavy elements, could be derived from the quasirelativistic many-body Breit – Pauli Hamiltonian. There are two most significant types of relativistic effects, namely, the so-called scalar effects, namely, those in which operators do not contain the electronic spin variable, and spin – orbit relativistic effects, those in which operators depend on the electronic spin.

In this representation, scalar effects could be defined as the sum of the mass-velocity and Darwin corrections. In turn, mass-velocity correction arises due to the relativistic increase in the electron mass, affecting the kinetic energy of an electron, while Darwin correction originates in the so-called 'smearing' of the moving electron, resulting in a change in its potential energy. On the other hand, the spin – orbit effect originates in the interaction of an electron spin with its own angular momentum in relation to the position of the nucleus under consideration (one-electron effect), its own angular momentum in relation to the position of another electron (two-electron spin-same-orbit effect), or, on the other hand, with the angular momentum of another electron in relation to its own position (two-electron spin-other-orbit effect). Generally, the spin – orbit interactions result in the spin – orbit splitting of orbitals, namely, those with parallel and antiparallel spins relative to electron angular momentum, which in turn makes nuclear spin no longer a proper quantum number.

The relativistic effects can also be spitted up in the meaning of its inner/external origin. In this review, attention will be paid to the so-called HAHA and HALA effects. The acronym HAHA stands for the 'Heavy Atom on Heavy Atom effect', being of the inner-origin type and corresponding to a heavy-atom (relativistic) effect on the heavy-atom's own NMR parameters. On the other hand, the HALA effect, as will be used throughout the paper, refers to a 'heavy-atom effect on light-atom NMR parameters' and represents the external-origin type of effect. It is essential that in the case of molecules containing heavy elements, not taking into account relativistic effects at an appropriate level of theory cannot be compensated by using whatever high accuracy correlated *ab initio* nonrelativistic approaches.

At present, the development of relativistic approaches to the calculation of magnetic resonance parameters is of utmost importance, as outlined in a number of 'relativistic' reviews cited above. However, it should be recalled that the four-component relativistic methods are extremely computationally demanding compared to the two-component ZORA methods. Among the most widespread four-component methods for the calculation of NMR parameters are the relativistic random phase approximation (RRPA) or time-dependent Dirac – Hartree – Fock (TD-DHF) method and time-dependent relativistic four-component density functional theory (TD-RDFT) method or time-dependent Dirac – Kohn – Sham (TD-DKS) method.

The main idea of the present section was to provide general insight into the relativistic HAHA and HALA effects of heavy isotopes, ^{109}Ag, ^{113}Cd, ^{119}Sn, ^{125}Te, ^{195}Pt, ^{199}Hg, ^{205}Tl, and ^{207}Pb, in their NMR chemical shifts and spin – spin coupling constants, concentrating mainly on practical computational aspects and paying little attention to pure theoretical issues.

A more detailed description of relativistic effects in the NMR spectra of compounds containing heavy nuclei could be found in a recent review by Rusakova and Krivdin.†

† I.L.Rusakova, L.B.Krivdin. *Mendeleev Commun.*, **28**, 1 (2018)

2.2. ^{109}Ag NMR

Silver belongs to the so-called 'Cinderella nuclei' group. This term was introduced by Mann[29] to specify those 1/2 spin isotopes that are most difficult to observe: ^{57}Fe, ^{89}Y, ^{103}Rh, ^{109}Ag, ^{169}Tm, ^{183}W, and ^{187}Os. Term 'Cinderella nuclei' refers in a rather pathetic way to the very fact that NMR sensitivity of those nuclei is extremely low, so that generally they are of very limited interest and that this situation could dramatically change in the future along with a general progress in NMR technique (like that with Cinderella from the known fairytale). Indeed, along with marked progress in NMR software and hardware, this situation has been slightly improved in recent years, while theoretical calculations of the NMR parameters of 'Cinderella nuclei' at the modern levels of theory are still in a cradle.

One of the most comprehensive papers dealing with the computation of NMR chemical shifts of ^{109}Ag, the isotope from the 'Cinderella nuclei' series, is that by Alkorta *et al.*[30] reporting calculation of ^{109}Ag NMR chemical shifts of eight trinuclear Ag(I) complexes with pyrazolate ligands **1**–**8** shown in Figure 1 at the relativistic two-component Zeroth Order Regular Approximation (ZORA) level. In that publication, relativistically corrected ^{109}Ag NMR chemical shifts were calculated using the BP86 functional in combination with the full-electron QZ4P basis set within the relativistic ZORA spin–orbit Hamiltonian. All geometry optimizations were carried out with the B3LYP functional and jul-cc-pVDZ basis set for light atoms together with aug-cc-pVDZ-pp for silver.

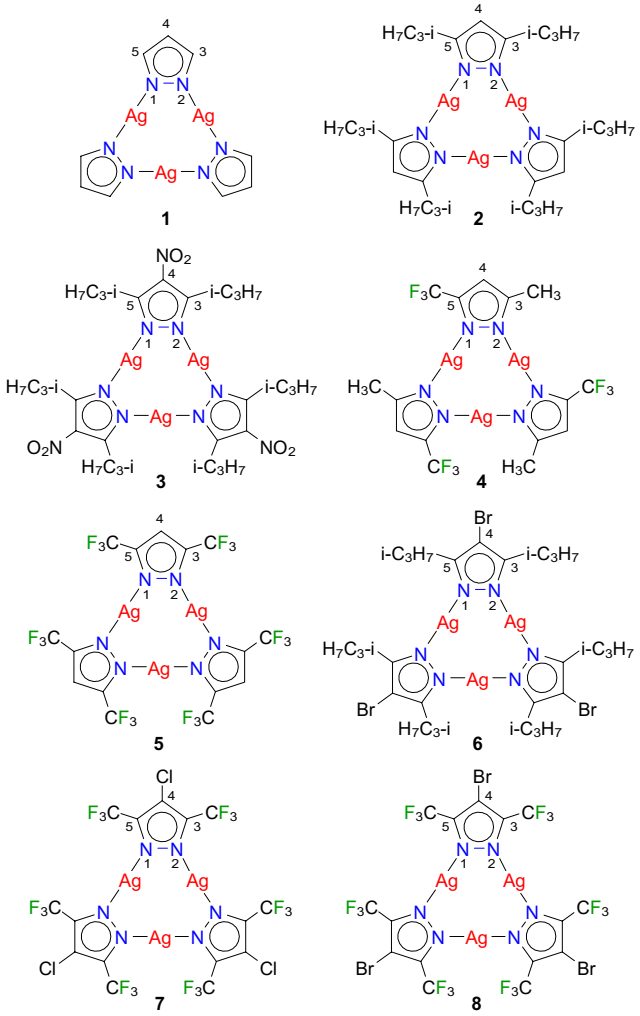
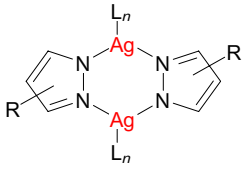


Figure 1. The structures of eight representative silver complexes. Reproduced with minor editing privilege from Alkorta *et al.*[30] with the permission of *John Wiley and Sons*.

The calculated ^{109}Ag NMR chemical shifts were found to be accordingly 508.1, 535.5, 489.0, 478.5, 425.4, 509.8, 393.9, and 394.4 ppm for **1** to **8**, in good agreement with the experimental value of 434.1 ppm for **5** measured in that publication and referenced to $AgNO_3$ on the D_2O scale (0.0 ppm).

Another very recent paper by the same principal authors[31] reported on the relativistically corrected NMR shielding constants in the series of dinuclear silver pyrazolates **9** calculated at the ZORA level with BP86 functional and full electron QZ4P basis set on the geometries, optimized at the MP2 level with the same basis set. The calculated ^{109}Ag shielding constants of all systems studied in that paper spread over the range of as much as approximately 1200 ppm. A good relationship between silver chemical shielding and intramolecular Ag–Ag distance in this series was established. Additionally, those results showed that six-membered rings in that series possessed nonaromatic character, while pyrazole rings did not change their aromatic character upon complexation.

Structure 9



R = H, 4-NO_2, 3,5-Me, 4-Cl;
L = N_2, OH_2, NCH, SH_2, NH_3, PH_3, CNH (n = 0, 1, 2, 4)

In the earlier paper by Kauch and Pecul,[32] one-bond silver-nitrogen spin–spin coupling constants of Ag^+ cations intercalated between imidazole rings in DNA chains with nitrogens-15 of neighboring silver-bound imidazole pairs, $^1J_{Ag,N}$, were calculated within the density functional theory (DFT) framework with relativistic effects taken into account at the two-component ZORA relativistic level both with and without accounting for spin–orbit coupling effects (Fig. 2). Three different basis sets of triple and quadruple zeta quality with polarization functions, TZP, TZ2P, and QZ4P, were employed in that study. A number of different exchange-correlation functionals, namely, PBE0, revPBE, PW91, BP86, BEE, KT1 and KT2, were tested and compared to the most common B3LYP. The range of calculated $^1J_{Ag,N}$ was between 85.3 and 107.2 Hz when the scalar ZORA approximation was used, and between 84.4 and 106.1 Hz when the spin–orbit coupling effects were included, which was in fairly good agreement with the available experimental value of 92 Hz.[33]

Among the three basis sets tested in that study, the most convenient was the all-electron basis set of quadruple zeta quality with an extended core, QZ4P. The most popular hybrid functional, B3LYP, gave a somewhat overestimated (compared to experiment) result, while the revPBE, BEE, hybrid PBE0, BP86, and PW91 functionals produced results that were very close to each other and to experiment. The spin–orbit term was not very important and thus could safely be omitted in the related calculations of the formally

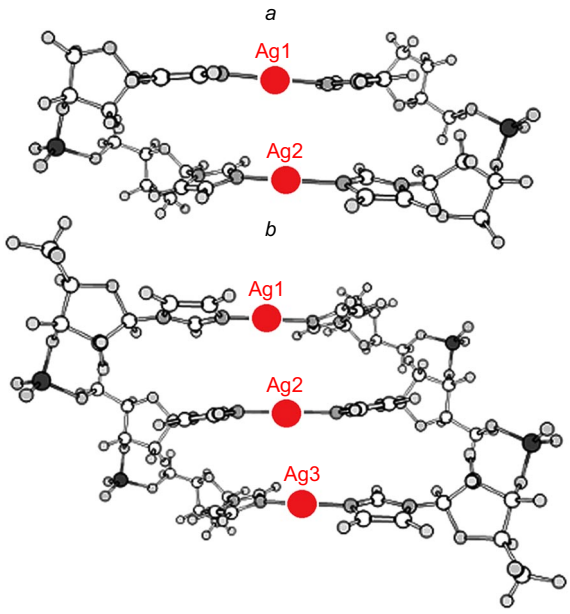


Figure 2. Models of two and three silver-bound imidazole pairs in double (*a*) and triple (*b*) systems. Reproduced with minor editing privilege from Kauch and Pecul [32] with the permission of *John Wiley and Sons*.

one-bond spin – spin coupling constant, $^1J_{Ag,N}$. Indeed, the numerical value of $^1J_{Ag,N}$ is too small to treat it as a genuine *one-bond* coupling constant, as mentioned by one of the referees.

Another interesting finding of the performed study [32] deals with the results of the silver-nitrogen bond stretching monitored in the values of the $^1J_{Ag,N}$ coupling constant, which is illustrated in Figure 3. It was found that $^1J_{Ag,N}$ did not change much in the range of the deformation parameter

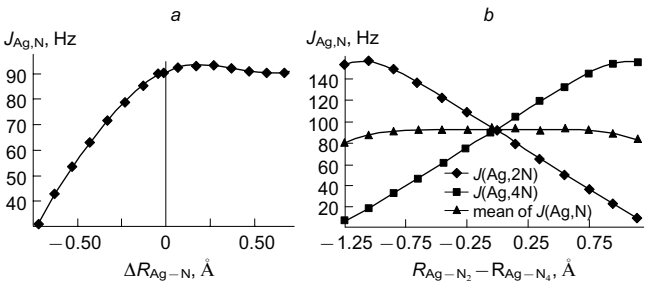


Figure 3. Effect of stretching of the silver – nitrogen bond on the $^1J_{Ag,N}$ coupling constant: (*a*) symmetric bond stretching and (*b*) asymmetric bond stretching. Reproduced with minor editing privilege from Kauch and Pecul [32] with the permission of *John Wiley and Sons*.

ΔR_{Ag-N} between 0.0 and 0.7 Å. As the Ag – N distance became shorter, the coupling constant $^1J_{Ag,N}$ decreased almost linearly. This coupling constant also appeared to be dependent on the position of the Ag^+ ion in the molecule. Based on these results, it was concluded that the one-bond silver – nitrogen coupling constant was strongly dependent on the geometry changes.

Finally, calculations performed for systems containing two and three silver ions resulted in a coupling constant between two silver nuclei, $^1J_{Ag,Ag}$, of approximately 1 Hz (1.18 Hz for the double system and about 0.96 Hz for the triple one). The small value of this coupling was explained by the authors [32] as arising from the long distance between silver ions of almost 4 Å.

Wodyński *et al.*[34] performed two-component ZORA calculations of $^1J_{Ag,C}$ and $^1J_{Ag,N}$ coupling constants of the silver cyanide dimer AgCN···AgCN with different non-relativistic (NR) exchange-correlation functionals and triple zeta Dyall's basis set (Table 1). Hybrid functionals B3LYP and PBE0 generally led to good agreement with the experimental data, while the BVP86 values were apparently underestimated. Another nonhybrid functional of Keal – Tozer's KT2 leads to even smaller values than those provided by BVP86.

Much earlier, Bryce and Wasylishen [35] performed relativistic ZORA calculations of $^1J_{Ag,C}$ on simple fragments to model ordered (model I) and disordered (model II) sites of silver cyanide in the solid state. In those calculations, the Vosko – Wilk – Nusair (VWN), Becke 88, and Perdew 86 functionals in combination with the triply polarized TZP Slater-type basis set were employed. 'Ordered' model I stood for the case when all cyanide groups were oriented in the same direction within a given AgCN chain. Thus, in the case of the 'ordered' silver cyanide chain, all silver atoms lied in sites where silver was bonded to one carbon atom and one nitrogen atom. 'Disordered' model II applied to the case when there was no perfect parallel ordering of the cyanide groups within a given AgCN chain. Thus, a 'disordered' silver site referred to the situation when Ag was bonded with two carbon atoms, as shown below:

Ordered: NC – Ag – NC – Ag (model I)
Disordered: NC – Ag – CN – Ag (model II)

Performed calculations resulted in $^1J_{Ag,C} = -308$ Hz for model 1 and −234 Hz for model 2, compared to -297 ± 15 and -201 ± 15 Hz derived from the experimental ^{109}Ag NMR. The performed calculations did not produce quantitative agreement with the experiment because of the simplicity of the model systems. Nevertheless, the calculated magnitudes of $^1J_{Ag,C}$ were within the known experimental range, and the difference in spin – spin coupling constants for an ordered and a disordered site of

Table 1. Spin – spin coupling constants (Hz) of silver cyanide dimer calculated at the nonrelativistic level and relativistic two-component level using scalar (sc-ZORA) and spin – orbit (so-ZORA) approaches, the latter with four different functionals. Compiled from Wodyński *et al.*[34]

Coupling constant	B3LYP/TZP			so-ZORA/TZP				Experiment [a]
	NR	sc-ZORA	so-ZORA	BVP86	B3LYP	PBE0	KT2	
$^1J_{Ag,C}$	−254	−317	−315	−273	−315	−303	−252	(−)297 ± 15
$^1J_{Ag,N}$	58.6	67.9	67.4	60.2	67.4	68.0	56.1	
$^2J_{Ag,N}$	10.2	10.7	11.1	9.0	11.1	12.5	7.4	

[a] The sign in parentheses was not experimentally determined.

74 Hz was in good agreement with the experimental value of 96 ± 30 Hz.

2.3. ^{113}Cd NMR

Cadmium possesses two NMR active isotopes with spin 1/2, ^{111}Cd and ^{113}Cd, with very similar nuclear properties. Among those two, ^{113}Cd is the most commonly used isotope due to its higher NMR sensitivity. Additionally, ^{113}Cd NMR chemical shifts spread over a large range of almost 1000 ppm, which makes it a remarkable NMR probe for structural studies of cadmium complexes.

One of the most representative studies dealing with the calculation of ^{113}Cd NMR chemical shifts is that by Casella *et al.*[36] who tested several DFT protocols at the nonrelativistic and relativistic scalar and spin–orbit ZORA levels for the calculation of cadmium chemical shifts for a number of cadmium complexes **10**–**35** with different local coordination environments on the metal center, which are shown in Figures 4 and 5.

At the nonrelativistic level, the Gauge-Including Atomic Orbitals (GIAO) shielding tensor calculations of ^{113}Cd in Cd_2Et were performed with various combinations of functionals and basis sets, as presented in Figure 6. All calculated ^{113}Cd NMR chemical shifts obtained with the DZVP basis set on cadmium and 6-31G(d,p) and/or cc-pVDZ basis sets on light atoms demonstrated a fairly good performance with all protocols except for, surprisingly, M06-L, for which the chemical shift values appeared to be quite underestimated. The performance of B3PW91 and B3LYP functionals in combination with different basis sets extracted from the same publication is illustrated in Figure 7.[36]

It was found that relativistic spin–orbit effects did not strongly affect the calculated ^{113}Cd NMR chemical shifts, most likely due to their partial cancelation in the difference between the reference and a sample. Relativistic scalar corrections showed no appreciable improvement with respect to the nonrelativistic methods, indicating on a noticeable basis set dependence of the calculated ^{113}Cd NMR chemical shifts when using DZP and TZ2P.

In an earlier publication by Kauch and Pecul,[37] the indirect isotropic ^{113}Cd–^{1}H spin–spin coupling constants separated formally by five chemical bonds were calculated in a model rubredoxin complex **36**, consisting of four cysteine molecules and a cadmium cation, as shown in Figure 8. Those calculations were performed using one-component and two-component Hamiltonians, the latter including the spin–orbit coupling term. Several exchange-correlation functionals have been tested, namely, B3LYP, PBE0, revPBE, BVP86, BEE, PW91, KT1, and KT2, in

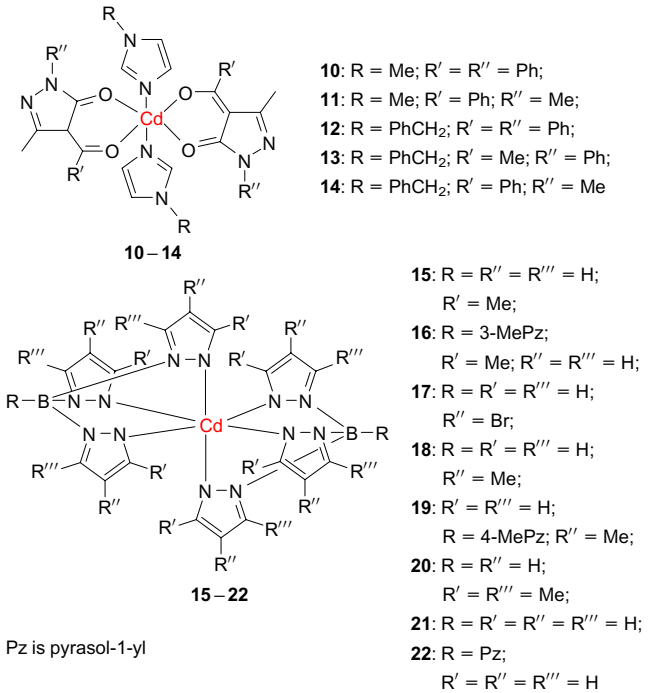


Figure 4. The structures of the representative cadmium complexes **10**–**22**. Reproduced with minor editing privilege from Casella *et al.*[36] with the permission of *Elsevier*.

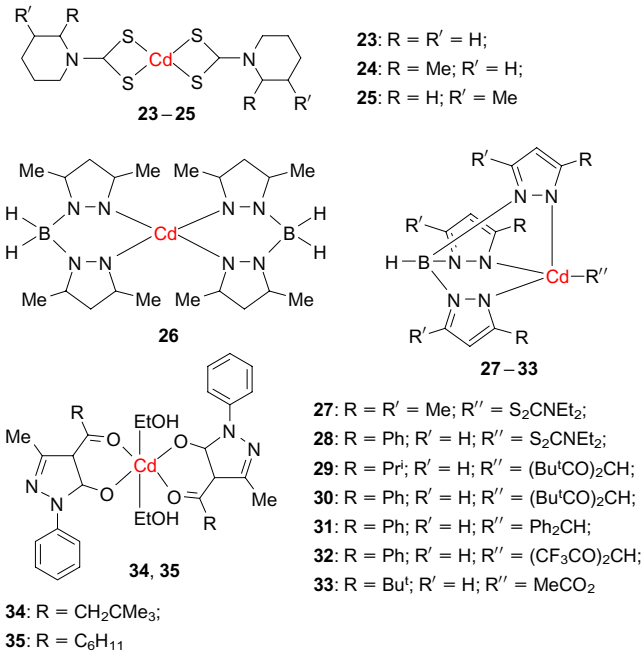


Figure 5. The structures of the representative cadmium complexes **23**–**35**. Reproduced with minor editing privilege from Casella *et al.*[36] with the permission of *Elsevier*.

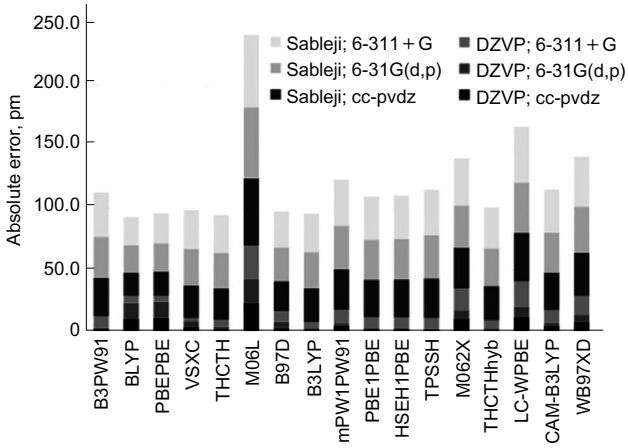


Figure 6. Absolute errors (ppm) between calculated and experimental ^{113}Cd NMR chemical shifts of Et_2Cd with respect to Me_2Cd. Reproduced with minor editing privilege from Casella *et al.*[36] with the permission of *Elsevier*.

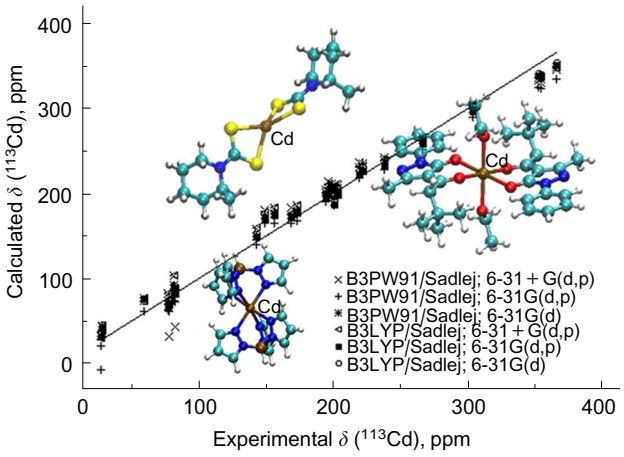


Figure 7. Correlation of calculated ^{113}Cd NMR chemical shifts in the series of **23**–**35** *vs.* experiment. Reproduced with minor editing privilege from Casella *et al.*[36] with the permission of *Elsevier*.

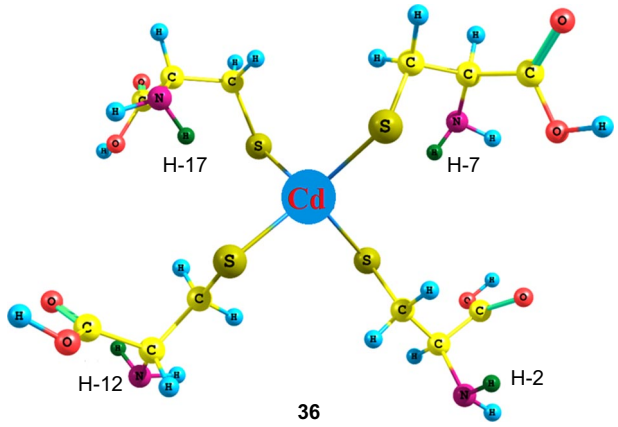


Figure 8. The structure of the model rubredoxin complex. Considered protons coupled to cadmium (H-2, H-7, H-12, and H-17) are shown in green. Reproduced with minor editing privilege from Kauch and Pecul,[37] with the permission of the *American Chemical Society*.

combination with triple zeta polarized and doubly polarized TZP and TZ2P basis sets together with a quadruple zeta quadruply polarized QZ4P basis set.

The main result of that study was that the choice of the functional did not affect much calculated couplings, as illustrated by the results of the performed calculations compiled in Table 2. Moreover, the sign of the calculated coupling constant was never affected by the choice of the functional, and the magnitudes of calculated cadmium – proton couplings varied in a very narrow range. In particular, the results obtained using the hybrid functionals B3LYP and PBE0 did not differ much from each other and were similar to those obtained by means of the nonhybrid functionals, with the corresponding difference being approximately 0.1 Hz. Even less variation was observed when the cadmium – proton coupling constants were calculated using different nonhybrid functionals KT1, KT2, revPBE, BEE, BVP86, and PW91 on cadmium atoms. Unfortunately, very small values of those couplings (approximately 0.5 Hz) made those conclusions far from any practical interest.

At approximately the same period of time, Roukala *et al.*[38] investigated the performance of Breit – Pauli perturbation theory (BPPT) against a fully relativistic four-component method in computing the ^{113}Cd NMR chemical shifts of dimethyl cadmium. Geometry optimization was performed at the DFT BP86/aug-cc-pVTZ level, while calculation of ^{113}Cd NMR chemical shifts was performed at the four-component relativistic level within the Gaussian nuclear charge distribution model applying both restricted kinetic balance (RKB) and unrestricted kinetic balance (UKB) prescriptions. It was generally shown that five out of the sixteen BPPT correction terms were responsible for most of the relativistic corrections applied to the chemical shift of cadmium.

Table 3 compiled from that publication[38] summarizes the final ^{113}Cd NMR chemical shifts of dimethyl cadmium obtained at the BPPT level with three different functionals and within the HF scheme compared to the fully relativistic Dirac – Hartree – Fock (DHF) four-component results. A similar dependence on the amount of exact exchange in the functionals was observed, with the anisotropy decreasing from BLYP to BHandHLYP. Additionally, a notable difference between the best calculated (BHandHLYP functional) shielding and the experimental result was found to be approximately 740 ppm (22%).

Some a decade earlier Krauss *et al.*[39] performed calculations of ^{113}Cd NMR chemical shifts of the metal ion binding sites of dicadmium phosphotriesterase, including full amino acid side chains, representing the protein environment surrounding the cadmium active sites. One to three water molecules were included in the active site in addition to the bridging hydroxide. All ^{113}Cd NMR isotropic shielding calculations were performed at the nonrelativistic level using the B3LYP functional with the uncontracted form of the first-order polarized basis set of Kellö and Sadlej[40] on cadmium and Pople's 6-31G(d) on the rest of the atoms.

Table 2. Isotropic spin – spin coupling constants ^{113}Cd – ^{1}H (Hz) of the model rubredoxin complex, calculated at the scalar two-component level with the all-electron TZ2P basis set. Compiled from Kauch and Pecul.[37]

Functional	*J*(Cd,H-2)	*J*(Cd,H-7)	*J*(Cd,H-12)	*J*(Cd,H-17)
KT1	0.32	0.58	0.45	0.70
KT2(+VWN)	0.32	0.57	0.45	0.67
revPBE	0.30	0.61	0.40	0.62
BEE(+VWN)	0.30	0.55	0.41	0.64
BVP86	0.31	0.60	0.42	0.70
PW91	0.31	0.59	0.41	0.68
B3LYP	0.40	0.36	0.46	0.42
PBE0	0.32	0.40	0.36	0.47
Experiment		0.56 ± 0.03	0.30 ± 0.03	0.56 ± 0.03

Table 3. Relativistic four-component Dirac – Hartree – Fock (DHF) and Breit – Pauli perturbation theory (BPPT) results for the shielding anisotropy (ppm) of dimethyl cadmium. Compiled from Roukala *et al.*[38]

Term	BPPT				DHF	Experiment
	BLYP	B3LYP	BHandHLYP	HF		
NR	2703	2625	2488	2252		
BPPT	224	202	172	112		
Total	2927	2827	2660	2364	2497	3400

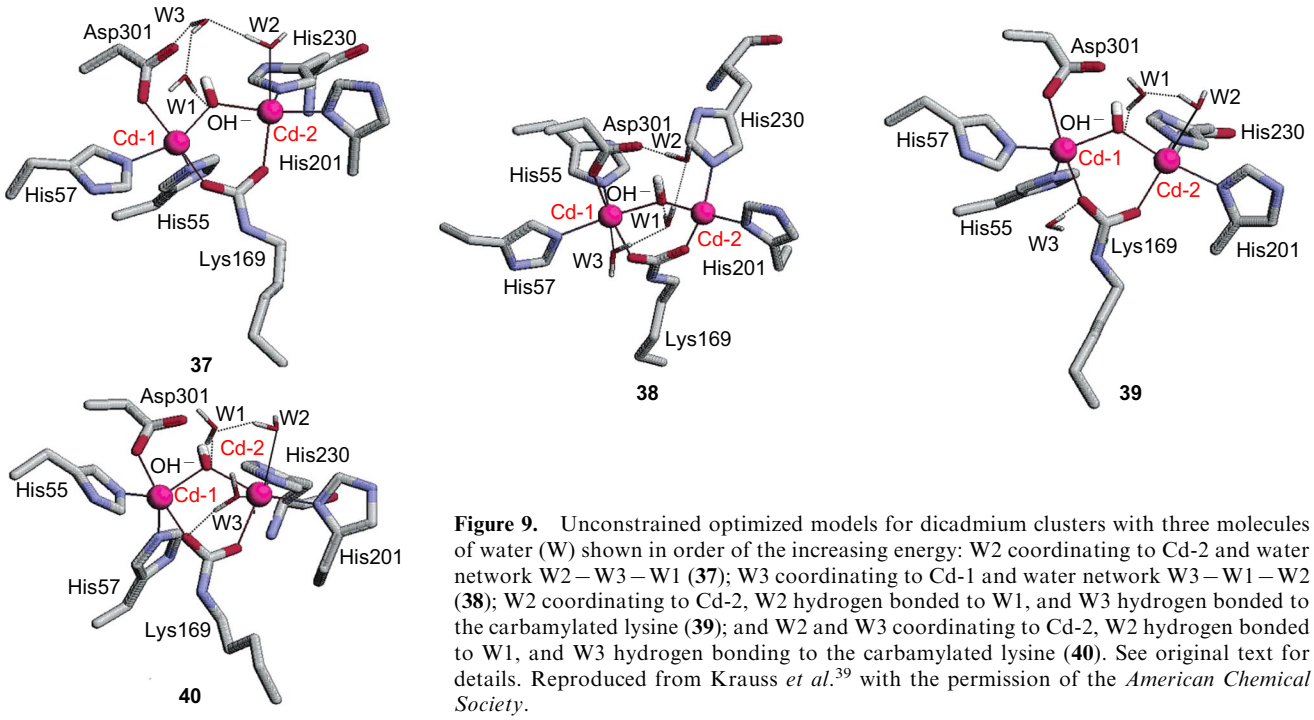


Figure 9. Unconstrained optimized models for dicadmium clusters with three molecules of water (W) shown in order of the increasing energy: W2 coordinating to Cd-2 and water network W2–W3–W1 (**37**); W3 coordinating to Cd-1 and water network W3–W1–W2 (**38**); W2 coordinating to Cd-2, W2 hydrogen bonded to W1, and W3 hydrogen bonded to the carbamylated lysine (**39**); and W2 and W3 coordinating to Cd-2, W2 hydrogen bonded to W1, and W3 hydrogen bonding to the carbamylated lysine (**40**). See original text for details. Reproduced from Krauss *et al.*[39] with the permission of the *American Chemical Society*.

The calculated isotropic shielding constants correlated with the coordination number of the metal ions, indicating that dicadmium phosphotriesterase had one more ligand in the highfield shift region than in the lowfield region. Theoretically, a number of energetically close structures were found for dicadmium phosphotriesterase complexed with water molecules, as illustrated by the model structures **37**–**40** involving three water molecules shown in Figure 9. The results of the performed calculations are presented in Table 4 retrieved from the title publication.[39] The most important factor determining ^{113}Cd NMR isotropic shielding in the case of dicadmium phosphotriesterase was the coordination number of the metal ions. Independent of which of the two sites is occupied with cadmium, a six-coordinated site had the highest shielding of 3754–3772 ppm. Accordingly, a five-coordinated site had a ^{113}Cd NMR shielding that was approximately 100 ppm lower, and the only four-coordinated site was approximately 100 ppm less shielded.

A number of early papers appeared in the previous decade (*i.e.* those published in the interim of 2000–2010) dealt with different aspects of the early computations of ^{113}Cd NMR chemical shifts and spin–spin coupling constants involving ^{113}Cd isotopes, which are briefly reviewed below.

Table 4. Calculated ^{113}Cd NMR isotropic shielding constants (ppm) for the geometry optimized metal ion binding sites of the dicadmium phosphotriesterase clusters. Compiled from Krauss *et al.*[39]

Cluster	Atom Cd1		Atom Cd2	
	Coordination number	Isotropic shielding	Coordination number	Isotropic shielding
37	5	3630	5	3683
38	6	3763	4	3558
39	5	3679	5	3691
40	5	3639	6	3754

In continuation of the earlier studies by Ellis *et al.*[41] and Higashioji *et al.*[42] dealing with the calculation of ^{113}Cd NMR chemical shifts of dimethyl- and diethylcadmium, in three related publications by Kidambi *et al.*,[43–45] ^{113}Cd NMR chemical shifts were calculated in a number of cadmium complexes with inorganic, organic, and bioinorganic ligands.

Thus, in the first publication,[43] such calculations were performed using the Hartree–Fock and DFT methods for dimethylcadmium, $CdMe_2$, diethylcadmium, $CdEt_2$, methylethylcadmium, CdMeEt, cadmium nitrate tetrahydrate, $Cd(NO_3)\cdot 4\,H_2O$, and cadmium acetate dihydrate, $Cd(OAc)\cdot 2\,H_2O$. Theoretical and experimental chemical shifts were compared to determine the effectiveness of theoretical calculations in determining cadmium chemical shifts. The effect of different cadmium basis sets on calculated cadmium chemical shifts was also studied. The DFT results matched the experimental chemical shifts much better than the Hartree–Fock calculations. Additionally, the agreement between the theoretical and experimental values significantly improved with the explicit inclusion of a sufficient number of water molecules into the calculation space.

In the second paper from this series, Kidambi and Ramamoorthy[44] presented a detailed theoretical study of isotropic and anisotropic ^{113}Cd NMR chemical shifts of several biologically active complexes exemplified in Figure 10 with bis(2,2′-dipyridylamine)dinitratocadmium (**41**), bis(2-aminomethylpyridine)dinitratocadmium (**42**), mesoporphyrincadmium complex (**43**), pyridyl-mesoporphyrincadmium complex (**44**), cadmiumalaninate (**45**), and cadmiumglycinate (**46**) with different coordination numbers of cadmium ranging between 4 and 8. Isotropic and anisotropic cadmium chemical shifts were calculated using the B3PW91 hybrid functional in combination with the Kellö–Sadlej basis set[40] for Cd and Pople's 6-311+G for

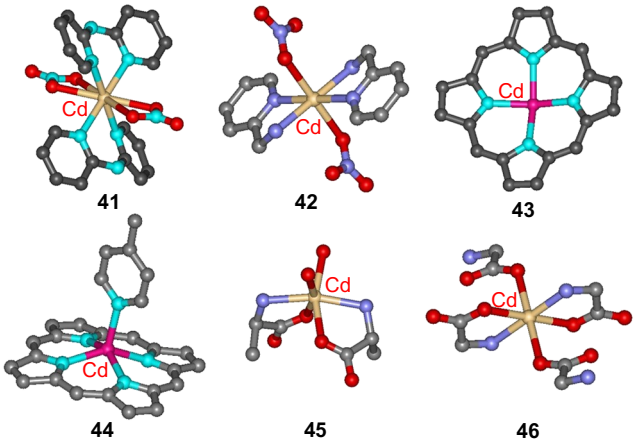


Figure 10. Neutron diffraction or optimized X-ray structures of the representative cadmium complexes. Cadmium is inscribed explicitly, and the colors of other elements are as follows: carbon — gray, nitrogen — aquamarine or purple, oxygen — red. Hydrogen atoms are omitted for clarity. Reproduced with minor editing privilege from Kidambi and Ramamoorthy[44] (Supplementary Material) with the permission of the *American Chemical Society*.

the rest of the atoms. Performed calculations demonstrated that nonrelativistic calculations of ^{113}Cd NMR chemical shifts of cadmium complexes could provide valuable information about the structure of discrete cadmium species.

In the third communication,[45] experimental measurements were performed, which were substantiated by the B3PW91 calculations of ^{113}Cd NMR chemical shifts in crystalline anhydrous cadmium formate (**47**) and acetate dehydrate (**48**) shown in Figure 11. The performed calculations showed fairly good agreement with the ^{113}Cd chemical shift anisotropy tensors determined in the solid-state NMR experiments on powder samples.

In the paper by Hemmingsen *et al.*[46] of the same period of time, ^{113}Cd isotropic NMR shielding constants were calculated for a number of metal ion binding sites in proteins using the GIAO-B3LYP and GIAO-HF methods with the uncontracted polarized basis set of Kellö and Sadlej[40] on cadmium and Pople's 6-31G(d) on ligands. The computational results showed that the calculated ^{113}Cd chemical shifts of the metal ion-containing proteins

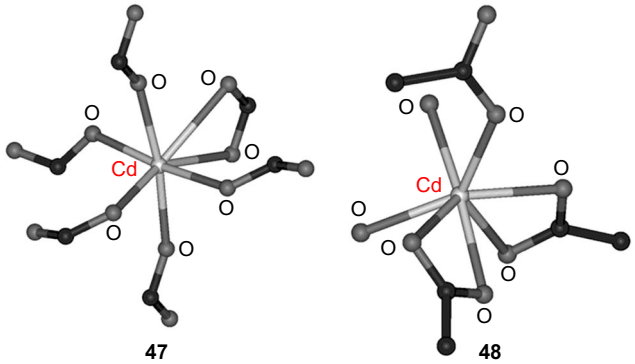


Figure 11. Crystal structures of anhydrous cadmium formate (**47**) and cadmium acetate dehydrate (**48**) used in the calculations of their isotropic and anisotropic ^{113}Cd NMR chemical shifts. Reproduced with minor editing privilege from Kidambi *et al.*[45] with the permission of the *American Chemical Society*.

were in good agreement with the experimental data. The effect of different ligand types (thiolate, imidazole, water, and monodentate carboxylate), coordination number, and deviations of the coordination geometry from the ideal structures on cadmium chemical shifts were also investigated. In particular, the ligand type and coordination number were found to be the important factors influencing the values of ^{113}Cd NMR chemical shifts.

Four years later, Li *et al.*[47] presented a DFT study of ^{113}Cd NMR chemical shifts of the ^{113}Cd(II) ion solvated in aqueous solution. The ^{113}Cd NMR shielding constant was computed using a perturbation theory formalism, which included the nonrelativistic and relativistic contributions to the nuclear magnetic shielding tensor. The paramagnetic nonrelativistic contribution was found to be most sensitive to the dynamic changes in the system and was mainly responsible for the solvent effects in solution. It was found that relativistic correction provided very little sensitivity to the chemical environment and could safely be disregarded in theoretical calculations due to the mutual cancelation between individual relativistic corrections.

2.4. ^{119}Sn NMR

The story of computational ^{119}Sn NMR begins with the simplest molecule of stannane, SnH_4, and its derivatives, the objects of a number of early studies reporting calculations performed mainly at the nonrelativistic and/or the two-component relativistic level, which are exemplified by a number of early publications.[48 – 56]

In one of the most essential publications of that period, Bagno, Casella, and Saielli[57] calculated at the two-component ZORA level ^{119}Sn nuclear shielding constants and spin – spin coupling constants $^1J_{Sn,C}$, $^1J_{Sn,H}$, and $^2J_{Sn,H}$ in stannane, tetramethylstannane, methyltin halides $Me_{4-n}SnX_n$ (X = Cl, Br, I; n = 1 – 3), and tin halides together with related stannyl ions. In the calculation of tin chemical shifts, the Becke 88 exchange plus the Perdew 86 correlation functional in combination with the all-electron TZ2P basis set (specially optimized for the ZORA calculations) was used for all atoms, while spin – spin coupling constants were calculated with the BP functional. Those data are exemplified in Table 5.

The calculated ^{119}Sn NMR chemical shifts generally correlated well with the experimental values, except when several heavy halogen atoms, especially iodine, were chemically bound to tin. In such cases, the calculated chemical shifts were almost constant, falling out of the correlation at the scalar (spin-free) ZORA level; only at the spin – orbit level was a good correlation found for all compounds examined (Fig. 12).

For spin – spin coupling constants involving tin, also given in Table 5, a large relativistic contribution was revealed at both sc-ZORA and so-ZORA levels. As an example, in the parent stannane, the nonrelativistic value of $^1J_{Sn,H}$ obtained at the BP/TZ2P level was −1283 Hz, compared to −1600 and −1550 Hz obtained accordingly at the sc-ZORA and so-ZORA levels, which revealed a relativistic contribution of approximately −300 Hz. The same tendency was found for the $^1J_{Sn,C}$ coupling constants. Surprisingly, all calculated values of $^2J_{Sn,H}$ were dramatically underestimated. In general, the correlation between calculated at both scalar and spin – orbit ZORA quasirelativistic levels spin – spin coupling constants involving tin *vs.* experiment was rather good, as illustrated in Figure 13. This finding was in contrast to the corresponding results

Table 5. Calculated at the ZORA level and experimental ^{119}Sn NMR chemical shifts (ppm) and ^{119}Sn–^{13}C and ^{119}Sn–^{1}H spin–spin coupling constants (Hz) of the stannane derivatives. Compiled from Bagno, Casella, and Saielli.[57]

Compound/ Ion	δ_{Sn}			$^{1}J_{Sn,C}$ and $^{1}J_{Sn,H}$			$^{2}J_{Sn,H}$		
	sc-ZORA	so-ZORA	Experiment	sc-ZORA	so-ZORA	Experiment	sc-ZORA	so-ZORA	Experiment
$SnMe_4$	0	0	0	−115.9	−104.8	−340	8.45	6.74	53.9
SnH_4	−600	−632	−500	−1599.6	−1549.5	−1930			
SnH_3^-	−1042	−1072		26.6	81.2	109.4			
SnH_3^+	1074	1132	−186	−2188.7	−2093.7	−2960			
Me_3SnCl	185	185	164	−124.0	−112.9	−379.7	6.3	4.5	58.2
Me_2SnCl_2	203	188	141	−172.9	−162.4	−468.4	6.9	5.3	68.2
$MeSnCl_3$	108	43	21	−310.4	−300.5		17.3	15.9	96.9
$SnCl_4$	−23	−210	−150						
Me_3SnBr	198	136	128	−113.2	−102.9	−368.9	5.7	3.9	57.8
Me_2SnBr_2	268	71	70	−145.2	−135.4	−442.7	4.6	2.7	66.7
$MeSnBr_3$	233	−261	−165	−248.3	−236.4	−640	11.2	9.0	
$SnBr_4$	128	−973	−638						
Me_3SnI	198	28	39	−98.7	−88.4		4.9	3.2	
Me_2SnI_2	337	−190	−159	−103.9	−89.4		2.1	−0.2	
$MeSnI_3$	395	−865	−700	−150.8	−116.5		2.8	−1.5	
SnI_4	356	−2193	−1701						

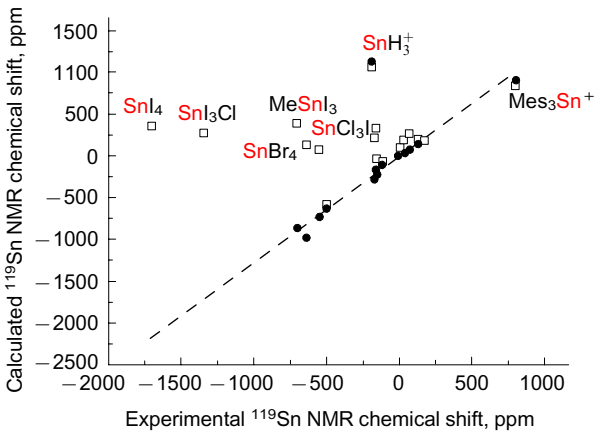


Figure 12. Correlation between calculated at the ZORA level and experimental ^{119}Sn NMR chemical shifts in the representative series of tin compounds: scalar (empty squares) and spin–orbit (filled circles) levels. Reproduced with minor editing privilege from Bagno, Casella, and Saielli [57] with the permission of the *American Chemical Society*.

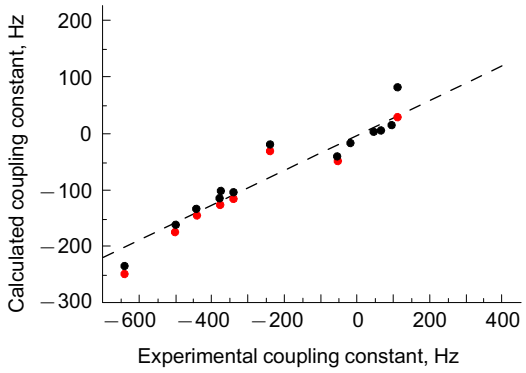


Figure 13. Correlation between calculated at the scalar (red circles) and spin–orbit (black circles) relativistic levels and experimental spin–spin coupling constants $^{1}J_{Sn,C}$, $^{1}J_{Sn,H}$, and $^{2}J_{Sn,H}$ in the representative series of tin compounds. Reproduced with minor editing privilege from Bagno, Casella, and Saielli [57] with the permission of the *American Chemical Society*.

dealing with the calculation of ^{119}Sn chemical shifts, where scalar ZORA proved to be entirely unsuccessful in reproducing experimental chemical shifts in heavy tin halides.

In the same 2006 year, Lantto *et al.*[58] investigated a principal relativistic heavy-atom effect on the NMR shielding tensor of the heavy atom itself (known as the 'HAHA effect') for tin in a series of closed-shell Sn^{2+}, Sn^{4+}, SnH_2, and SnH_3^- systems. It was found that the second-order spin–orbit mechanism, *i.e.* the second-order SO mechanism arising from the cross-term contribution of the Fermi contact hyperfine interaction and the relativistically modified spin-Zeeman interaction (known as 'FC/SZ-KE') was isotropic and practically independent of the electron correlation effects, as well as of the chemical environment of heavy atoms. The third-order spin–orbit terms depended on those factors and contributed both to the heavy-atom shielding anisotropy and the ^{119}Sn NMR chemical shifts.

Table 6 shows the nonrelativistic tin shieldings, the most essential relativistic FC/SZ-KE corrections, and the total values of the calculated ^{119}Sn NMR shielding constants compared to the fully relativistic four-component Dirac–Hartree–Fock (DHF) calculations. First, it should be noted that relativistic FC/SZ-KE corrections were found to be essentially the same for all four systems, falling into a very narrow range of 1617–1619 ppm. Second, the ^{119}Sn NMR shielding constants calculated at that level were in fairly good agreement with the fully relativistic four-component DHF results.

Several years later, in two related publications dealing with the calculation of ^{119}Sn NMR chemical shifts in the

Table 6. ^{119}Sn NMR shielding constants (ppm) calculated at different levels of theory. Compiled from Lantto *et al.*[58]

System	NR	Relativistic correction (FC/SZ-KE)	Total	Four-component (DHF)
Sn^{2+}	5074.2	1618.2	6450.2	6130.5
Sn^{4+}	5057.9	1617.3	6433.6	6113.7
SnH_2	725.5	1618.4	1705.0	1788.7
SnH_3^-	3571.1	1618.5	4919.3	4537.8

Table 7. ^{119}Sn NMR chemical shifts (ppm) calculated at different levels of theory. Compiled from Maldonado *et al.*[59]

Compound	relPPA (RPA)	PBE0	B3LYP	BLYP	Experiment
$SnCl_4$	−124.9	317.2	376.3	481.6	−150
$SnCl_3Br$	−253.2	149.4	186.7	264.0	−263
$SnCl_2Br_2$	−376.2	−21.4	−3.9	46.0	−385
$SnClBr_3$	−498.8	−192.7	−193.2	−169.8	−508
$SnCl_3I$	−576.2	−208.8	−208.5	−151.9	−557
$SnBr_4$	−619.0	−363.0	−379.2	−381.5	−638
$SnCl_2BrI$	−693.6	−377.5	−392.3	−359.9	−672
$SnClBr_2I$	−812.2	−544.9	−572.9	−563.8	−796
$SnBr_3I$	−924.6	−710.1	−748.9	−762.5	−916
$SnCl_2I_2$	−983.8	−718.8	−755.7	−735.8	−955
$SnClBrI_2$	−1092.3	−879.6	−924.9	−925.6	−1068
$SnBr_2I_2$	−1194.7	−1036.4	−1088.0	−1108.6	−1187
$SnClI_3$	−1347.5	−1195.2	−1249.1	−1255.8	−1347
$SnBrI_3$	−1437.7	−1340.5	−1396.4	−1420.8	−1447
SnI_4	−1655.2	−1628.5	−1681.9	−1707.1	−1701

series of halogenostannanes, $SiH_{4-n}X_n$ with X = H, F, Cl, Br, I and n = 0 – 4, Maldonado *et al.*[59,60] studied relativistic and electron correlation effects resulting in core- and ligand-dependent relativistic corrections to tin nuclear magnetic shielding constants (and chemical shifts) in this series. Compiled in Table 7 are the ^{119}Sn NMR chemical shifts in the series of halogenostannanes calculated at the DFT level using popular B3LYP, BLYP, and PBE0 functionals and at the Relativistic Polarization Propagator Approach (RelPPA) at the Random Phase Approximation (RPA) level compared to the experiment. In fact, all DFT methods take into account electron correlation effects in an implicit way, while the uncorrelated RPA level does not.

It is seen from those data that the results obtained within the RelPPA at the RPA level show the most reliable results compared to the experiment, so that this approach can be taken as the benchmark relativistic method for the ^{119}Sn NMR chemical shifts, even for the very heavy molecular systems. On the other hand, the calculated DFT chemical shifts were not in good agreement with their experimental values for light systems, although the DFT performance was significantly improved with the weight of the molecules. For the lightest molecule in this series, $SnCl_4$, all DFT chemical shifts were positive, while the experimental shifts were negative. Additionally, there was a large difference between the values obtained with different DFT functionals. However, for heavier systems, the performance of the DFT calculations was improved, and the results obtained with different functionals were closer to each other and to the experiment. In the case of heavier molecular systems, the calculated ^{119}Sn NMR chemical shifts were in good agreement with the experimental results, and the differences between them were very small.

In a more recent study by Křístková *et al.*,[61] relativistic four-component calculations of $^1J_{Sn,H}$ in stannane were performed using an efficient evaluation of the exchange-correlation response kernel. The authors reported the development and implementation of a new scheme for the efficient calculation of indirect nuclear spin – spin coupling constants in the framework of the four-component matrix Dirac – Kohn – Sham (DKS) approach, which took advantage of the restricted magnetic balance formalism for the rapid evaluation of the DFT exchange-correlation response kernels. The new approach aimed to speed up the evaluation of matrix elements of the kernel of the exchange-correlation potential and tested on a series of as many as 63 indirect nuclear spin – spin coupling constants involving that of $^1J_{Sn,H}$ in stannane. The resulting relativistic value was $^1J_{Sn,H}$ = −1742.9 Hz, as compared to experimental value of −1933.3 Hz. At the same time, the nonrelativistic value was −1241.4 Hz, leaving as much as approximately 500 Hz for the relativistic contribution.

Three years later, Demissie[62] reported manifestation of scalar and spin – orbit relativistic effects in the ^{119}Sn NMR chemical shifts and spin – spin coupling constants in three tin alkynyl compounds, $Sn(C{\equiv}C-CH_3)_4$ (**49**), $(CH_3)_2Sn(C{\equiv}C-CH_3)_2$ (**50**), and $(CH_3)_3Sn-C{\equiv}C-H$

Table 8. ^{119}Sn NMR chemical shifts (ppm) and ^{119}Sn – ^{1}H and ^{119}Sn – ^{13}C spin – spin coupling constants (Hz) calculated at different levels of theory compared to the experiment. Compiled from Demissie.[62]

Compound	Formula	NMR parameter	Total values				Relativistic corrections			Experiment
			NR	so-ZORA	sc-ZORA	DKS	scalar	spin – orbit	total	
49	$Sn(C{\equiv}C-CH_3)_4$	δ_{Sn}	−366.5	−460.3	−391.6	−397.0	−25.1	−5.4	−30.5	
		$^1J_{Sn,C}$	−957.1	−1073.6	−1243.8	−1223.7	−286.8	20.2	−266.6	−1168.0
		$^2J_{Sn,C}$	−213.1	−254.9	−277.8	−276.3	−64.6	1.5	−63.1	−241.0
		$^3J_{Sn,C}$	−19.0	−18.7	−25.5	−25.3	−6.5	0.3	−6.2	−19.5
		$^4J_{Sn,H}$	19.7	20.3	27.3	26.7	7.7	−0.6	7.0	17.0
50	$(CH_3)_2Sn(C{\equiv}C-CH_3)_2$	δ_{Sn}	−167.2	−209.8	−180.2	−179.3	−13.0	0.9	−12.1	
		$^1J_{Sn,Me}$	−366.3	−363.1	−446.0	−440.4	−79.7	5.6	−74.1	−496.2
		$^1J_{Sn,C{\equiv}}$	−580.9	−550.4	−632.2	−613.1	−51.3	19.2	−32.2	−654.6
		$^2J_{Sn,C{\equiv}}$	−135.0	−141.2	−151.8	−150.0	−16.8	1.8	−15.0	−141.8
		$^3J_{Sn,Me}$	−13.8	−11.3	−16.5	−16.2	−2.7	0.3	−2.4	−12.8
		$^2J_{Sn,H}$	67.7	44.7	89.0	68.2	21.3	−20.8	0.5	68.8
		$^4J_{Sn,H}$	16.1	14.3	20.3	19.6	4.2	−0.7	3.5	13.1
51	$(CH_3)_3Sn-C{\equiv}C-H$	δ_{Sn}	−104.0	−131.3	−111.8	−111.8	−7.8	0.1	−7.8	
		$^1J_{Sn,Me}$	−302.2	−279.9	−344.3	−339.2	−42.1	5.1	−36.9	−403.5
		$^1J_{Sn,C{\equiv}}$	−379.2	−298.6	−343.6	−326.8	35.6	16.8	52.4	−415.5
		$^2J_{Sn,C{\equiv}}$	−89.7	−83.4	−87.1	−85.4	2.6	1.7	4.3	−85.6
		$^2J_{Sn,H}$	46.1	39.9	53.5	55.1	7.3	1.7	9.0	61.0
		$^3J_{Sn,H}$	−29.4	−25.8	−35.2	−34.1	−5.8	1.1	−4.7	−34.0

(**51**), derived from the nonrelativistic as well as from the two- and four-component relativistic DFT calculations. The main relativistic effect in these molecules was shown to be not due to spin–orbit coupling (as might be expected) but rather due to the scalar relativistic contraction of the *s*-shells. It was found that for a variety of spin–spin coupling constants involving tin, the four-component relativistic DFT approach using Perdew's hybrid exchange-correlation functional PBE0 gave results in better agreement with the experiment (compared to other functionals). The indirect spin–spin coupling constants calculated using the spin–orbit ZORA were in good agreement with the results obtained from the four-component relativistic calculations, which are illustrated in Table 8. It is well known from the comparison of two- and four-component relativistic methods that spin–orbit contributions are dominant for absolute shielding constants. Interestingly, some predicted chemical shifts had opposite signs of the experimental chemical shift, but since the chemical shift relies on an arbitrary reference compound, there is no physical difference between negative and positive chemical shift.

Scalar effects were generally found to prevail for spin–spin coupling constants involving tin, which is due to the relativistic increase in density and spin density at the position of the nucleus. This was also confirmed by the results of the performed study for ^{119}Sn NMR chemical shifts and spin–spin coupling constants, as one can unambiguously conclude from those data. For three closely related compounds **49**–**51**, the total relativistic corrections were found to be spread over *ca.* 20 ppm (from −7.8 to 30.5 ppm) for ^{119}Sn NMR chemical shifts and over more than 300 Hz (from −266.6 to +52.4 Hz) for spin–spin coupling constants involving ^{119}Sn.

In continuation of the investigation of the transmission mechanisms of tin spin–spin coupling across triple carbon-carbon (acetylenic) bonds, Jakubowska *et al.*[63] reported calculations of the one-bond and geminal tin–carbon coupling constants, $^{1}J_{\mathrm{Sn,C}\equiv}$ and $^{2}J_{\mathrm{Sn,C}\equiv}$, in ethynylstannane, $HC{\equiv}CSnH_3$, performed at both the nonrelativistic coupled cluster single and double excitation model (CCSD) and DFT level, the latter in the nonrelativistic and relativistic four-component approach with different exchange-correlation functionals and basis sets, to estimate the effects of the electron correlation and relativity.

Three different exchange-correlation functionals, BLYP, B3LYP, and BHLYP, and two different basis set combinations were used. In the first one, for all atoms, the all-electron augmented triple zeta basis set with polarization functions (ATZP) was used. In the second basis set, Sauer's aug-cc-pVTZ-J was used on carbons and hydrogens, while the ATZP basis set was used on tin. All of those basis sets were employed in the uncontracted form. The nonrelativistic DFT calculation of the vibrationally averaged spin–spin coupling constants was performed with the B3LYP functional.

As shown in Table 9, the B3LYP values of $^{1}J_{\mathrm{Sn,C}\equiv}$ and $^{2}J_{\mathrm{Sn,C}\equiv}$ were the closest to the benchmark CCSD results. Taking everything into account, the performance of the B3LYP functional was found to be the most satisfactory, so that it was recommended to be used in all related relativistic DFT calculations. The difference between relativistic (4c-B3LYP) and nonrelativistic (B3LYP) results was approximately 50 Hz for $^{1}J_{\mathrm{Sn,C}\equiv}$ and some 20 Hz for $^{2}J_{\mathrm{Sn,C}\equiv}$, indicating that relativistic effects were well pronounced for both couplings.

Table 9. ^{119}Sn−^{13}C spin–spin coupling constants (Hz) of ethynylstannane calculated at different levels of theory compared to the experimental values. Compiled from Jakubowska *et al.*[63]

Coupling constant	BLYP	B3LYP	BHLYP	CCSD	4c-B3LYP	Experiment [a]
$^{1}J_{\mathrm{Sn,C}\equiv}$	−439.8	−526.9	−677.6	−597.3	−575.9	−344.2 (−445.4)
$^{2}J_{\mathrm{Sn,C}\equiv}$	−122.2	−124.7	−120.8	−128.0	−143.4	−64.7 (−103.3)

[a] Experimental values for $HC{\equiv}CSn(C_2H_5)_3$, estimated experimental values for $HC{\equiv}CSnH_3$ in parenthesis.

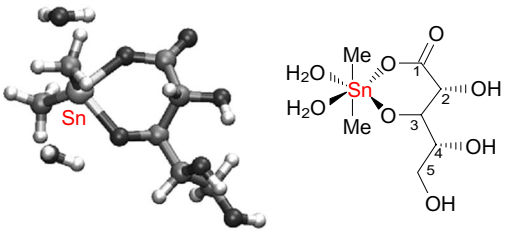
Turning to the discussion of organotin compounds studied by computational ^{119}Sn NMR, a pioneering paper by Bagno *et al.*[64] should first be recalled together with some more recent contributions from his group.[65–68] Thus, in the former publication,[64] the structure of the complex of D-ribonic acid with dimethyltin(IV) was evaluated based on the experimental and theoretical ^{119}Sn NMR study, which allowed the determination of its stable conformation in solution as well as the detection of a dimerization process. Moreover, evidence was given of the active coordination of tin by solvent.

In that study, geometry optimization was performed at the DFT level using the B3PW91 hybrid functional combined with the 6-31G(d,p) basis set on C, H, and O and the DZVP basis set on Sn. Shielding constants were calculated using B3LYP and B3PW91 hybrid functionals with IGLO-II for tin and 6-31G(d,p) basis sets for the light atoms.

The dimerization process and solvent effects were taken into account by explicitly considering coordinating solvent molecules in three different monomer model structures exemplified in Figure 14 for the structure with two molecules of water **52** and two dimer models **53** and **54** shown in Figure 15. DFT calculations of the geometry and ^{119}Sn NMR chemical shifts supported the proposed structures of the monomer and dimer forms of D-ribonic acid with dimethyltin(IV) in solution.

In a more recent publication by Bagno *et al.*[68] the performance of the DFT protocols, both at the scalar relativistic ZORA and the nonrelativistic levels of theory for the calculation of the $^{3}J_{\mathrm{Sn,H}}$ and $^{3}J_{\mathrm{Sn,C}}$ couplings for a series of flexible organotin(IV) *erythro* (**55**) and *threo* (**56**) derivatives was tested.

Geometry optimizations were performed by using the common B3LYP functional. The correlation-consistent



52

Figure 14. Monomer model of D-ribonic acid with dimethyltin(IV) having two water molecules coordinated to tin. Reproduced with minor editing privilege from Bagno *et al.*[64] with the permission of *John Wiley and Sons*.

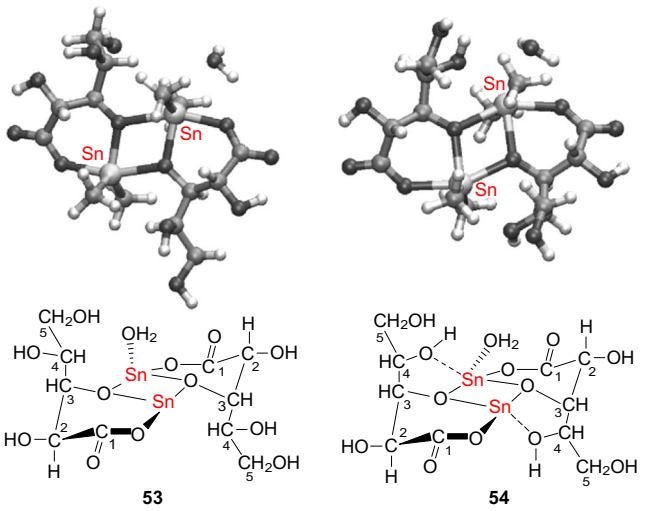
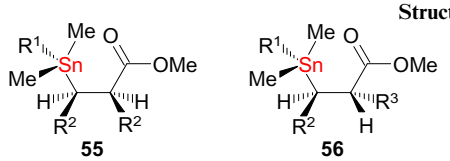


Figure 15. Dimer models of D-ribonic acid with dimethyltin. For clarity, methyl groups on tin in bottom structures are not shown. In both cases, the two tin atoms are nonequivalent due to a coordinating water molecule on only one tin atom. Reproduced with minor editing privilege from Bagno *et al.*[64] with the permission of *John Wiley and Sons*.

polarized triple zeta valence basis set cc-pVTZ was used for light atoms, while an effective core potential coupled with a cc-pVTZ quality valence contracted basis set was applied for tin. The vicinal coupling constants were calculated on the optimized geometries with the nonrelativistic protocol using the BLYP functional with Pople's 6-31G(d,p) basis set for light atoms and the all-electron double zeta valence with polarization basis set, DZVP, for tin.

A satisfactory agreement between experimental and calculated vicinal couplings was achieved by taking into account conformational beheviour of **55** and **56**. The protocols used in that study, mainly the relativistic protocol, were found to give a correct picture of the overall performance in calculating vicinal tin couplings. Both protocols satisfactorily described conformer populations; however, the relativistic approach resulted in a better performance for $^{3}J_{Sn,H}$ and $^{3}J_{Sn,C}$ in that series. It was found that the nonrelativistic approach suffered from a systematic underestimation of both vicinal couplings, implying that calculated coupling constants should be rescaled depending on the chemical systems under study.

Structures 55, 56



R^1 = Me, Cl; R^2, R^3 = Me, Ph

Casella *et al.*[65] tested several computational protocols at the nonrelativistic DFT level of theory for the calculation of $^{1}J_{Sn,C}$ and $^{2}J_{Sn,H}$ spin–spin coupling constants in di- and trimethyltin(IV) derivatives together with penta- and hexacoordinated tin complexes with different ligands. Quite good agreement with the experimental data was found for a number of different hybrids and some pure functionals, as illustrated for tetramethylstannane in Table 10. In those

Table 10. Spin–spin coupling constants $^{1}J_{Sn,C}$ and $^{2}J_{Sn,H}$ (Hz) of tetramethylstannane calculated at the nonrelativistic DFT level using different functionals compared to the experiment. Compiled from Casella *et al.*[65]

Hybrid functionals	$^{1}J_{Sn,C}$	$^{2}J_{Sn,H}$	Pure functionals	$^{1}J_{Sn,C}$	$^{2}J_{Sn,H}$
B3PW91	−353.4	48.1	BP86	−279.1	34.9
B3LYP	−351.3	39.7	BLYP	−289.0	28.2
PBE1PBE	−372.7	50.6	PBEPBE	−288.5	34.0
B971	−352.4	36.5	PW91PW91	−286.4	34.9
B98	−359.5	40.9	OLYP	−322.0	43.1
mPW91PW91	−373.5	52.9	OPW91	−322.4	52.6
mPWB1K	−393.1	49.6	G96LYP	−284.6	32.7
B3P86	−345.9	45.6	Experiment	−336.9	54.7
O3LYP	−354.0	47.3			
mPW3LYP	−350.5	38.8			
Experiment	−336.9	54.7			

nonrelativistic calculations, the 6-31G(d,p) basis set was used for all of the atoms except tin, for which the all-electron contracted DZVP39 basis set was employed.

A number of penta- and hexacoordinated tin complexes exemplified with structures **57**–**59** were also investigated in that study by means of the calculation of their ^{119}Sn NMR chemical shifts compared to the experiment (Table 11). For complex **57**, three different isomers were considered, namely, hexacoordinated tin(IV) with methyl groups arranged in the *trans* configuration (**57a**); pentacoordinated tin(IV) where double chelation was lost (**57b**); and hexacoordinated tin(IV) with *cis* methyl groups (**57c**). It was found that the calculated $^{1}J_{Sn,C}$ and $^{2}J_{Sn,H}$ for **57a** were in disagreement with their experimental values, whereas the calculated coupling constants for **57c** were in good agreement with the experiment, giving reasoning for the existence of that particular isomer. Accordingly, the calculated values of $^{1}J_{Sn,C}$ and $^{2}J_{Sn,H}$ were found to be closer to structures **58a** and **59a** than to their diverse isomers **58b** and **59b**.

In two related papers by Casella *et al.*[66,67] the dihedral angle beheviour of $^{3}J_{Sn,H}$ and $^{3}J_{Sn,C}$ was investigated to verify their Karplus-type dependences together with the effect of the heteroatom X (X = N, O, S) in the coupling

Structures 57–59

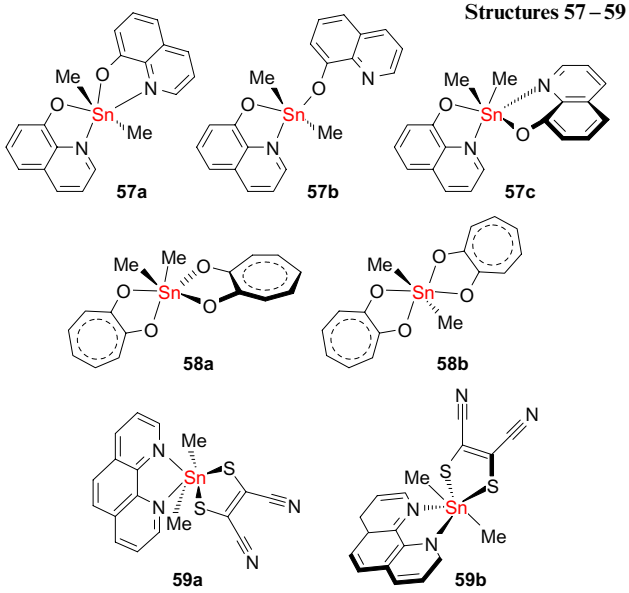


Table 11. Calculated spin–spin coupling constants $^{1}J_{Sn,C}$ and $^{2}J_{Sn,H}$ (Hz) of penta- and hexacoordinated tin complexes compared to the experimental values. Compiled from Casella *et al.*[65]

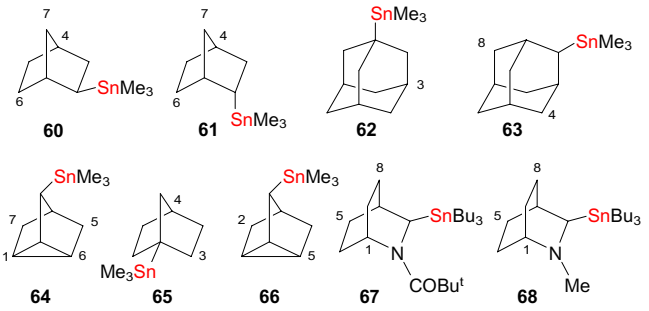
Compound	$^{1}J_{Sn,C}$		$^{2}J_{Sn,H}$	
	Calculated	Experiment [a]	Calculated	Experiment
57a	−790.3	(−)632	86.7	71.2
57b	−643.6		73.0	
57c	−599.5		67.5	
58a	−626.0	(−)643	68.0	72.2
58b	−843.7		92.4	
59a	−497.5		59.4	65.0
59b	−690.9		83.4	

[a] The sign in parentheses was not experimentally determined.

path at both nonrelativistic and relativistic scalar ZORA levels.

Thus, in the first paper,[66] a calibration of the computational schemes, performed by comparing experimental and calculated couplings, both at the nonrelativistic and two-component scalar relativistic DFT levels, for a set of rigid molecules exemplified with structures **60**–**68**, revealed their high predictive power. In particular, relativistic results for $^{3}J_{Sn,C}$, compared to the experiment, had a mean absolute error of only 2 Hz over a range of almost 70 Hz, as illustrated in Table 12. It was also found that the presence of the multiple paths connecting coupled nuclei was of great importance in view of the fact that the magnitude of $^{3}J_{Sn,C}$ decreased significantly by increasing the number of coupling paths between tin and carbon. Considering the overall results, a very high correlation coefficient between calculations and experiment was observed for both protocols, nonrelativistic and two-component relativistic. Generally, closer agreement with the calculated values of the relativistic protocol was documented. However, the slopes of the fitting lines were either higher or lower than unity. A clearer picture was obtained by considering $^{3}J_{Sn,C}$ and $^{3}J_{Sn,H}$ couplings separately. For $^{3}J_{Sn,C}$, the performance of the relativistic protocol was indeed very high.

Structures 60–68



Generally, both coupling constants, $^{3}J_{Sn,H}$ and $^{3}J_{Sn,C}$, were found to follow the well-known Karplus-type dependence, as illustrated in Figure 16 for $^{3}J_{Sn,H}$ in 1-(trimethylstannyl)propane (**69**) and 2-hydroxy-1-(trimethylstannyl)-

Structures 69, 70

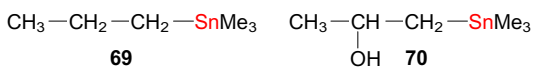


Table 12. Vicinal spin–spin coupling constants $^{3}J_{Sn,C}$ (Hz) of the representative tin derivatives of polycycloalkanes calculated at the nonrelativistic and two-component scalar relativistic DFT levels compared to the experimental values. Compiled from Casella *et al.*[66]

Compound	Coupled nuclei	NR	Relativistic sc-ZORA	Experiment [a]
60	Sn,C(4)	−9.5	−11.3	(−)12.7
	Sn,C(6)	−48.7	−69.5	(−)67.4
	Sn,C(7)	−0.9	2.6	0.0
61	Sn,C(4)	−17.4	−22.2	(−)23.4
	Sn,C(6)	−28.3	−38.1	(−)36.0
	Sn,C(7)	−44.1	−60.5	(−)56.6
62	Sn,C(3)	−34.8	−49.1	(−)51.1
63	Sn,C(4)	−6.7	−7.3	(−)8.5
	Sn,C(8)	−42.7	−61.0	(−)60.0
64	Sn,C(1)	−41.4	−51.1	(−)53.6
	Sn,C(5)	−7.1	−5.2	(−)9.7
	Sn,C(6)	−6.0	−5.6	(−)8.0
	Sn,C(7)	−41.8	−52.8	(−)57.8
65	Sn,C(3)	−38.2	−50.5	(−)51.9
	Sn,C(4)	−50.7	−65.4	(−)65.8
66	Sn,C(2)	−49.6	−66.2	(−)67.5
	Sn,C(5)	−8.1	−9.2	(−)11.9
67	Sn,C(1)	−0.3	2.9	(±)11.8
	Sn,C(5)	−37.7	−50.9	(−)52.7
	Sn,C(8)	−13.7	−16.5	(−)14.8
68	Sn,C(1)	−23.3	−35.2	(−)30.5
	Sn,C(5)	−46.7	−65.5	(−)62.5
	Sn,C(8)	−9.9	−9.7	(−)12.0
	Sn,Me	−4.7	1.5	(±)5.8

[a] The sign in parentheses was not experimentally determined.

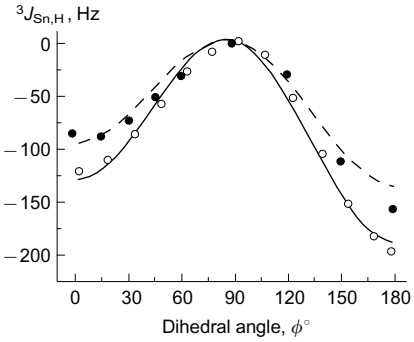


Figure 16. Dihedral angle dependence of $^{3}J_{Sn,H}$. Open circles: 1-(trimethylstannyl)propane (**69**); solid circles: 2-hydroxy-1-(trimethylstannyl)propane (**70**). Reproduced with minor editing privilege from Casella *et al.*[66] with the permission of *John Wiley and Sons*.

propane (**70**). However, it was shown that the influence of the substituents, as well as the presence of the multiple paths connecting coupled nuclei known as the multipath coupling mechanism, affected the form of the Karplus curve in each particular case, which necessarily should be taken into account in related studies.

In another paper by the same authors,[67] the Karplus-type beheviour of $^{3}J_{Sn,C}$ transmitted *via* two coupling paths, $^{119}Sn-C-C-^{13}C$ and $^{119}Sn-C-N-^{13}C$, was established, as exemplified for (tributylstannyl)piperidines **71**–**73** by the data presented in Table 13 together with their graphical representations shown in Figure 17. Inclusion at the relativistic level of one water molecule into computational space in an explicit way (indicated in the

Structures 71e, 71a, 72e, 72a

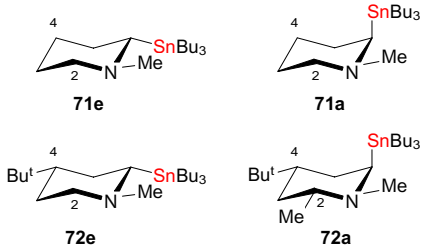


Table 13. Vicinal spin – spin coupling constants $^3J_{Sn,C}$ (Hz) of (tributylstannyl)piperidines calculated at the nonrelativistic and two-component scalar relativistic DFT levels compared to the experimental values. Compiled from Casella *et al.*[67]

Compound	Coupled nuclei	NR	Relativistic		Experiment [a]
			ZORA	ZORA (+H_2O)	
71e	Sn,C(2)	−42.1	−55.3	−48.8	(−)20.3
	Sn,C(4)	−38.2	−50.8	−40.1	(−)24.6
	Sn,Me	−9.2	−9.5	−10.3	(−)8.8
71a	Sn,C(2)	−14.0	−15.4	−13.4	(−)20.3
	Sn,C(4)	−18.5	−21.1	−19.4	(−)11.8
	Sn,Me	−9.9	−8.2	−14.6	(−)8.8
72e	Sn,C(2)	−37.9	−52.1	−45.8	(−)25.5
	Sn,C(4)	−42.0	−57.8	−46.8	(−)27.5
	Sn,Me	−6.5	−5.9	−7.6	(−)5.3
73a	Sn,C(2)	−2.3	−17.9	−15.7	(−)17.4
	Sn,C(4)	−15.7	−18.7	−17.7	(−)21.8
	Sn,Me	−17.8	−12.2	−18.1	(−)9.0

[a] The sign in parentheses was not experimentally determined.

table as 'ZORA + H_2O') did not result in any regular changes of $^3J_{Sn,C}$; however, a neat effect of such inclusion in some particular cases was found to be rather essential (of up to 10 Hz or 20% of the total value).

At the nonrelativistic level, spin – spin coupling constants were calculated at the BLYP/DZVP(Sn) + 6-31G**(light atoms) level on geometries optimized at the B3LYP/TZVP(ECP) and B3LYP/DZVP(Sn) + 6-31G**(light atoms) levels, respectively, where DZVP is an all-electron polarized double zeta basis set for tin. At the scalar relativistic level, the BLYP functional and the all-electron Slater type TZ2P basis set were used throughout.

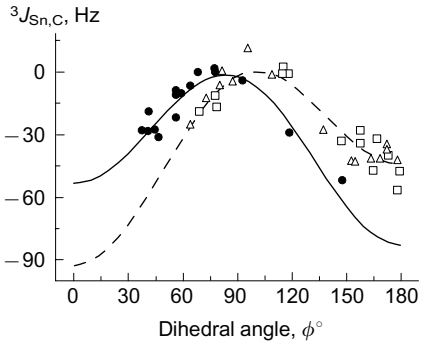


Figure 17. Karplus curves of $^3J_{Sn,C}$ in *N*-methyl-2-(trimethylstannyl)piperidines for different coupling paths. Empty squares: Sn – C – C – C; empty triangles: Sn – C – N – C; filled circles: Sn – C – N – Me. Reproduced with minor editing privilege from Casella *et al.*[67] with the permission of *The Royal Society of Chemistry*.

2.5. ^{125}Te NMR

Basic theoretical principles of the two- and four-component relativistic calculations of ^{125}Te NMR shielding constants (chemical shifts) and spin – spin coupling constants involving tellurium are presented in two recent reviews.[15,69] Herewith, we will not go into this area, forwarding the reader to those reviews and focusing our interest on pure practical applications of such calculations.

Among several early publications[70–72] dealing with the calculation of ^{125}Te NMR shielding constants and tellurium spin – spin coupling constants is that by Hada *et al.*[71] dealing with the evaluation of a quasirelativistic Hamiltonian including the spin-free relativistic, one- and two-electron spin – orbit, and relativistic magnetic interaction terms. Those calculations for tellurium shielding constants were performed in a series of simple tellurium-containing molecules involving TeH_2, TeF_6, $Te(CH_3)_2$, $Te(CH_3)_4$, and $Te(CH_3)_2Cl_2$, as represented in Table 14. The main result of the performed calculations was that relativistic effects amounting to as much as 1300 ppm were very important for qualitatively reproducing the absolute values of ^{125}Te shielding constants obtained experimentally. On the other hand, for ^{125}Te NMR chemical shifts, relativistic effects were less important because they cancelled each other between a sample and a reference.

Some eight years ago, Jaszuński and Olejniczak[73] performed an extensive nonrelativistic HF, CCSD, and

Table 14. Calculated and experimental ^{125}Te NMR chemical shifts (ppm) in a series of simple tellurium-containing compounds. Compiled from Hada *et al.*[71]

Compound	Level	Shielding constant				δ_{calc}	Experiment
		Paramagnetic	Diamagnetic	Spin – orbit	Total		
$Te(CH_3)_2$	nonrelativistic	−2228	5436		3208	0	0
	quasirelativistic	−2334	5161	1898	4725	0	
TeH_2	nonrelativistic	−1602	5374		3772	−564	−621
	quasirelativistic	−1684	5099	1895	5310	−585	
TeF_6	nonrelativistic	−2626	5633		3007	201	543 ± 130
	quasirelativistic	−2859	5358	1956	4455	270	
$Te(CH_3)_4$	nonrelativistic	−2195	5505		3310	−102	−67
	quasirelativistic	−2247	5230	1785	4768	−42	
$Te(CH_3)_2Cl_2$	nonrelativistic	−2657	5563		2906	302	734
	quasirelativistic	−2804	5288	1774	4258	467	

Table 15. ^{125}Te NMR shielding constant (ppm) of TeH_2 calculated at the nonrelativistic and relativistic four-component Dirac–Coulomb levels using different basis sets. Compiled from Jaszuński and Olejniczak.[73]

Basis set	Nonrelativistic			Relativistic		
	HF	CCSD	CCSD(T)	4c-HF	4c-DFT	4c-SDFT
uWTBS	3720.8	3835.7	3846.3	4832.5	4701.6	4744.6
dyall.cv3z	3702.7	3772.1	3787.1			
dyall.acv3z				4802.5	4675.2	4722.9
c-o.cv3z	3701.0	3769.7	3784.7			
dyall.v4z				4815.9	4688.3	4736.8
dyall.cv4z				4806.2	4677.9	4725.7
dyall.acv4z	3696.0	3764.9	3780.2	4804.5	4677.1	4725.9
dyall.acv4z-unc(H)	3695.3	3764.0	3779.8			

CCSD(T) study and the four-component Hartree–Fock, DFT, and spin-density functional theory (SDFT) relativistic calculations of $^1J_{Te,H}$ in TeH_2. Relativistic effects were described by applying the Dirac–Coulomb Hamiltonian, commonly used in relativistic four-component calculations. The role of the level of theory, basis sets, electron correlation, relativistic and rovibrational effects was thoroughly investigated. As an example, the role of the level of theory (both at the nonrelativistic and four-component relativistic levels) applied together with triple and quadruple zeta basis sets augmented with different valence and core-valence functions is presented in Table 15 compiled from that publication.

The nonrelativistic calculations of the tellurium shielding constant essentially underestimated the relativistic results (by as much as *ca.* 1000 ppm). The CCSD approach recovered a major part of the electron correlation effects, with the CCSD and CCSD(T) values being very much the same. At this the CCSD(T) values of the ^{125}Te NMR shielding constants were approximately 2% larger than the HF values. At the relativistic level (performed with the KT2 functional in both DFT and SDFT calculations), the basis set dependence of the ^{125}Te NMR shielding constant was very similar in all the approximations, meaning that the essential differences observed for a particular shielding constant between various levels of approximation were almost independent of the basis set. Finally, the ZPV corrections and temperature effects were studied at the CCSD level, combining the c-o.cv3z basis set for tellurium and the uncontracted aug-cc-pVTZ basis for hydrogens. The ZPV correction for TeH_2 was -76.02 ppm, and at 300 K, the total rovibrational effect was -79.87 ppm.

Taking into account all these accuracy factors (level of theory and electron correlation, quality of a basis set, relativistic effects, rovibrational and temperature corrections), it was found that a reasonable estimate of the tellurium shielding constant in TeH_2 was 4809 ± 70 ppm.

Rusakova *et al.*[74] performed calculations of ^{125}Te NMR chemical shifts at the four-component relativistic level by taking into account solvent and vibrational corrections in a series of organotellurium compounds **74**–**87** with dimethyl telluride (**74**) used as a reference.

In the ^{125}Te NMR chemical shift scale referenced to dimethyl telluride, relativistic corrections varied in the range of 17–369 ppm, which gave on average 26% of the total relativistic values of tellurium chemical shifts. Table 16 compiled from this publication [74] shows that total relativistic corrections to ^{125}Te NMR chemical shifts ($\Delta\delta_{rel}$) were deshielding because the relativistic shielding constant of dimethyl telluride used as a standard was the largest in the series. It followed that relativistic corrections to tellurium chemical shifts varied in a wide range, so that there were no evident cancellation of relativistic effects found, which might be the result of the subtraction of the tellurium shielding constants of the compounds under consideration and that of a standard.

Structures 74–87

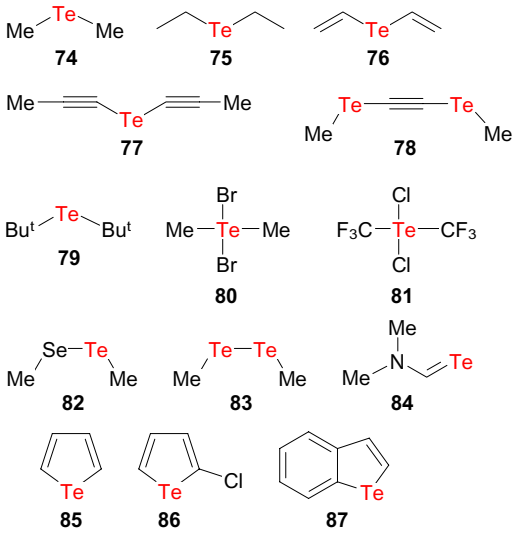


Table 16. ^{125}Te NMR chemical shifts (ppm) calculated at the nonrelativistic and four-component relativistic DFT levels using the PBE0 functional. Compiled from Rusakova *et al.*[74]

Compound	NR (δ_{NR})	Relativistic correction ($\Delta\delta_{rel}$)	Relativistic (δ_{rel})	Experiment
75	293	38	331	374
76	455	113	568	534
77	242	107	349	338
78	132	55	187	215
79	762	166	928	993
80	567	230	797	858
81	793	369	1162	1114
82	437	30	467	512
83	1	28	29	63
84	845	17	862	599
85	597	161	758	782
86	696	181	877	905
87	597	139	736	727

Table 17. ^{125}Te NMR chemical shifts (δ_{total}, ppm) in several representative compounds calculated with the PBE0 functional taking into account relativistic ($\Delta\delta_{rel}$), solvent ($\Delta\delta_{solv}$), and vibrational ($\Delta\delta_{vib}$) corrections (ppm) to the corresponding nonrelativistic values (δ_{NR}). Compiled from Rusakova *et al.*[74]

Compound	Solvent	δ_{NR}	$\Delta\delta_{rel}$	$\Delta\delta_{solv}$	$\Delta\delta_{vib}$	δ_{total}	Experiment
75	C_6D_6	293	38	−2	20	349	374
76	C_6D_6	455	113	15	−13	570	534
77	C6D6	242	107	36	−61	324	338
80	$PhCH_3$	567	230	138	−45	890	858
85	$(CD_3)_2CO$	597	161	71	−22	807	782
86	$(CD_3)_2CO$	696	181	78	−39	916	905

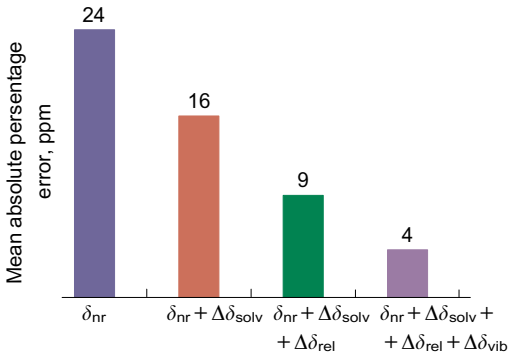


Figure 18. Mean absolute percentage errors of ^{125}Te NMR chemical shifts, calculated at the nonrelativistic (δ_{nr}) and 4c-relativistic levels using the PBE0 functional taking into account solvent ($\Delta\delta_{solv}$), relativistic ($\Delta\delta_{rel}$), and vibrational ($\Delta\delta_{vib}$) corrections in comparison to the experimental results. Reproduced from Rusakova *et al.*[74] with minor editing privilege with the permission of the *American Chemical Society*.

The absence of the cancelation of relativistic effects in this series and the finding that they cancelled each other between a sample and a reference in the series of TeH_2, TeF_6, $Te(CH_3)_2$, $Te(CH_3)_4$, and $Te(CH_3)_2Cl_2$, as was reported by Hada,[71] might be explained by the dramatic difference between the chemical structures in those series of compounds.

Another interesting issue raised by the authors [74] was the solvent effects and vibrational corrections to ^{125}Te NMR chemical shifts compared to relativistic effects, exemplified for a series of representative compounds **75**–**77**, **80**, **85**, and **86** in Table 17. It was found that relativistic correction ($\Delta\delta_{rel}$) averaged over those six compounds amounted to 22% in relation to the total tellurium chemical shifts (δ_{total}). At that time, solvent ($\Delta\delta_{solv}$) and vibrational ($\Delta\delta_{vib}$) effects reached absolute values as much as *ca.* 138 and 61 ppm, respectively. On average, $\Delta\delta_{solv}$ and $\Delta\delta_{vib}$ amounted to 8 and 6%, respectively.

The final results of that study dealing with the relative contributions of relativistic, solvent, and vibrational effects on ^{125}Te NMR chemical shifts are summarized in Figure 18. The mean absolute percentage error of the calculation of ^{125}Te NMR chemical shifts consequently decreased from 24 ppm for the nonrelativistic level to only 4 ppm when relativistic, solvent, and vibrational effects were taken into account.

Rusakov *et al.*[75] performed a high-level correlated calculation of spin–spin coupling constants involving tellurium, $^2J_{Te,H}$ and $^3J_{Te,H}$, of divinyl telluride (**76**) and tellurophene (**85**) taking into account relativistic effects, vibrational corrections, and solvent effects. At the nonrelativistic level, a very well approved Sauer's polarization propagator methods SOPPA(MP2), SOPPA(CC2), and SOPPA(CCSD) were applied at the two-component ZORA level together with the B3LYP and PBE0 functionals within the DFT framework. A full-electron basis set av3z-J derived in that paper was employed for tellurium, while Sauer's contracted basis set, aug-cc-pVTZ-J, was used for the hydrogens involved in spin–spin coupling with tellurium. At that, a standard Dunning's cc-pVDZ basis set was used on all uncoupled atoms. Proposed in that paper, tellurium basis set av3z-J was specifically optimized for the correlated calculations of spin–spin coupling constants involving tellurium using the technique applied earlier for the creation of the aug-cc-pVTZ-J family of basis sets.[76, 77] Scalar relativistic corrections were calculated within the ZORA formalism with the B3LYP functional, while vibrational and solvent corrections were evaluated at the nonrelativistic B3LYP level with the former using the ZPVE approach and the latter within the IEF PCM scheme for chloroform.

The nonrelativistic values of the ^{125}Te–^{1}H coupling constants of tellurophene calculated at different SOPPA

Table 18. Geminal and vicinal spin–spin coupling constants ^{125}Te–^{1}H (Hz) of tellurophene (**85**), including relativistic (ΔJ_{rel}), solvent (ΔJ_{solv}), and vibrational (ΔJ_{vib}) corrections (Hz), to their total nonrelativistic values (TO). Compiled from Rusakov *et al.*[75]

Coupling constant	Method	Nonrelativistic results					Relativistic, solvent, and vibrational corrections			J_{total}
		DSO	PSO	SD	FC	TO	ΔJ_{rel}	ΔJ_{solv}	ΔJ_{vib}	
$^2J_{Te,H}$	DFT–B3LYP	0.3	14.2	−0.3	−114.5	−100.3	−17.6	−0.1	−0.1	−118.1
	DFT–PBE0	0.3	14.0	−0.2	−108.5	−94.4	−17.6	−0.1	−0.1	−112.2
	SOPPA(MP2)	0.3	11.4	−0.6	−101.9	−90.8	−17.6	−0.1	−0.1	−108.6
	SOPPA(CC2)	0.3	11.1	−0.5	−100.8	−89.9	−17.6	−0.1	−0.1	−107.7
	SOPPA(CCSD)	0.3	11.4	−0.6	−98.5	−87.4	−17.6	−0.1	−0.1	−105.2
	Experiment	14.2	−0.3	−114.5	−100.3	−17.6	−0.1	−0.1	−118.1	−101.7
$^3J_{Te,H}$	DFT–B3LYP	0.5	−0.4	−1.2	−20.4	−21.5	5.1	0.6	−0.6	−16.4
	DFT–PBE0	0.5	−0.6	−1.3	−17.9	−19.3	5.1	0.6	−0.6	−14.2
	SOPPA(MP2)	0.5	−0.7	−0.9	−27.8	−28.9	5.1	0.6	−0.6	−23.8
	SOPPA(CC2)	0.5	−0.6	−0.9	−28.1	−29.1	5.1	0.6	−0.6	−24.0
	SOPPA(CCSD)	0.5	−0.7	−0.9	−26.3	−27.4	5.1	0.6	−0.6	−22.3
	Experiment	−0.4	−1.2	−20.4	−21.5	5.1	0.6	−0.6	−16.4	−20.2

and DFT levels together with relativistic, solvent, and vibrational corrections in comparison with the experimental results are compiled in Table 18. For both couplings, $^{2}J_{Te,H}$ and $^{3}J_{Te,H}$, the Fermi contact contribution dominated over the noncontact terms. However, for the vicinal coupling constant $^{3}J_{Te,H}$, the overall contribution of the noncontact terms was almost negligible, while for the geminal coupling constant $^{2}J_{Te,H}$, the contribution of the paramagnetic spin–orbit term was approximately 11 Hz (at the SOPPA level) or even 14 Hz (at the DFT level), which was essentially more than 10% of its total value, thus being far from negligible. ZPVE and PCM corrections (accordingly, ΔJ_{vib} and ΔJ_{solv}) were of minor importance for both $^{2}J_{Te,H}$ and $^{3}J_{Te,H}$ couplings, while scalar relativistic effects (ΔJ_{rel}) contributed to the calculated values of these couplings of up to *ca.* −18 and +5 Hz, respectively, which totaled 17 and 23% of their nonrelativistic values. This meant that taking into account relativistic corrections essentially worsened the DFT results and dramatically improved the performance of the SOPPA methods; the latter results were in very good agreement with the experimental results.

According to the NBO analysis performed in that study,[75] the tellurium atom possessed two different lone pairs, one of almost pure *p*-character (*p*-type), and another one providing a considerable amount of *s*-character (*σ*-type), the latter being in the orthogonal position to the former. Figure 19 shows the naturally localized molecular orbitals describing lone pairs of both types in tellurophene and divinyl telluride. It was found that the lone pair of a *σ*-type provided the so-called *orientational lone pair effect* upon the values of ^{125}Te–^{1}H coupling constants.

Finally, the authors of that publication [75] calculated the dihedral angle dependences of geminal and vicinal ^{125}Te–^{1}H couplings, $^{2}J_{Te,H}$ and $^{3}J_{Te,H}$, in divinyl telluride with respect to the internal rotation around the Te–C bond, as shown in Figure 20. The negative geminal coupling, $^{2}J_{Te,HX}$, provided the most striking beheviour decreasing (increasing in absolute value) by more than 100 Hz (!) on going from the *s-trans* ($\varphi = 0^{\circ}$) to the *s-cis* ($\varphi = 180^{\circ}$) arrangement of the vinyl group rotating around the Te–C bond, which corresponded to accordingly, *transoidal* and *cisoidal* orientations of the tellurium lone pair towards the geminal ^{125}Te–^{1}H coupling pathway.

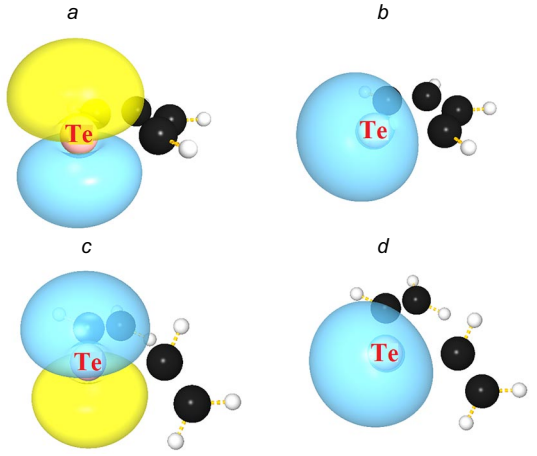


Figure 19. The tellurium lone pairs of accordingly *p*- (*a*, *c*) and *σ*- (*b*, *d*) types in tellurophene, as follows from the NBO analysis. Reproduced with minor editing privilege from Rusakov *et al.*[75] with the permission of *The Royal Society of Chemistry*.

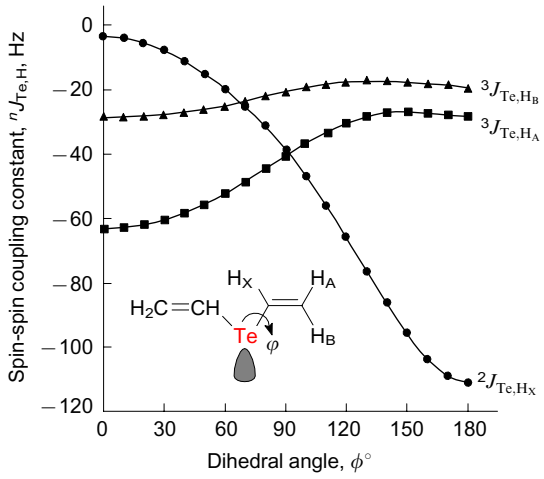


Figure 20. Dihedral angle dependences of $^{2}J_{Te,H}$ and $^{3}J_{Te,H}$ coupling constants in divinyl telluride calculated at the SOPPA (CCSD) level. The value of $\varphi = 0^{\circ}$ is assigned to the *s-trans* orientation of the vinyl group rotating around the Te–C bond. Reproduced with minor editing privilege from Rusakov *et al.*[75] with the permission of *The Royal Society of Chemistry*.

Thus, a marked stereospecificity of geminal and vicinal ^{125}Te–^{1}H spin–spin coupling constants originating in the orientational lone pair effect of tellurium was found in that study,[75] which was reestablished later for a representative set of organotellurium compounds,[78] providing a new guide in stereochemical studies of organic derivatives of tellurium.

One of the referees suggested giving some general notes on the nature of the lone pair effect. Herewith, we will not go far into this issue in view of the fact that the topic of the present review deals with the computational NMR of heavy nuclei rather than intermolecular interactions and lone pair effects in particular. In general, the origin of the latter consists of the orbital interaction of the heteroatom lone pair with the bonding molecular orbitals of the adjacent carbon–hydrogen and/or carbon–carbon bonds, resulting in a marked shielding of the adjacent proton and/or carbon in *cis*-orientation to the lone pair and, as a result, in the increase of the adjacent carbon–hydrogen and/or carbon–carbon spin–spin coupling constant.[79] In the original publications, we observed this effect for lone nitrogen pairs, and from the data of the present review, we see that these effects are also manifested by lone pairs of heavy atoms, exemplified here for tellurium.

Recently Rusakova *et al.*[80] performed a high-level calculation of the one-bond tellurium–carbon spin–spin coupling constants, $^{1}J_{Te,C}$, in a series of four classical organotellurium compounds, $Te(CH_3)_2$, $Te(CF_3)_2$, $Te(C{\equiv}CH)_2$, and tellurophene, with scrutiny relativistic effects, vibrational corrections, and solvent effects. All calculations of $^{1}J_{Te,C}$ were performed using different locally dense basis set schemes implying Dyall's dyall.xv3z (x = a, c, ac, none) basis sets on tellurium and Sauers's triple zeta aug-cc-pVTZ-J on α-carbons (*i.e.* those coupled with tellurium) together with Dunningig's cc-pVDZ basis sets for the rest of the atoms. The vibrational corrections and solvent effects were calculated at the nonrelativistic DFT-PBE0 and RPA levels of theory. The results of the calculations at different levels of theory and with different basis sets performed in that study are exemplified for $Te(CH_3)_2$ and tellurophene in Table 19.

Table 19. One-bond spin – spin coupling constants $^{125}Te-{}^{1}H$ and $^{1}J_{Te,C}$ (Hz) of the representative organotellurium compounds calculated using different basis sets at the DFT-PBE0 and RPA levels, including relativistic (ΔJ_{rel}), solvent (ΔJ_{solv}), and vibrational (ΔJ_{vib}) corrections (Hz), to their total values (TO). Compiled from Rusakova *et al.*[75]

Compound	Basis set (Te)	SOPPA(MP2)	DFT-PBE0				RPA				Experiment
			ΔJ_{rel}	ΔJ_{solv}	ΔJ_{vib}	TO [a]	ΔJ_{rel}	ΔJ_{solv}	ΔJ_{vib}	TO [a]	
$Te(CH_3)_2$	av3z-J	73.3	70.6	−6.6	9.5	146.8	142.8	−15.8	11.4	211.7	158.0
	dyall.v3z	73.7	70.5	−6.5	9.5	147.2	142.2	−15.3	11.4	212.0	
	dyall.av3z	73.5	70.6	−6.6	9.5	147.0	142.8	−15.8	11.4	211.9	
	dyall.cv3z	112.8	69.6	−6.3	9.5	185.6	140.3	−14.9	10.9	249.1	
	dyall.acv3z	112.2	69.8	−6.4	9.5	185.1	140.7	−15.4	10.9	248.3	
Tellurophene	av3z−J	159.6	137.3	−2.1	10.8	305.6	181.2	−8.6	13.0	345.2	302.4
	dyall.v3z	159.1	137.1	−1.8	10.8	305.1	180.1	−7.3	13.0	344.9	
	dyall.av3z	159.7	137.3	−2.1	10.8	305.6	181.2	−8.6	13.0	345.3	
	dyall.cv3z	204.4	136.0	−1.8	12.8	351.5	177.8	−7.1	12.8	387.9	
	dyall.acv3z	204.7	136.3	−2.0	12.8	351.7	192.2	−8.3	12.8	401.4	

[a] Evaluated as SOPPA(MP2) + ΔJ_{rel} + ΔJ_{solv} + ΔJ_{vib} .

The usage of Dyall's core-valence correlation-consistent and all-electron core-valence correlation-consistent basis sets of triple-zeta quality, dyall.cv3z and dyall.acv3z, dramatically increased the value of calculated $^{1}J_{Te,C}$ at the SOPPA(MP2) level. We associate this fact with the unpredictable influence of the 'all-electron' functions in the general contraction scheme of the dyall.acv3z basis set.

It followed that relativistic corrections played a major role in the calculation of $^{1}J_{Te,C}$, reaching as much as almost 50% of their total values, while solvent and vibrational corrections were found to be much less significant, being accordingly up to 4 and 6%, respectively (Fig. 21). Taking into account all types of corrections essentially improved the agreement of the nonrelativistic SOPPA(MP2) results with the experiment demonstrating the importance mainly of the relativistic corrections and, to a much less extent, the solvent and vibrational corrections in the calculations of the one-bond spin – spin coupling constants involving tellurium and carbon. The overall accuracy of the hybrid scheme 'SOPPA(MP2) + DFT corrections' with the av3z-J basis set on tellurium, aug-cc-pVTZ-J basis set on α-carbon and cc-pVDZ basis sets on the rest of atoms and using the non-relativistic MP2 optimized geometries was found to be sufficiently high giving the MAPE of as much as 5.7% with respect to experimental data.

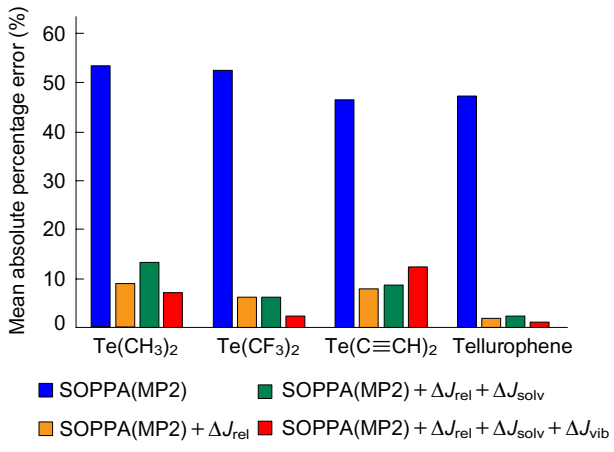


Figure 21. Contribution of relativistic, solvent, and vibrational effects to the mean absolute percentage error of calculation of the one-bond $^{125}Te-{}^{13}C$ spin – spin coupling constants. Reproduced with minor editing privilege from Rusakova *et al.*[80] with the permission of *John Wiley and Sons*.

Rusakov and Rusakova[81] developed a family of tellurium basis sets, acvXz-J (X = 2, 3, and 4), for the calculation of indirect nuclear spin – spin coupling constants involving the tellurium nucleus. In those basis sets, the saturation of angular spaces was performed in an even-tempered manner until achieving the convergence of tellurium spin – spin coupling constants under consideration. Saturated basis sets were contracted by approximately 30% using the coefficients obtained from the atomic self-consistent field closed shell calculations of tellurium anion, Te^{2-}. The saturation of basis sets was studied on spin – spin coupling constants $^{125}Te-{}^{1}H$ and $^{125}Te-{}^{13}C$, calculated within the SOPPA(CCSD) and CCSD methods by taking into account relativistic effects, solvent effects, and vibrational corrections.

Relativistic corrections (ΔJ_{rel}) were evaluated as the differences between coupling constants obtained using relativistic four-component Dirac – Kohn – Sham Hamiltonian and those of the so-called '10c limit scheme'. This scheme implied an increase in the speed of light by 10 times in the relativistic four-component calculations (which is common for the relativistic calculations of the second-order molecular properties), resulting in a sufficiently accurate approximation of the relativistic property values.

Shown in Table 20 are the calculated spin – spin coupling constants involving different carbons and hydrogens of TeH_2, $Te(CH_3)_2$, and tellurophene. All four-component calculations were performed at the DFT level using the local density approximation (LDA) functional implying the unrestricted kinetic balance scheme. Solvent effects (ΔJ_{solv}) were evaluated as the differences between their values obtained in gas and liquid phases at the DFT level, implying the exchange correlation functional LDA. Vibrational corrections (ΔJ_{vib}) were calculated at the SOPPA(MP2) level at zero temperature.

The developed basis set acvXz-J showed high accuracy in the calculation of $^{n}J_{Te,H}$ and $^{n}J_{Te,C}$ (n = 1, 2, and 3) in the series of TeH_2, $TeMe_2$, and tellurophene, as illustrated in Table 20.

In continuation of the abovementioned studies, very recently, Rusakov and Rusakova[82] reported the results of the high-level calculations of the one-bond $^{125}Te-{}^{31}P$

Table 20. Spin–spin coupling constants $^{n}J_{Te,H}$ and $^{n}J_{Te,C}$ (n = 1, 2, and 3), Hz, in the series of TeH_2, $Te(CH_3)_2$, and tellurophene calculated at the CCSD level with the acv3z-J basis set taking into account relativistic effects (ΔJ_{rel}), solvent effects (ΔJ_{solv}), and vibrational corrections (ΔJ_{vib}), Hz, compared to the experiment. Compiled from Rusakov and Rusakova.[81]

Compound	Coupling constant	CCSD	ΔJ_{rel}	ΔJ_{solv}	ΔJ_{vib}	Total	Experiment [a]
TeH_2	$^{1}J_{Te,H}$	−223.7	131.2	−12.6	29.3	−75.8	(−)59.0
$Te(CH_3)_2$	$^{1}J_{Te,C}$	99.5	48.5	−3.8	18.8	163.0	158.0
	$^{2}J_{Te,H}$	−11.6	−5.0	0.9	−1.1	−16.8	(−)21.0
Tellurophene	$^{1}J_{Te,C}$	167.3	107.5	−0.2	10.8	285.4	302.0
	$^{2}J_{Te,C}$	−0.9	6.6	0.8	1.0	7.5	5.3
	$^{2}J_{Te,H}$	−93.7	−18.0	0.2	3.0	−108.5	(−)101.7
	$^{3}J_{Te,H}$	−25.0	1.4	−0.3	−0.3	−24.2	(−)20.2

[a] The sign in parentheses was not experimentally determined.

spin–spin coupling constants in the series of phosphine tellurides evaluated within the composite nonrelativistic scheme based on the correlated SOPPA(CC2) and CCSD methods applied for the nonrelativistic values of $^{1}J_{Te,P}$ and the DFT level for the four-component relativistic corrections. In more detail, the combined 'relativistically corrected' computational scheme derived from the highly correlated *ab initio* SOPPA(CC2) and CCSD methods for the nonrelativistic values and the 4-DFT(KT2) method for relativistic corrections was examined against the 'pure relativistic' 4-DFT(KT2) scheme by comparing the theoretical results of both schemes with experimental data.

The accuracy of the combined and pure schemes was found to be 12 and 8%, respectively, indicating that the 'pure' relativistic 4-DFT scheme performed better. The combined scheme, employing double excitation approaches in the nonrelativistic composite counterpart, provided reasonable accuracy; however, it was advised that one should consider a higher-level configuration space to obtain better results for this particular type of tellurium coupling constant. Four-component relativistic corrections to $^{1}J_{Te,P}$ were calculated in the series of 14 phosphine tellurides, with an average of 18% (Table 21). The calculated $^{1}J_{Te,P}$ together with their relativistic corrections, ΔJ_{rel}, presented in this table, were shown to be strongly dependent on the substituents at phosphorus.

Table 21. Four-component relativistic corrections to $^{1}J_{Te,P}$ coupling constants (Hz) of phosphine tellurides. Compiled from Rusakov and Rusakova.[82]

Compound	J_{rel} (see [a])	J_{nr} (see [b])	ΔJ_{rel} (see [c])	ΔJ_{rel} (%) [d]
$Me_3P{=}Te$	1969.5	1502.9	466.6	24
$Et_3P{=}Te$	1900.0 (1743) [e]	1559.8	340.2	18
$Pr^{i}_3P{=}Te$	1919.3	1536.5	382.8	20
$Bu^{t}_3P{=}Te$	1844.2 (1600)	1535.6	308.6	17
$(H_3Si)_3P{=}Te$	1203.9	1199.4	4.5	0
$(F_3C)_3P{=}Te$	2432.4	2039.4	393.0	16
$(CH_2{=}CH)_3P{=}Te$	2143.1	1674.4	468.7	22
$(HC{\equiv}C)_3P{=}Te$	2247.5	1791.0	456.5	20
$(CH_3CO)_3P{=}Te$	1888.1	1515.6	372.5	20
$(N{\equiv}C)_3P{=}Te$	2439.8	2008.5	431.3	18
$(Me_2N)_3P{=}Te$	2266.0 (2095)	1768.0	498.0	22
$(O_2N)_3P{=}Te$	2624.7	2285.6	339.1	13
$(MeO)_3P{=}Te$	2653.4	2011.7	641.7	24
$F_3P{=}Te$	3443.5	2629.5	814.0	24

[a] Total four-component relativistic value. [b] Total nonrelativistic value. [c] Relativistic contribution. [d] Relative percentage of relativistic contribution. [e] Experimental values are given in parenthesis.

Very few papers deal with the calculation of ^{125}Te NMR parameters in ditellurides, namely, those involving tellurium chemical shifts and tellurium spin–spin coupling constants between two tellurium nuclei, which are expected to contain essential relativistic contributions arising from both Heavy Atom on Heavy Atom (HAHA) and Heavy Atom on Vicinal Heavy Atom (HAVHA) effects.

One of the most recent papers in this area is that by Bortolli *et al.*,[83] which is devoted to the calculation of ^{125}Te NMR chemical shift, δ_{Te}, in classical diphenyl ditelluride, $C_6H_5{-}Te{-}Te{-}C_6H_5$, existing in a mixture of two conformers, known as 'open' (**88a**) and 'closed' (**88b**), named so by an analogy with the open and closed gate, as shown in Figure 22. The performed calculations resulted in shielding constants of 2095.4 and 2390.2 ppm for the open and closed conformations, respectively, calculated in chloroform solvent (taken into account within the COSMO formalism) at the ZORA-OPBE/QZ4Pae level of theory on the ZORA-OPBE/TZ2P geometries. This difference in tellurium shielding constants corresponded to the ^{125}Te NMR chemical shifts of δ_{Te} = 574.8 and 280.0 ppm from $TeMe_2$, indicating that phenyl orientation strongly affected tellurium chemical shifts.

For a comparison with the experimental value of δ_{Te} of diphenyl ditelluride of 420.8 ppm,[84] the authors of the abovementioned paper[83] computed δ_{Te} of 476.8 and 184.5 ppm in accordingly, the open and closed conformer with the Boltzmann averaged value of δ_{Te} being 389.1 ppm.

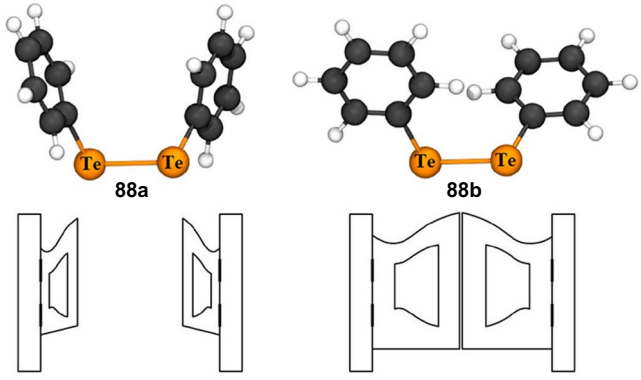


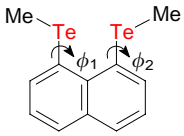
Figure 22. 'Open' (**88a**) and 'closed' (**88b**) conformers of diphenyl ditelluride optimized at the ZORA-OPBE/TZ2P level, corresponding to the 'open' and 'closed' gates. Reproduced with minor editing privilege from Bortolli *et al.*[83] from the open-access journal operating on the Creative Commons Attribution 4.0 International Public License.

Those calculations were performed with the inclusion of spin – orbit coupling at the so-ZORA-OPBE/QZ4Pae//ZORA-OPBE/TZ2P level of theory. In the case of the open and closed conformers, for which the values of the C – Te – Te – C dihedral angle were practically the same, spin – orbit effects were adopted as a constant correction. However, the neat spin – orbit effect was rather large of approximately 100 ppm, and it was explained to be most entirely due to the HAHA effect. Since the molecule of diphenyl ditelluride has two adjacent tellurium atoms, while the reference, $TeMe_2$, possesses only one tellurium, the HAVHA effect on the shielding constant was not cancelled in the calculation of the tellurium chemical shift of the former compound, so that it should be taken into consideration separately. In other words, the HAVHA effect deserves special consideration when calculating the tellurium chemical shifts in this series.

Tellurium – tellurium spin – spin coupling constants separated formally by four chemical bonds but possessing coupled tellurium nuclei in close vicinity to each other and thus containing a noticeable through-space contribution have been thoroughly investigated in two related publications [85, 86] by the same principal authors.

In the first paper,[85] a detailed conformational analysis of 1,8-bis(methyltellanyl)naphthalene (**89**), where two coupled tellurium nuclei are separated by four chemical bonds but spatially are very close, was performed together with the two-dimensional dihedral angle mapping of the corresponding $^4J_{Te,Te}$, as shown in Figure 23. The upper 2D plots represent the potential energy with the minimum labeled *CCt* (see notations in the caption to figure). There is a huge flat area (light yellow) that extends well into what would be classified as *AB* conformation. The second of the 2D plots represents the $J_{Te,Te}$ coupling surface, which looks quite different. Here, a structure with the *CCt* conformation has a $J_{Te,Te}$ value of approximately 2500 Hz, while a structure in the *AB* region lies much lower *ca.* 1500 Hz. From the flatness of the potential energy surface, it follows that this system samples large areas in the conformational space around the minima.

Structure 89



89

The same conclusion was drawn by the authors from the analysis of the tellurium – tellurium coupling pathway in **89** through the inspection of the coupling deformation density shown in Figure 24. The spatial overlap of the tellurium lone pairs was the determining mechanism of the transmission of tellurium – tellurium spin – spin coupling, rather than its ordinary transmission through the framework of four chemical bonds. It was concluded that this should be taken as evidence for the importance of the $LP_{Te} \rightarrow \sigma^*_{TeC}$ orbital interaction in the transmission of tellurium-tellurium coupling.

In a forthcoming paper by the same principal authors,[86] the conformational beheviour of $^{125}Te - ^{125}Te$ spin – spin coupling constants was investigated with a special emphasis on the through-space transmission mechanism in a series of

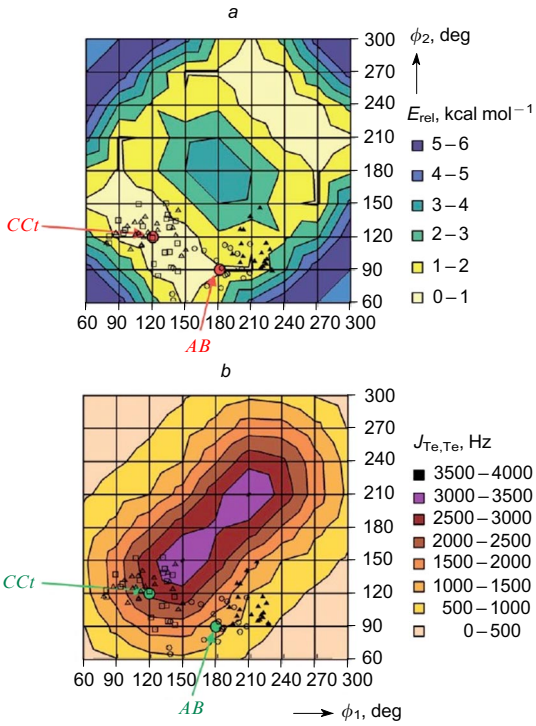


Figure 23. Relative energies (*a*) and $^{125}Te - ^{125}Te$ coupling constants (*b*) in 1,8-bis(methyltellanyl)naphthalene (**89**) as a function of the conformation, as defined by the two specified dihedral angles. **Note.** *CCt* and *AB* represent the following conformations: roughly perpendicular (*A*), in-plane (*B*), or in-between (*C*), both *cis* (*c*) or both *trans* (*t*). Reproduced with minor editing privilege from Bühl *et al.*[85] with the permission of *John Wiley and Sons*.

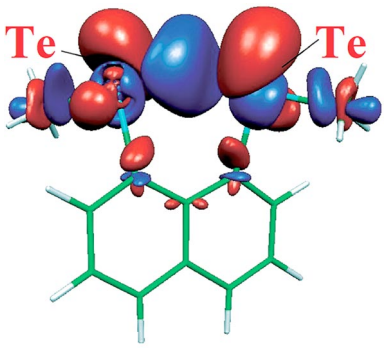
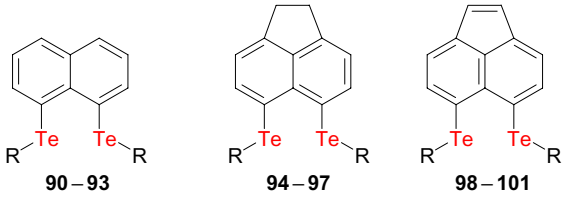


Figure 24. Total tellurium – tellurium coupling deformation density in 1,8-bis(methyltellanyl)-naphthalene (**89**). Reproduced with minor editing privilege from Büh *et al.*[85] with the permission of *John Wiley and Sons*.

Scructures 90 – 101



90 – 93
naphthalene (bis)tellurides

94 – 97
acenaphthalene (bis)tellurides

98 – 101
acenaphthylene (bis)tellurides

R = Ph (**90**, **94**, **98**), Tol (**91**, **95**, **99**), p-An (**92**, **96**, **100**), Mes (**93**, **97**, **101**)

Table 22. Selected interatomic distances (Å) from X-ray crystallography and B3LYP optimizations and ^{125}Te–^{125}Te spin–spin coupling constants (Hz) from the solution-state NMR studies and the so-ZORA-B3LYP computations in the series of naphthalene, acenaphthalene, and acenaphthylene (bis)tellurides. Adapted from Knight *et al.*[86]

Compound	Te–Te interatomic distance		^{125}Te–^{125}Te coupling constant	
	Calculated	X-ray	Calculated	Experiment
90		3.287	2779	2505
91		3.271	3078	2587
92		3.266	3191	2640
93		3.262	3153	3848
94	3.438	3.367	2604	2110
95	3.440	3.329	2699	2147
96	3.448	3.320	2842	2213
97		3.338	2738	3398
98	3.451	3.393	2798	2057
99	3.453	3.353	2879	2166
100	3.466	3.334	2978	
101		3.342	2918	3565

naphthalene, acenaphthalene, and acenaphthylene (bis)tellurides, exemplified with structures **90**–**101** shown below.

Exceptionally large through-space $J_{Te,Te}$ coupling constants (3289–3848 Hz) were observed for the derivatives substituted with bulky mesityl and triisopropylbenzyl groups, indicating that these species adopted a predominant *CCt* conformation (for notations *CCt* and *AB*, see caption to Figure 23). This finding was supported by the performed DFT calculations, providing a computed trend following the experimentally obtained $J_{Te,Te}$ values with a single minima found for each compound in the *CCt* conformation. In contrast, compounds substituted with less bulky aryl groups displayed much lower $J_{Te,Te}$ values of 2050–2676 Hz, which suggested that those compounds were mostly in their *AB* conformers, providing lower couplings. Computed $J_{Te,Te}$ values for naphthalenes **90**–**93** were essentially overestimated, while observed couplings for the remaining set of compounds **94**–**101**, for which both *CCt* and *AB* minima were found, were between the values computed for those conformers (Table 22). This fact was consistent with the previous finding[85] that an equilibrium should exist between the *CCt* and *AB* conformers due to the small difference in their potential energies.

In one of the most recent papers, dos Reis Lino *et al.*[87] calculated ^{125}Te NMR chemical shifts and spin–spin coupling constants involving tellurium using spin–orbit ZORA and four-component Dirac–Kohn–Sham relativistic methods in four recently synthesized tellurium-containing complexes **102**–**105**, as shown in Figure 25. For those complexes, the influence of different conformers, basis sets, functionals and methods to treat relativistic and solvent effects was examined (Table 23).

All NMR parameters of the title complexes were evaluated in the gas phase within the DFT framework at both nonrelativistic and two-component relativistic ZORA levels, the latter including spin–orbit effects (so-ZORA). The calculations of ^{125}Te NMR chemical shifts and indirect spin–spin coupling constants involving tellurium were carried out with the PB86, PBE, B3LYP, and PBE0 exchange-correlation functionals, employing the TZ2P and QZ4P basis sets. The calculation of spin–spin coupling constants was also performed with the TZ2P-J and QZ4P-J basis sets, which were especially designed and optimized for such calculations. The ^{125}Te NMR parameters were also calculated using the four-component DKS relativistic Hamiltonian with the PBE0 exchange correlation functional together with Dyall's relativistic all electron valence triple zeta basis set.

Based on the performed calculations of ^{125}Te NMR chemical shifts and spin–spin coupling constants involving tellurium in the series of **102**–**105**, the authors[87] came to the following basic conclusions:

Functionals and basis sets. The PBE0 functional presented the most negative ^{125}Te NMR chemical shift, while B3LYP resulted in the best agreement with the experimental results. On the other hand, the BP86 and PBE GGA functionals led to the largest chemical shifts. At this the hybrid PBE0 and B3LYP functionals underestimated the experimental data, while the GGA PBE and BP86 overestimated them. Regarding the effect of varying the functional on the calculation of the one-bond spin–spin coupling constants involving tellurium, the PBE functional presented the most

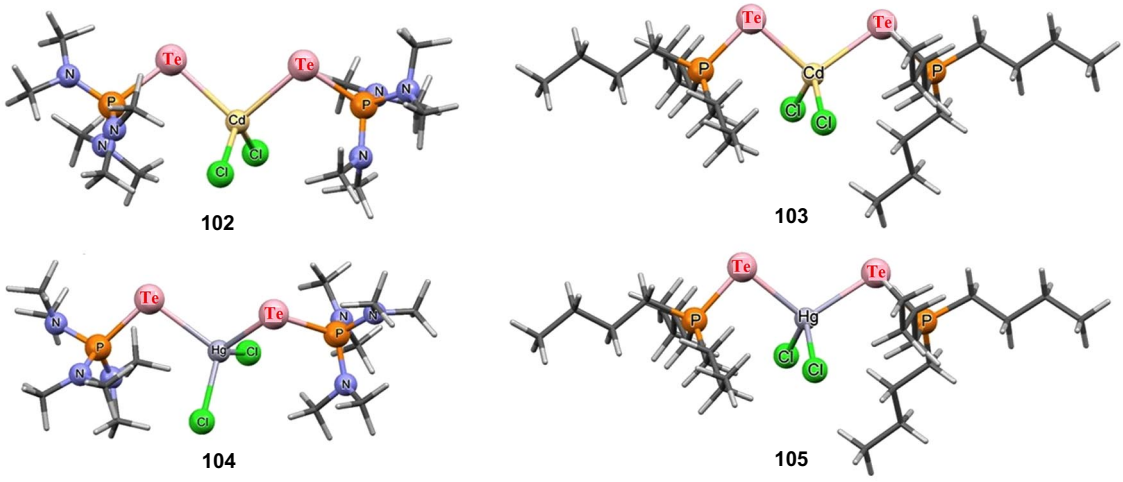


Figure 25. Stereochemical structure of the tellurium-containing cadmium and mercury complexes. Reproduced with minor editing privilege from dos Reis Lino *et al.*[87] with the permission of the *American Chemical Society*.

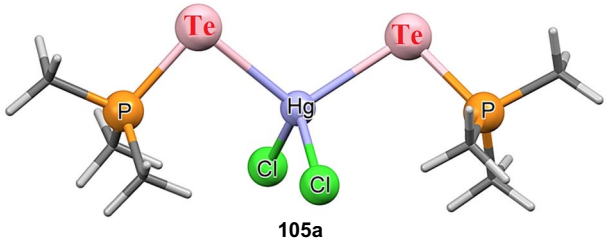
Table 23. ^{125}Te NMR chemical shifts (ppm) and spin–spin coupling constants (Hz) involving tellurium calculated at the so-ZORA level using different functionals and basis sets. Compiled from dos Reis Lino *et al.*[87]

Compound	δ_{Te}				$^1J_{Te,P}$			
	Functional	Basis set	Calculated	Experiment	Functional	Basis set	Calculated	Experiment
102	PBE0	TZ2P	−539	−728	PBE0	TZ2P-J	2041	1617
		QZ4P	−567			QZ4P-J	2021	
103					PBE0	TZ2P	1299	1287
						QZ2P-J	1525	
104	PBE0	TZ2P	−389	−480	PBE0	TZ2P-J	2045	1606
		QZ4P	−413			QZ4P-J	2025	
105	PBE0	TZ2P	−508	−478	PBE0	TZ2P-J	1192	1262
	B3LYP	TZ2P	−485		B3LYP	TZ2P-J	1770	
	PBE	TZ2P	−465		PBE	TZ2P-J	1300	
	BP86	TZ2P	−418		BP86	TZ2P-J	1310	

accurate result. The BP86 and B3LYP functionals also overestimated the experimental data, and the latter yielded the poorest result. Finally, the hybrid PBE0 functional underestimated the $^1J_{Te,P}$ value by only 70 Hz, which was 5.5% of the experimental value. The general result was that in the calculation of ^{125}Te NMR chemical shifts and spin–spin coupling constants involving tellurium, the PBE0 functional exhibited the overall best performance in combination with the TZ2P and QZ4P basis sets for chemical shifts and TZ2P-J and QZ4P-J basis sets for spin–spin coupling constants.

Solvent effects. In general, the addition of solvent effects using the COSMO model in the so-ZORA/PBE0 calculations did not improve the agreement of the performed calculations of complex **105** with experiment, as compared to the gas phase results. The solvent effect correction was found to be 56 ppm for the ^{125}Te NMR chemical shifts, which was approximately twice the difference between the gas phase result and experiment. For the one-bond spin–spin coupling constants involving tellurium, $^1J_{Te,P}$, the solvent effect correction was 209 Hz, but adding the solvent correction resulted in a worse agreement of computational data with experiment.

Relativistic effects. Finally, the performance of the two-component spin–orbit ZORA and four-component DKS relativistic methods in the calculation of ^{125}Te NMR chemical shifts and spin–spin coupling constants involving tellurium was studied on the reduced structure of complex **105** (labelled **105a**), as shown in Figure 26, to evaluate the effect of relativistic effects. In those calculations, the PBE0 functional was used, together with the relativistic triple zeta Dyall's basis set for both chemical shifts and spin–spin coupling constants. The relativistic correction to chemical shift of tellurium in **105a** was found to be 212 ppm at the two-component so-ZORA level and 184 ppm at the four-component DKS level, while relativistic corrections to $^1J_{Te,P}$ coupling constant were accordingly, 125 and 218 Hz.



105a

Figure 26. Reduced structure of complex **105** (labelled **105a**) used for the 4-component DKS calculations. Reproduced with minor editing privilege from dos Reis Lino and co-workers[87] with the permission of the *American Chemical Society*.

In general, the authors of that paper[87] performed a deep study of different accuracy factors involving the influence of different functionals and basis sets, solvent effects, and, most essentially, relativistic effects contributing to tellurium chemical shifts and spin–spin coupling constants. It was demonstrated that the PBE0 functional exhibited the overall best performance in combination with the TZ2P and QZ4P basis sets for chemical shifts and the TZ2P-J and QZ4P-J basis sets for spin–spin coupling constants. Surprisingly, the addition of solvent did not improve the agreement of the performed calculations with the experiment compared to the gas phase results. The relativistic correction to tellurium chemical shifts and spin–spin coupling constants was found to be essential, contributing 212 ppm at the two-component so-ZORA level and 184 ppm at the four-component DKS level, while relativistic corrections to the $^1J_{Te,P}$ coupling constant were accordingly 125 and 218 Hz.

An interesting paper by Rusakov and Rusakova[88] has just appeared dealing with accurate quantum chemical modeling of ^{125}Te NMR spectra in a variety of organotellurium compounds at the DFT level. Excellent accuracy against an experiment was reported, which could be effectively applied for routine calculations of tellurium chemical shifts. The role of solvent, vibrational, and relativistic corrections has been thoroughly investigated. Special attention was focused on the effect of taking into account scalar relativistic effects during geometry optimizations and the calculation of tellurium chemical shifts.

This study was performed in a series of nineteen representative tellurium compounds with ^{125}Te NMR chemical shifts covering a wide range of approximately 3000 ppm. As many as seventy-two combined and nine pure 4c-DFT schemes were examined. An interesting and practically important result was that the B3LYP+SVWN5 computational scheme appeared to be the most accurate when nonrelativistic equilibrium geometries were used.

It was also found that relativistic corrections to tellurium chemical shifts provided a decrease in MAE by approximately 28.9 ppm compared to that evaluated at the nonrelativistic level by taking into account solvent corrections. The latter were shown to play a less important role. Thus, taking into account solvent effects for tellurium

shielding constants resulted in the MAE decrease by approximately 12.4 ppm compared to the nonrelativistic gas phase result. On the other hand, zero-point vibrational corrections were shown to be overall insignificant, and it was not recommended to take them into account unless a very high precision was required.

One more interesting question raised in that study [88] dealt with the influence of the so-called 'relativistic geometry factor', *i.e.* the effect of using relativistically optimized geometry compared to the nonrelativistic geometry in the calculation of tellurium chemical shifts. Thus, despite what might have been expected, taking into account scalar relativistic effects during geometry optimization resulted in a noticeable effect on the overall accuracy of calculation. Namely, the decrease in MAE, evaluated for the relativistic four-component model, resulted in an 8.7 ppm effect, which was approximately two-thirds of that due to solvent effects.

Sauer and co-workers published in 2020 a number of papers (see, for example, references [89–93]) dealing with the noniterative corrections to the random phase and higher random phase approximations for the singlet and triplet excitation energies and related items that could also be applied to heavy nuclei. Herewith, we will not go into much detail of this pure theoretical material forwarding reader to the original publications.

2.6. ^{195}Pt NMR

We start this section with a brief historical introduction of the pioneering papers by Autschbach and co-workers [94–99] of the beginning of the century dealing with the calculation of different types of spin–spin coupling constants involving platinum in platinum complexes, namely those of platinum–carbon,[96,98] platinum–phosphorus,[94,95] platinum–platinum,[97,98] and platinum–thallium.[94,99] The basic conclusion derived from those early studies was that at the two-component ZORA level, used to compute those coupling constant, the scalar and/or spin–orbit mechanisms together with solvent effects, evaluated mostly at the COSMO level, were of prime importance. These findings were derived from the ZORA calculations of $^{n}J_{Pt,X}$ (X = C, P, Pt, and Tl) in a number of platinum complexes.

A decade later, Krykunov, Ziegler, and van Lenthe [100] applied the so-ZORA formalism for the calculation of ^{195}Pt NMR chemical shifts of Pt(II) square-planar complexes presented in Table 24. Those calculations were performed using the ZORA Hamiltonian with spin–orbit coupling and polarized valence triple (TZP) and/or doubly polarized valence triple (TZ2P) basis sets in combination with the B3LYP, BP86, and BLYP functionals.

The results of the performed calculations with pure functionals, as well as with a hybrid B3LYP, were found to be in good agreement with the experimental trends. As an example, the ^{195}Pt NMR chemical shifts of PtX_2L_2 (where X is Cl, Br, or I) became more negative in the row from Cl to I for each L (where L is SMe_2, NH_3, PMe_3, or $AsMe_3$). Additionally, the chemical shifts of the $PtX_2(NH_3)_2$ compounds were more positive than those of $PtX_2(PMe_3)_2$ or $PtX_2(AsMe_3)_2$. The B3LYP functional yielded better agreement with the experimental results than BP86 and BLYP. Thus, the comparison of the RMSD value for B3LYP (265 ppm) against the BLYP (298 ppm) and BP86 (323 ppm) values showed that the B3LYP chemical shifts agreed better with the experiment than those evaluated with the BLYP and BP86 functionals. The general conclusion of the performed study [100] was that application of the hybrid B3LYP functional yielded smaller deviations of calculated

Table 24. ^{195}Pt NMR chemical shifts (ppm) of the Pt(II) square-planar complexes calculated at the so-ZORA/TZP level compared to the experiment. Compiled from Krykunov, Ziegler, and van Lenthe.[100]

Compound	BP86		BLYP		B3LYP		Experiment
	so-ZORA	Total	so-ZORA	Total	so-ZORA	Total	
cis-$PtCl_2(SMe_2)_2$	0	0	0	0	0	0	0
trans-$PtCl_2(SMe_2)_2$	−327.4	614.7	−335.1	633.7	−296.5	759.4	127
cis-$PtBr_2(SMe_2)_2$	−137.4	−352.4	−135.4	−360.5	−123.7	−388.4	−328
trans-$PtBr_2(SMe_2)_2$	−520.3	16.5	−528.9	19.4	−469.6	129.7	−348
cis-$PtI_2(SMe_2)_2$	−366.4	−932.7	−353.9	−949.7	−333.6	−1048.7	
trans-$PtI_2(SMe_2)_2$	−936.0	−1112.9	−946.7	−1147.2	−857.4	−1068.1	−1601
cis-$PtCl_2(NH_3)_2$	−315.7	1283.7	−333.5	1420.0	−313.6	1535.8	1447
trans-$PtCl_2(NH_3)_2$	−231.4	1202.6	−246.4	1288.6	−221.7	1526.4	1450
cis-$PtBr_2(NH_3)_2$	−463.4	802.5	−476.1	925.9	−444.3	1031.4	1092
trans-$PtBr_2(NH_3)_2$	−358.9	676.6	−367.0	753.1	−315.5	1000.9	
cis-$PtI_2(NH_3)_2$	−746.6	−137.2	−735.9	−44.9	−692.8	20.5	283
trans-$PtI_2(NH_3)_2$	−664.8	−313.7	−659.6	−266.1	−583.7	−27.2	
cis-$PtCl_2(PMe_3)_2$	51.5	−362.2	63.5	−383.3	93.0	−598.2	−857
trans-$PtCl_2(PMe_3)_2$	10.3	−202.9	19.9	−187.5	−6.2	−297.1	−399
cis-$PtBr_2(PMe_3)_2$	−63.1	−582.3	−62.4	−618.9	−28.3	−869.1	−1085
trans-$PtBr_2(PMe_3)_2$	−159.7	−749.7	−154.0	−743.9	−129.4	−837.3	−922
cis-$PtI_2(PMe_3)_2$	−231.3	−911.8	−247.3	−975.0	−203.9	−1256.3	−1037
trans-$PtI_2(PMe_3)_2$	−474.7	−1700.2	−479.4	−1730.0	−389.7	−1816.4	−1988
cis-$PtCl_2(AsMe_3)_2$	−66.5	−392.2	−57.9	−404.7	−18.2	−554.9	−740
trans-$PtCl_2(AsMe_3)_2$	−58.7	−120.3	−50.5	−93.5	−59.5	−131.5	−229
cis-$PtBr_2(AsMe_3)_2$	−208.9	−686.6	−204.0	−709.0	−151.0	−878.6	−1074
trans-$PtBr_2(AsMe_3)_2$	−227.3	−684.7	−223.0	−666.0	−191.2	−705.1	−827
cis-$PtI_2(AsMe_3)_2$	−442.5	−1166.6	−448.0	−1214.2	−385.6	−1421.7	
trans-$PtI_2(AsMe_3)_2$	−543.2	−1721.3	−548.5	−1736.6	−462.6	−1795.3	−1967
RMSD, ppm		323		298		265	

^{195}Pt NMR chemical shifts from experiment in that series, compared to the pure BLYP and BP86 values. This occurred because for the majority of studied Pt(II) square complexes, the local density functionals (BLYP and BP86) underestimated in absolute value experimental ^{195}Pt NMR chemical shifts.

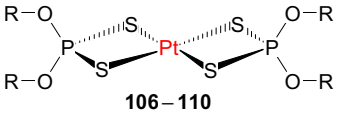
In continuation of earlier experimental studies,[101–105] Roukala *et al.*[106] performed a solid-state experimental and computational investigation of ^{195}Pt NMR chemical shifts and ^{195}Pt – ^{31}P spin – spin coupling constants in a series of bis(dialkyldithiophosphato)Pt(II) complexes **106** – **110**. The measured anisotropic platinum chemical shifts afforded more detailed chemical and structural information than the isotropic ^{195}Pt NMR chemical shifts and ^{195}Pt – ^{31}P spin – spin coupling constants. Advanced theoretical modeling at the DFT level, including both crystal lattice and the important relativistic spin – orbit effects, qualitatively reproduced the measured chemical shift tensors, supported the experimental analysis, and provided extensive stereochemical information. A particular correction model for the nonnegligible lattice effects was adopted, allowing one to avoid a severe deterioration of the ^{195}Pt NMR anisotropic parameters due to the high requirements posed on the pseudopotential quality in such calculations.

Table 25 shows the characteristic isotropic ^{195}Pt NMR chemical shifts and ^{195}Pt – ^{31}P spin – spin coupling constants measured and calculated in that study.[106] The calculated isotropic ^{195}Pt NMR shielding constants were found to be nearly equivalent in all compounds, with the spin – orbit coupling term being the dominant. The calculated isotropic ^{195}Pt NMR chemical shifts were in acceptable agreement with the experimental results, especially for compounds **108** and **110**. The ^{195}Pt solid-state NMR asymmetry parameters showed only small variations between complexes **106** – **110**, while the calculated values were slightly larger than their experimental counterparts. These findings favored the idea that the central part of those complexes was more or less invariant to different ligands, and therefore, the platinum shielding tensors were nearly equivalent for platinum complexes with ligands belonging to the same class.

The geminal spin – spin coupling constants $^2J_{Pt,P}$, transmitted *via* the double path coupling mechanism, were found to have a negative sign, with the absolute values in the range of 401 – 428 Hz, which is close to the experimental values varying in the range of 431 – 456 Hz. The differences between complexes **106** – **110** were found to be very small, down to only a few Hertz. The use of a hybrid functional was found to be vital for obtaining $^2J_{Pt,P}$ values that were close to the experimental observations. Thus, the coupling constants calculated with the pure PBE functional were only of about – 250 Hz, so inclusion of the 25% fraction of the exact exchange in PBE0 resulted in a 63 – 78% increase in the magnitude of the calculated coupling constant. The spin – orbit coupling term yielded only negligible corrections (only a few Hz) to the spin – spin coupling constants of that type compared to other coupling contributions. Scalar relativistic effects were found to be much larger, somewhat of about 100 Hz, compared to the nonrelativistic values.

Very recently, ^{195}Pt NMR chemical shifts of simple square-planar platinum complexes, cisplatin (**111**) and transplatin (**112**), together with fourteen derivatives (**113** – **126**), were reported in two recent publications by Semenov *et al.*[107,108] The structures of **111** – **126** were optimized at the DFT/dyall.ae2z level, and their ^{195}Pt NMR chemical shifts were evaluated within nonrelativistic and fully relativistic four-component approaches (Table 26). The most essential result of that study was that relativistic

Structures 106 – 110



106 – 110

R = E (**106**), Pr^i (**107**), Bu^i (**108**), Bu^s (**109**), c-Hex (**110**)

Table 25. Isotropic ^{195}Pt NMR chemical shifts (ppm) and ^{195}Pt – ^{31}P spin – spin coupling constants (Hz) in the series of bis(dialkyldithiophosphato)Pt(II) complexes. Compiled from Roukala *et al.*[106]

Compound [a]	^{195}Pt NMR chemical shift		^{195}Pt – ^{31}P coupling constant	
	Calculated [b,c]	Experiment [c]	Calculated [b]	Experiment [d]
106	0.0	0.0	– 428	(–)444.4
107	70.9	28.0	– 401	(–)431.1
108 (*A*)	6.3	0.3	– 410	(–)443.2
108 (*B*)	– 14.2		– 416	
109 (*A*)	38.2	140.0	– 407	*ca.* (–)456
109 (*B*)	67.6		– 403	
110	61.7	66.4	– 411	(–)433.2

[a] *A* or *B* refer to the two different conformations of the same complex in the crystallographic unit cell. [b] Calculated at the so-ZORA level of theory using the PBE0 hybrid functional. [c] All chemical shifts are reported relative to the complex with the largest absolute experimental chemical shift. [d] The sign in parentheses was not experimentally determined.

Structures 111 – 126

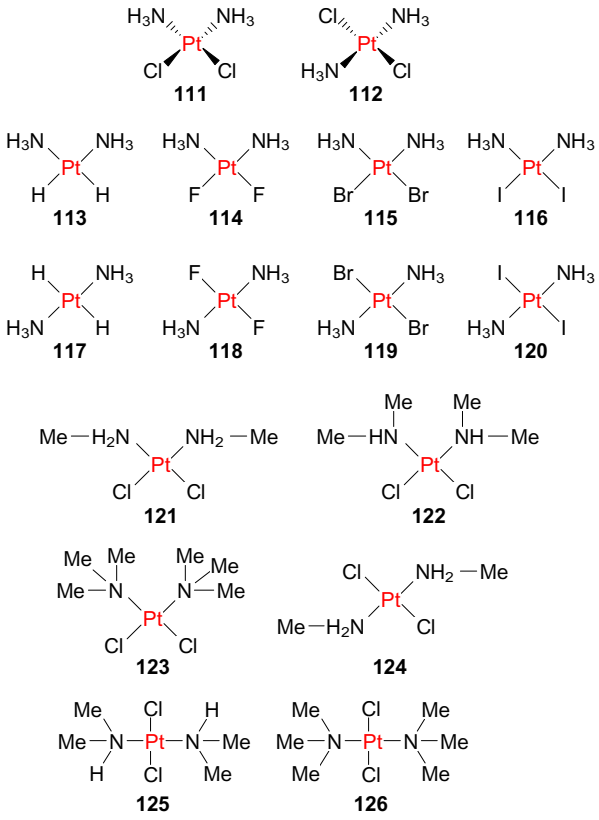


Table 26. ^{195}Pt NMR chemical shifts (ppm) of platinum complexes **111**–**126** calculated at the four-component relativistic level with the KT2 functional and dyall.ae2z basis set on all atoms. Compiled from Semenov *et al.*[108]

Compound	Nonrelativistic chemical shift, δ_{nr}	Relativistic chemical shift, δ_{rel}	Relativistic contribution, $\Delta\delta_{rel}$	$\Delta\delta_{rel}$ (%)
111	−1517.1	−2043.7 (−2101.0) [a]	−526.6	25.7
112	−1658.7	−2155.4 (−2104.0)	−496.7	23.0
113	−3315.3	−3459.5	−144.2	4.2
114	20.5	−898.5	−919.0	102.2
115	−1900.4	−2438.9	−538.5	22.1
116	−2703.5	−3462.3	−758.8	21.9
117	−2066.7	−2915.5	−848.8	29.1
118	1937.2	−1100.8	−3038.0	275.9
119	−2034.7	−2626.5	−591.8	22.5
120	−2846.5	−3812.8	−966.3	25.3
121	−791.6	−2736.8	−1945.2	71.1
122	−799.3	−2852.1	−2052.8	72.0
123	−620.1	−2197.6	−1577.5	71.8
124	−865.3	−2468.8	−1603.5	64.9
125	−1037.9	−2554.0	−1516.1	59.4
126	−874.3	−2360.3	−1486.0	63.0

[a] Experimental values are given in parenthesis.

corrections to ^{195}Pt NMR chemical shifts were found to be very important, being on average as much as approximately 1500–2000 parts per million or 20–70% from their total relativistic values. Indeed, those results provided an unambiguous indication of marked relativistic effects in the ^{195}Pt NMR chemical shifts in the square-planar platinum complexes.

Another interesting aspect raised in the former publication[108] dealt with the solvent effects on the ^{195}Pt NMR chemical shifts of the square-planar Pt(II) complexes exemplified with structures **111**–**126**. A noticeable improvement with the experiment was gained by using the supermolecular solvation model considering two solvent molecules of water directly added into the calculation space of those species to form solvation complexes in the IEF-PCM medium, as shown in Figure 27.

The results of the performed study[108] of the accuracy factors in the calculation of ^{195}Pt NMR chemical shifts in

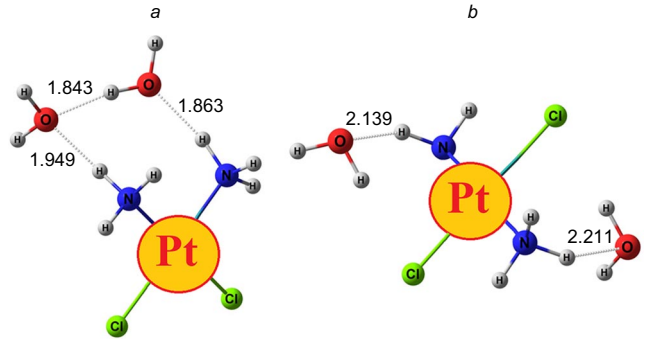


Figure 27. Supermolecular solvation complexes of cisplatin (*b*) and transplatin (*a*) with two molecules of water. Reproduced from Semenov *et al.*[108] with the permission of the *American Chemical Society*.

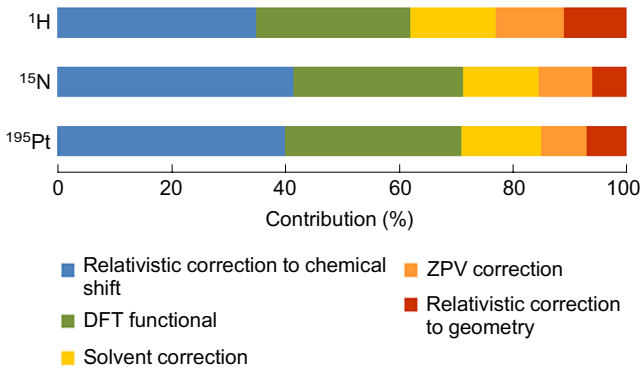


Figure 28. Relative contributions of different accuracy factors to the calculated ^{195}Pt NMR chemical shifts of the derivatives of cisplatin and transplatin. Reproduced from Semenov *et al.*[108] with the permission of the *American Chemical Society*.

the series of **111**–**126** involving relativistic effects, geometrical factors, functionals and basis sets, solvent effects, and vibrational corrections are generalized in Figure 28. The most essential accuracy factor in the calculation of the ^{195}Pt NMR chemical shifts of the square-planar Pt(II) complexes was a relativistic correction amounting to as much as *ca.* 40% of the total value, while relativistic correction to geometry was only 5–10% being the most insignificant factor. As usual, one of the most critical accuracy factors of the performed DFT calculations was a proper choice of a functional. For the studied series of compounds **111**–**126**, it amounted to approximately 30% of the total values of the ^{195}Pt NMR chemical shift and was indeed one of the most essential accuracy factors. Solvent effects and ZPVE corrections were found to be much less significant, being, accordingly, approximately 15 and 10%, respectively.

The most general conclusions derived from the performed calculation of the ^{195}Pt NMR chemical shifts of cisplatin and transplatin and derivatives at the four-component relativistic level[107, 108] were as follows:

(a) Calculation of platinum chemical shifts in the nonrelativistic approximation did not allow the authors to reach any practical results with any of the examined functionals because no relativistic effects amounting to as much as *ca.* 40% of the total value was taken into account at this level;

(b) Accounting for those effects at the stage of geometry optimization, as well as correcting the resulting equilibrium geometry with ZPVE and solvent corrections, resulted in a rather small increase in the accuracy of calculation;

(c) Essential improvement in accuracy could be achieved when relativistic effects are taken into account at the four-component relativistic level;

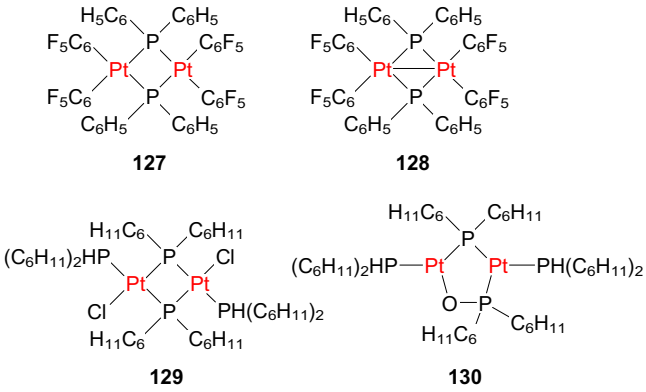
(d) Large uncertainty dealt with a proper choice of the DFT functional, which is an unavoidable source of errors in any of the DFT calculations.

Recent calculations of various accuracy factors involving stereoelectronic, solvent, and relativistic effects in the series of square-planar 4*d* and 5*d* transition metal complexes, performed by Marek and co-workers[109–111] and Kaupp *et al.*,[112] revealed a number of interesting effects in platinum complexes. According to the results of the molecular orbital analysis of cisplatin and related square-planar Pt(II) complexes performed in those studies, there was an

essential σ-donation from the occupied ligand's HOMO to the Pt(II) LUMO together with a π-back-donation process from the occupied metal *d*-orbitals to the antibonding orbitals of ligands. The former process decreased the electron density on ligands and increased it on platinum, while the latter reduced the electron density on platinum and increased it on ligands. This was because the values of the ^{195}Pt NMR chemical shift were extremely sensitive to the electronic nature of the ligands. Indeed, calculation of ^{195}Pt NMR chemical shifts of the square-planar Pt(II) complexes while taking into account relativistic effects represented a challenging effort and was of the utmost theoretical importance.

As a part of a detailed study on phosphanido bridged platinum complexes,[113–121] in two related papers by Mastrorilli *et al.*[122] and Todisco *et al.*[123] the ^{195}Pt NMR chemical shifts were reported for the structurally related complexes, $(n\text{-}Bu_4N)_2[(C_6F_5)_2Pt(\mu\text{-}PPh_2)_2Pt(C_6F_5)_2]$ (**127**), $[(C_6F_5)_2Pt(\mu\text{-}PPh_2)_2Pt(C_6F_5)_2]$ (*Pt – Pt*) (**128**), *anti*-[(PHCy)ClPt(μ-PCy_2)$_2$Pt[(PHCy)Cl] (**129**), and [$(PHCy_2)$Pt(μ-PCy_2)(κ^2*P*,*O*-μ-$POCy_2$)Pt($PHCy_2$)] (*Pt – Pt*) (**130**)

Structures 127 – 130



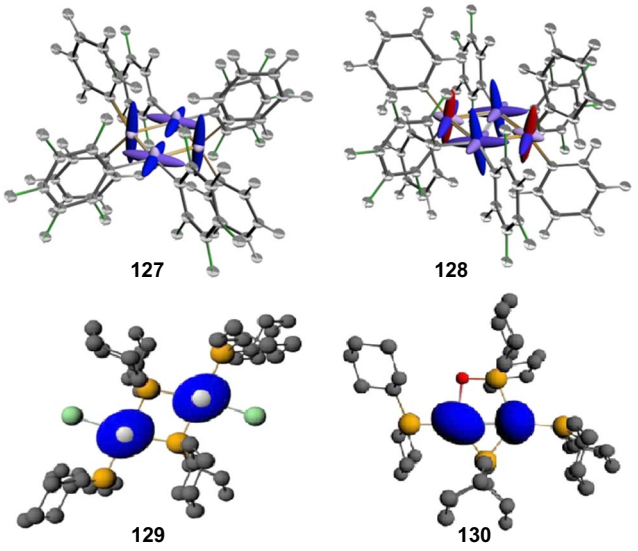


Figure 29. Orientation of the shielding tensors of the ^{195}Pt nucleus (shown in blue) of compounds **127** – **130**. Reproduced with minor editing privilege from Mastrorilli *et al.*[122] and Todisco *et al.*[123] with the permissions of the American Chemical Society and *The Royal Society of Chemistry*.

Table 27. Isotropic ^{195}Pt NMR chemical shifts, calculated at the so-ZORA-BP86/TZP level, compared to experiment (all values are in ppm). Compiled from Mastrorilli *et al.*[122] and Todisco *et al.*[123]

Compound	Isotropic shielding constant, σ_{iso}	Isotropic chemical shift, δ_{iso}	Experiment
127	4593	−3199	−3795
128	5953	−4561	−5298
129	4914	−3521	−3970
130 (Pt1)	5667	−4275	−4833
130 (Pt2)	5911	−4519	−5188

shown in Figure 29, with the adopted orientation of the principal components of the platinum shielding tensors. Those calculations were performed at the so-ZORA level with the BP86 functional and triple zeta singly and/or doubly polarized Slater basis sets, TZP and/or TZ2P. The calculated isotropic ^{195}Pt NMR chemical shifts of **127** – **130** retrieved from those publications[122,123] are compiled in Table 27. It was found that paramagnetic and spin – orbit terms were the most important contributions to the ^{195}Pt NMR chemical shifts. The calculated isotropic shielding constants of ^{195}Pt were also in good agreement with the experimental values, except for a systematic shift of approximately −500 ppm, which might be ascribed to the ambiguous reference of ^{195}Pt shielding.

2.7. ^{199}Hg NMR

The simplest system studied very recently by means of the four-component relativistic calculation of its ^{199}Hg NMR chemical shifts and ^{199}Hg – ^{1}H spin – spin coupling constants was a molecular complex Hg···H_2O shown in Figure 30, consisting of one atom of mercury and one molecule of water,[124] a classical molecular van der Waals complex of mercury originally studied by Duval and Soep[125] in 1991. In this complex, two hydrogen atoms are not symmetrical: the one which is closer to mercury is labelled H-1, while the other is labelled H-2 (see Figure 30).

Those calculations were performed at the four-component Dirac – Kohn – Sham DFT level with the B3LYP functional used with the upcJ-3 basis set on light atoms and Dyall's triple zeta basis set on mercury. Geometry optimization was performed at the DFT and CCSD levels using the aug-cc-pVTZ basis set on hydrogen and oxygen atoms and the MDF60 effective core potential on mercury.

It was found that the mercury shielding constant at equilibrium geometry was 12 ppm smaller than that in isolated mercury atoms, with spin – orbit effects not playing an important role in that case. The dependencies of the through-space mercury – proton intermolecular spin – spin coupling constants, $J_{Hg,H\text{-}1}$ and $J_{Hg,H\text{-}2}$, on the distance

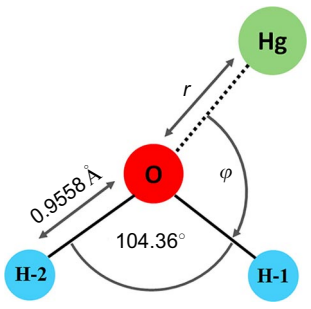


Figure 30. A molecular complex consisting of one atom of mercury and one molecule of water. Reproduced with minor editing privilege from Jakubowska and Pecul[124] with the permission of *Elsevier*.

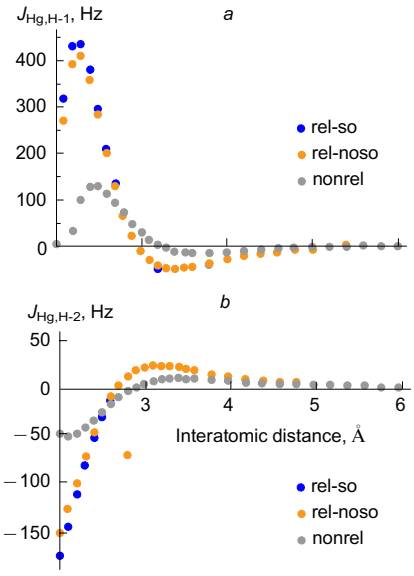


Figure 31. Dependence of spin–spin coupling constants $J_{Hg,H-1}$ (*a*) and $J_{Hg,H-2}$ (*b*) on interatomic distance Hg–O in the molecular complex consisting of one atom of mercury and one molecule of water; noso means not included spin–orbit effects. Reproduced with minor editing privilege from Jakubowska and Pecul [124] with the permission of *Elsevier*.

between oxygen and mercury atoms were found to be not monotonic, as all of them had at least one extremum, as illustrated in Figure 31.

In two related papers [126, 127] Autschbach and coworkers performed a detailed computational study of the mercury–mercury spin–spin coupling constants in $[Hg-Hg]^{2+}$ and $[Hg-Hg-Hg]^{2+}$ dications. The experimental values of those couplings are 284.1 kHz in a complex of $[Hg-Hg]^{2+}$ with crown ether 18-crown-6 reported by Malleier *et al.*[128] in 2001 and 139.7 kHz in the bare $[Hg-Hg-Hg]^{2+}$ ion measured in 1984 by Gillespie *et al.*[129] at −70°C in liquid SO_2. Interestingly, those couplings are the largest known experimentally observed spin–spin coupling constants. All calculations reported by Autschbach *et al.*[126, 127] were performed at the two-component scalar and spin–orbit ZORA levels with the Vosko–Wilk–Nusair local density functional, LDA, together with the gradient-corrected density functional, GGA, in combination with the triple zeta Slater-type basis sets with one polarization function, TZP, and those results are compiled in Table 28.

Both calculated one-bond couplings, $^1J_{Hg,Hg}$ (Hg_2^{2+}) and $^1J_{Hg,Hg}$ (Hg_3^{2+}), in the gas phase were dramatically overestimated compared to the experimental values. However, taking into account the solvent effect by an explicit introduction of solvent molecules (two molecules of crown ether 18-crown-6 in the case of Hg_2^{2+} and four molecules of water in the case of Hg_3^{2+}) into the calculation space brought calculated values of $^1J_{Hg,Hg}$ in almost ideal agreement with the experimental values: 278.4 *vs.* 284.1 kHz for Hg_2^{2+} and 142.3 *vs.* 139.7 kHz for Hg_3^{2+}.

In the second paper,[127] improved calculations were reported by performing geometry optimizations of $[Hg-Hg-Hg]^{2+}$ with up to 10 solvent molecules and/or with two counterions of AsF_6^-. Those calculations using the molecular dynamics simulation of solvent effects indicated that both the one-bond and two-bond $J_{Hg,Hg}$ were very sensitive to the presence of solvent. The final Born–Oppenheimer molecular dynamics simulation averaging resulted in approximately 150 kHz for $^1J_{Hg,Hg}$, which agreed well with the experimental spin–spin coupling of approximately 140 kHz measured in liquid SO_2. On the contrary, computations not considering explicit solvation at the quantum-mechanical level yielded one-bond coupling constants between 230 and 260 kHz, which was very far from the experimental value of 140 kHz.

In continuation of those studies, Bagno and Saielli [130] calculated $^nJ_{Hg,Hg}$ (n = 1, 2, and 3) coupling constants in Hg_4^{2+} dication (**131**) at the so-ZORA/TZ2P level on sc-ZORA/TZP geometry. Those data are compiled in Table 29. Unfortunately, dication appeared to be insufficiently stable in solution to allow for the experimental verification of its calculated $^nJ_{Hg,Hg}$ couplings. It follows that title $^nJ_{Hg,Hg}$ couplings are all positive in the kHz range; moreover, the one-bond couplings are all smaller than the two- and three-bond couplings, with the latter showing the largest total value.

Structure 131

$[Hg\text{-}1—Hg\text{-}2—Hg\text{-}3—Hg\text{-}4]^{2+}$

131

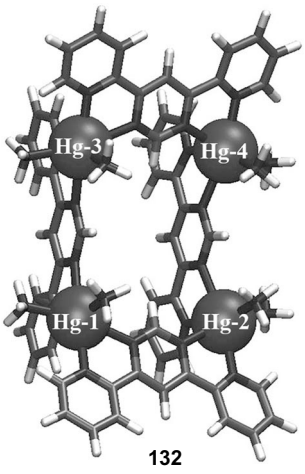
In continuation of the results on mercury–mercury coupling constants of Hg_4^{2+} dication, $^nJ_{Hg,Hg}$ coupling constants were theoretically studied in the so-called 'grid compounds' extensively studied by Lehn and co-workers,[131] which self-assemble to form extended networks containing metal centers (including mercury) at the regular positions of a grid. Thus, the $^nJ_{Hg,Hg}$ coupling constants were computed in the complex depicted in Figure 32, which gave rise to a simple 2 × 2 rectangular grid. The structure of that mercury grid involving as many as 148 atoms was optimized at the BP-ZORA scalar level, with the TZP basis set for mercury atoms and DZP for carbons, nitrogens, and hydrogens. The calculation of $^nJ_{Hg,Hg}$ coupling constants was run on the optimized structure, employing an all-electron basis set TZ2P for mercury and keeping the basis set for the other atoms at the DZP frozen-core level. The scalar ZORA method was used, and the performed calculation was restricted to the DSO, PSO and FC terms only (Table 30). The coupling constant between two ^{199}Hg nuclei across the 'horizontal' side was rather substantial, reaching −36 Hz,

Table 28. Spin–spin coupling constants $^{199}Hg-^{199}Hg$ (kHz) of $[Hg-Hg]^{2+}$ and $[Hg-Hg-Hg]^{2+}$ bare dications calculated at different levels of theory (gas phase) compared to the experiment (complex of $[Hg-Hg]^{2+}$ with crown ether 18-crown-6 in MeOH and complex of $[Hg-Hg-Hg]^{2+}$ with 2 AsF_6^- in liquid SO_2). Compiled from Autschbach *et al.*[126]

Method	$^1J_{Hg,Hg}$ (Hg_2^{2+})	$^1J_{Hg,Hg}$ (Hg_3^{2+})	$^2J_{Hg,Hg}$ (Hg_3^{2+})
sc-ZORA (LDA)	941.5	242.9	464.1
so-ZORA (LDA)	824.8	229.5	397.8
sc-ZORA (GGA)	935.8	241.8	460.4
so-ZORA (GGA)	819.8	241.0	452.6
Experiment	284.1	139.7	

Table 29. Calculated spin–spin coupling constants $^nJ_{Hg,Hg}$ (n = 1, 2, and 3), of the Hg_4^{2+} dication calculated at the so-ZORA/TZ2P level. Compiled from Bagno and Saielli.[130]

Coupling constant	PSO, Hz	FC + SD, kHz	Total, kHz
$^1J_{Hg\text{-}1,\ Hg\text{-}2}$	−1860	34.5	32.7
$^1J_{Hg\text{-}2,Hg\text{-}3}$	−377.1	100.0	99.6
$^2J_{Hg\text{-}1,Hg\text{-}3}$	−0.5	149.0	149.8
$^3J_{Hg\text{-}1,Hg\text{-}4}$	−29.4	178.0	178.0



132

Figure 32. A model Lehn's mercury 'grid compound'. The four mercury atoms define a rectangle with a *ca.* 7 Å side. Reproduced with minor editing privilege from Bagno and Saielli [130] with the permission of *Springer Nature*.

Table 30. Calculated spin – spin coupling constants $J_{Hg,Hg}$ (Hz) in Lehn's mercury 'grid compound' **132** containing four mercury atoms calculated at the so-ZORA/TZ2P level. Compiled from Bagno and Saielli.[130]

Coupling constant	DSO	PSO	FC	Total
$J_{Hg\text{-}1,Hg\text{-}2}$ ('horizontal')	0.06	0.04	−36.4	−36.3
$J_{Hg\text{-}1,Hg\text{-}3}$ ('vertical')	0.01	0.05	−17.9	−17.9
$J_{Hg\text{-}1,Hg\text{-}4}$ ('diagonal')	0.00	0.00	0.1	0.1

while the coupling constant across the 'vertical' side was −18 Hz, and only 0.1 Hz across the 'diagonal' side. The results of the performed study [130] again highlighted the extremely strong through-space spin – spin coupling that mercury nuclei could exhibit even when separated by large distances of up to 7 – 8 Å.

A good number of papers, exemplified by the most illustrative publications,[34, 38, 52, 56, 61, 94, 95, 132 – 136] deal with the two- and four-component relativistic calculations of ^{199}Hg NMR chemical shifts and spin – spin coupling constants involving mercury in simple inorganic compounds such as $HgMe_2$, HgMeCN, $Hg(CN)_2$, HgMeCl, HgMeBr, HgMeI, $HgCl_2$, $HgBr_2$, HgI_2 and related species. Early papers of that kind were well reviewed by Autschbach and Ziegler,[137] so in the present review, we concentrated on the three most illustrative recent examples of those studies reported by Kristkova *et al.*,[61] Gütz *et al.*,[136] and Wodinski *et al.*[34]

In the first paper,[61] a new method for the efficient calculation of indirect nuclear spin – spin coupling constants involving heavy nuclei (such as mercury) by applying the four-component matrix Dirac – Kohn – Sham approach was presented. The procedure of the fitting electron density for evaluations of the matrix elements of the exchange-correlation potential was extended by the authors to a relativistic framework and modified for the evaluation of the matrix elements of the kernel of the exchange-correlation potential. The new method was tested on a representative set of simple molecules exemplified in Table 31 for compounds **133** – **141**.

In the second paper,[136] the one-bond $^1J_{Hg,C}$ spin – spin coupling constants were calculated for $Hg(CH_3)_2$, $Hg(CH_3)Cl$, $Hg(CH_3)Br$, and $Hg(CH_3)I$, solvated with three molecules of dimethyl sulfoxide each, as shown in Figure 33. The authors presented a method for a subsystem-based calculation of indirect nuclear spin – spin coupling

Structures 133 – 141

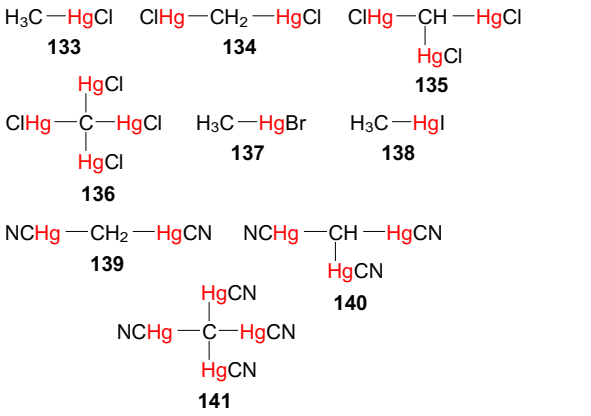


Table 31. Spin – spin coupling constants ^{199}Hg – ^{13}C and ^{199}Hg – 1H (Hz) calculated using the four-component matrix Dirac – Kohn – Sham approach compared to the experiment. Adopted from Křístková *et al.*[61]

Compound	$^1J_{Hg,C}$		$^2J_{Hg,H}$	
	Calculate	Experiment	Calculate	Experiment [a]
133	929	1678	−168	(−)221
134	966	1782	−142	(−)172
135	929	1827	−130	(−)124
136	739	1797		
137	820	1625	−168	(−)213
138	758	1543	−154	(−)180
139	811	1488	−144	(−)157
140	744	1455	−141	(−)127
141	595			

[a] The sign in parentheses was not experimentally determined.

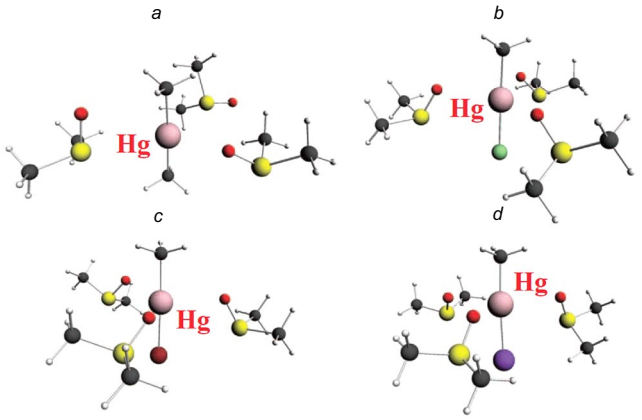


Figure 33. Structures of solvated mercury complexes: (*a*) $Hg(CH_3)_2$ + 3 DMSO, (*b*) $Hg(CH_3)Cl$ + 3 DMSO, (*c*) $Hg(CH_3)Br$ + 3 DMSO, (*d*) $Hg(CH_3)I$ + 3 DMSO. Element colors: mercury — dark pink, hydrogen — gray, carbon — black, oxygen — red, sulfur — yellow, chlorine — green, bromine — brown, iodine — purple. Reproduced with minor editing privilege from Götz *et al.*[136] with the permission of *Elsevier*.

tensors within the framework of the 'current-spin-density-functional theory'. That approach was based on the frozen-density embedding scheme within the DFT framework and extended a previously reported subsystem-based approach

Table 32. Mercury shielding constants (ppm) and spin–spin coupling constants involving mercury (Hz) of mercury di- and tetracyanides calculated at the nonrelativistic and two- and four-component relativistic levels. Compiled from Wodiński *et al.*[34]

Compound	NMR Parameter	NR	sc-ZORA	so-ZORA	4c-DKS [a]	Experiment [b]
$Hg(CN)_2$	σ_{Hg}	7353	7116	9980	12464	
	$^1J_{Hg,C}$	1742	2439	2362	2481	3140
	$^2J_{Hg,N}$	−62.6	−18.4	−37.3	−62.2	(−)101
$Hg(CN)_4^{2-}$	σ_{Hg}	6715	6109	8932		
	$^1J_{Hg,C}$	796	1578	1522		1540
	$^2J_{Hg,N}$	−23.4	−5.2	−5.3		(−)29 ± 2

[a] Calculated with B3LYP functional and dyall.v3z basis set on mercury and aug-cc-pVTZ-J basis set on carbon and nitrogen. [b] The sign in parentheses was not experimentally determined.

for the calculation of NMR shielding tensors to magnetic fields that coupled not only to orbital but also to the spin degrees of freedom. The studied series of methylmercury halides exhibited an exceptionally large shift of the one-bond $^{199}Hg-^{13}C$ spin–spin coupling constants between 233 and 699 Hz upon coordination with three molecules of dimethyl sulfoxide.

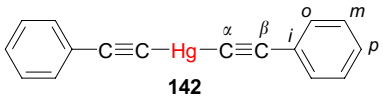
In the third paper,[34] calculations of mercury shielding constants and the one-bond mercury–carbon together with geminal mercury–nitrogen spin–spin coupling constants were performed for $Hg(CN)_2$ and $Hg(CN)_4^{2-}$ at the two- and four-component relativistic levels. The principal results of that study are compiled in Table 32.

From those data, it is seen that the scalar effects on the shielding constants of mercury are on average somewhat smaller than those for the spin–spin coupling constants. The scalar effects work in the opposite direction (leading to deshielding of the mercury nucleus) in comparison to spin–orbit coupling effects, but the latter were shown to be much larger. It was also demonstrated that the choice of a functional had a much smaller effect on the calculated mercury shielding constants than on spin–spin coupling constants involving mercury. The nonhybrid functional BVP86 systematically underestimated the mercury shielding constants calculated using the B3LYP hybrid functional, while PBE0 somewhat overestimated them. The KT2 results were between the BVP86 and B3LYP values. Taking into consideration the four-component DKS calculations, compared to the ZORA results, the ZORA calculation of the mercury shielding constant of $Hg(CN)_2$ led to the overestimation of the four-component DKS result by approximately 17%.

For the spin–spin coupling constants $^1J_{Hg,C}$ and $^2J_{Hg,N}$, relativistic effects evaluated within the sc-ZORA and so-ZORA methods were found to be dominating for $^1J_{Hg,C}$. In contrast, the difference between the scalar and spin–orbit results for $^2J_{Hg,N}$ was very small, but the nonrelativistic result was approximately five times larger than the so-ZORA value. The difference between $^1J_{Hg,C}$ calculated at the four-component level and the closest to experiment ZORA-B3LYP method indicated on the fact that ZORA value was much closer to the experiment. However, for $^2J_{Hg,N,}$ the four-component calculation led to a result closer to the experiment than that of ZORA: −62.2 *vs.* −37.3 Hz, as compared to the experimental coupling of (−)101 Hz.

Regarding organic derivatives of mercury, it should be recalled that some a decade ago, Gryff-Keller *et al.*[138] calculated at the scalar and spin–orbit ZORA-PBE0/TZP levels all $^nJ_{Hg,C}$ ($n = 1-6$) spin–spin coupling constants, both isotropic and anisotropic, of bis(phenylethynyl)mercury (**142**). The isotropic counterparts together with experimental values given in parentheses are presented below.

Structure 142



142

$^1J_{Hg,C-\alpha}$ = 2532 (2692) Hz; $^4J_{Hg,C-o}$ = −30.9 (15.0) Hz;
$^2J_{Hg,C-\beta}$ = 720 (675) Hz; $^5J_{Hg,C-m}$ = 6.1 (nd) Hz;
$^3J_{Hg,C-i}$ = 66.5 (57.5) Hz; $^6J_{Hg,C-p}$ = −7.3 (nd) Hz;
nd means not determinate

The anisotropies of the one-bond $^{199}Hg-^{13}C$ spin–spin coupling constants were determined with the aid of the temperature-dependent ^{13}C NMR spectra of **142** in the liquid–crystal phase. It was found that the performed theoretical calculations reproduced the experimental values of both isotropic and anisotropic NMR coupling constants quite well, especially when taking into account the high solvent sensitivity of those coupling constants.

Some three years earlier, Bryce *et al.*[139] performed scalar and spin–orbit ZORA calculations of $^{199}Hg-^{31}P$ isotropic and anisotropic spin–spin coupling constants in a series of mercury phosphine dimers $[HgP(C_6H_{12})_3(OCOCH_3)_2]_2$ and

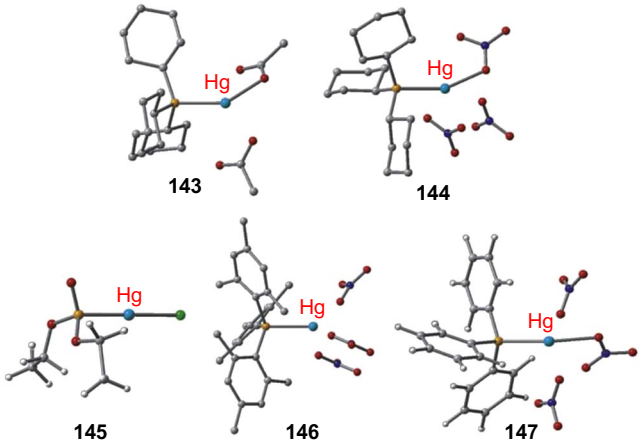


Figure 34. Structures of the models used for the calculations of indirect spin–spin coupling tensors: $[HgPCy_3(OAc)_2]_2$ (**143**); $[HgPCy_3(NO_3)_2]_2$ (**144**); $(EtO)_2P(O)HgCl$ (**145**); $[HgPMes_3(NO_3)_2]_2$ (**146**), and $[HgPPh_3(NO_3)_2]_2$ (**147**). Mercury is shown in indigo, phosphorus — in orange, chlorine in green, oxygen — in red, and carbon — in gray. Hydrogen atoms are omitted for clarity. Reproduced from Bryce *et al.*[139] with the permission of *Elsevier*.

derivatives. In view of the enormous computational expenses, one mercury – phosphorus moiety with the surrounding ligands and counterions was omitted to generate structures **143** – **147**, as shown in Figure 34.

The authors of that study [139] came to the following general conclusions:

(a) The spin – spin coupling tensor was axially symmetric in the systems studied, despite the lack of crystallographic symmetry requirements for this and although the chemical shift tensors for the coupled nuclei were often far from axially symmetric;

(b) The isotropic coupling constants and coupling anisotropies were dominated by the ZORA Fermi-contact-spin-dipolar cross term;

(c) ZORA spin – orbit relativistic corrections to coupling constants and coupling anisotropies were relatively small given the remaining discrepancies between experiment and theory;

(d) The crystal packing effects on computed values of ^{199}Hg-^{31}P isotropic and anisotropic spin – spin coupling constants could be rather substantial.

Turning to the organic derivatives of Hg^{2+} and Hg_2^{2+}, Bagno and Saielli [140] performed sc-ZORA calculations of δ_{Hg} together with $^1J_{Hg,N}$ and $^2J_{Hg,N}$ in mercury thymine adducts **148** and **149**. An interesting result of that study was that coordination of thymine with Hg_2^{2+}, resulting in structure **149**, resulted in $^2J_{Hg,N}$ being larger than $^1J_{Hg,N}$, as shown in Table 33.

Structures 148, 149

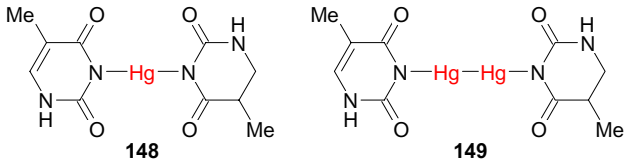


Table 33. Calculated mercury chemical shifts (δ_{Hg}, ppm) and one-bond and geminal mercury – nitrogen spin – spin coupling constants ($^1J_{Hg,N}$ and $^2J_{Hg,N}$, Hz) of the thymine adducts with mercury calculated at the sc-ZORA/TZ2P level. Compiled from Bagno and Saielli.[140]

Compound	δ_{Hg}	$^1J_{Hg,N}$	$^2J_{Hg,N}$
148	−1727	−670	
149	−1189	−159	−415

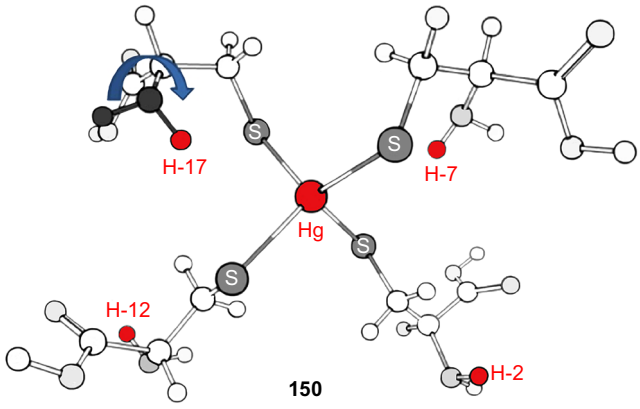


Figure 35. Enumeration of protons in the model system of mercury-substituted rubredoxin. Considered protons coupled to mercury (H-2, H-7, H-12, and H-17) are marked in red. Reproduced with minor editing privilege from Kauch and Pecul [37] with the permission of the *American Chemical Society*.

Kauch and Pecul [37] performed ZORA calculations of the five-bond ^{199}Hg – ^{1}H spin – spin coupling constants in the model system of mercury-substituted rubredoxin (**150**), as shown in Figure 35. In view of the fact that those coupled nuclei are located in close spatial vicinity to each other (being, however, formally separated by five chemical bonds), one should expect that their coupling transmission mechanism involves a considerable through-space contribution.

For geometry optimization, authors used the sc-ZORA Hamiltonian and the revPBE functional (the PBE functional with the revised exchange correction) in combination with the TZP basis set. The calculation of spin – spin coupling constants was carried out at the two-component sc-ZORA and so-ZORA levels. Three different all-electron basis sets (TZP, TZ2P, and QZ4P) were tested. A number of exchange-correlation functionals were chosen to check their beheviour in the calculation of the long-range mercury – proton coupling constants between spatially close nuclei in comparison to the experiment. The results of the performed calculations at the relativistic so-ZORA level are compiled in Table 34.

It was found that the calculated ^{199}Hg – ^{1}H coupling constants matched well with their experimental values, provided that the relativistic effects were taken into account. Indeed, relativistic effects dominated the total values of the mercury – proton coupling constants. The nonrelativistic absolute values were up to one order of magnitude times smaller than the values obtained using relativistic methods. As a whole, relativistic effects were by far dominated by the scalar term. At that time, the inclusion of scalar effects mainly influenced the Fermi contact term, while the paramagnetic term changed very slightly. The importance of the spin – orbit coupling effects depended on the spatial mercury – proton distance. The effects were negligible for the 'long-distance' (more than 4 Å) couplings, but they were substantial when the mercury – proton distance was below 4 Å.

Table 34. Five-bond mercury – proton spin – spin coupling constants (Hz) in the model system of mercury-substituted rubredoxin calculated at the so-ZORA level using different functionals and basis sets. Compiled from Kauch and Pecul.[37]

Functional	Basis set	$^5J_{Hg,H-2}$	$^5J_{Hg,H-7}$	$^5J_{Hg,H-12}$	$^5J_{Hg,H-17}$
revPBE	TZP	−0.59	−1.86	−1.17	−2.44
	TZ2P	−0.56	−2.03	−1.12	−2.70
	QZ4P	−0.56	−3.39	−1.10	−3.97
KT1	TZ2P	−0.72	−1.36	−1.35	−2.24
KT2 + VWN	TZ2P	−0.71	−1.43	−1.35	−2.28
BEE + VWN	TZ2P	−0.67	−1.46	−1.21	−2.24
BVP86	TZ2P	−0.65	−1.55	−1.21	−2.38
PW91	TZ2P	−0.65	−1.55	−1.20	−2.36
B3LYP	TZ2P	−0.86	−1.84	−1.27	−2.53
PBE0	TZ2P	−0.72	−2.00	−1.02	−2.51
Experiment [a]			(−)2.20 ± ± 0.1	(−)0.57 ± ± 0.1	(−)1.90 ± ± 0.2

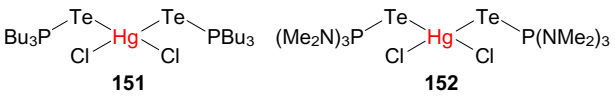
[a] The sign in parentheses was not experimentally determined.

The change in the basis set did not greatly affect the values of the calculated $^{199}Hg-{}^{1}H$ couplings. The extension of the basis set from TZ2P to QZ4P increased their absolute values, moving them further apart from the experiment. Thus, good agreement of the calculated and experimental values for the TZ2P basis set resulted from the so-called 'cancellation of errors', which in general is typical for the DFT calculations of spin–spin coupling constants. In contrast, the addition of polarization functions (when going from TZP to the TZ2P basis set) caused only the next to negligible effect on the calculated coupling constants (less than 5.0%).

In our opinion, despite the importance of the very informative particular results reported by Kauch and Pecul [37] on the model system of mercury-substituted rubredoxin, the absolute values of the calculated (and experimental) formally five-bond mercury–proton coupling constants are too small (*ca.* 1–2 Hz) for deriving any general conclusions.

Very recently, dos Reis Lino *et al.*[87] calculated at the quasirelativistic two-component ZORA-PBE0/TZ2P and fully relativistic four-component 4c-DKS/TZ2P (and/or TZ2P-J) levels mercury chemical shifts (δ_{Hg}) and geminal mercury–phosphorus spin–spin coupling constants ($^{2}J_{Hg,P}$) in two tellurium-containing mercury complexes **151** and **152**. The influence of different accuracy factors (level of theory, DFT functional, basis set, and solvent effects) on the values of computed δ_{Hg} and $^{2}J_{Hg,P}$ compared to the experiment are given in Table 35, compiled from the original data scattered along the parent publication.[87]

Structures 151, 152



151 **152**

Table 35. Accuracy factors of the calculation of δ_{Hg} (ppm) and $^{2}J_{Hg,P}$ (Hz) in the tellurium-containing mercury complexes. Compiled from dos Reis Lino *et al.*[87]

Compound	Accuracy factor	Item	δ_{Hg}	$^{2}J_{Hg,P}$ [a]
151	Level of theory	NR/TZ2P	−324.2	−32.4
		ZORA/TZ2P	−1583	−137.2
		NR/dyall.vtz	−84	−39.4
		4c-DCS/dyall.vtz [b]	−1596	−159.8
		Experiment	−1361	(−)128.8
151	Functional	PBE0	−1583	−135.0
		B3LYP	−1803	−200.3
		PBE	−1711	−95.8
		BP86	−1796	−95.8
		Experiment	−1361	(−)128.8
152	Basis set	TZ2P	−1554	−139.3
		TZ2P-J		−168.8
		QZ4P	−2098	−165.0
		QZ4P-J		−170.4
		Experiment	−1301	(−)195.6
151	Solvent effect	Gas phase	−1583	−135.0
		COSMO ($C_2H_4Cl_2$)	−1598	−163.3
		Experiment (CD_2Cl_2)	−1361	(−)128.8

[a] The sign in parentheses was not experimentally determined. [b] Data are given for a model compound with all PBu_3 groups in **151** substituted for PMe_3.

The basic conclusions arrived in that study [87] dealing with the accuracy factors of the calculation of mercury chemical shifts and mercury–phosphorus spin–spin coupling constants are outlined below.

Level of theory. The relativistic correction to the ^{199}Hg NMR chemical shift was approximately 1260 ppm, as evaluated at the ZORA/TZ2P level, which corresponded to approximately 90% of the experimental value. For the geminal mercury–phosphorus spin–spin coupling constant, that correction was 105 Hz evaluated at the same level of theory, which corresponded to approximately 80% of the experimental value, being very large compared to the nonrelativistic value of −32.4 Hz. For the mercury chemical shift, the relativistic correction was approximately 950 ppm evaluated at the two-component ZORA/TZ2P level and more than 1500 ppm calculated at the four-component DKS/dyall.vtz level. The ZORA approach thus reproduced approximately 60% of the relativistic corrections of the four-component DKS approach. Using the specialized coupling constant basis set TZ2P-J, the relativistic correction for $^{2}J_{Hg,P}$ was 96 Hz, while with the four-component DKS approach, the relativistic corrections were as much as 120 Hz. The ZORA/TZ2P level thus reproduced 80% of the DKS/dyall.vtz relativistic corrections for the $^{2}J_{Hg,P}$ coupling constant.

Functionals. The overall spread of the results dealing with the calculation of the ^{199}Hg NMR chemical shift at the two-component level with different functionals was approximately 220 ppm. The common B3LYP functional yielded the most negative chemical shift value, while PBE0 gave the least negative value and was not unexpectedly the most accurate result. All four functionals (PBE0, B3LYP, PBE, and BP86) underestimated the ^{199}Hg NMR experimental chemical shift value. Calculated with the specialized coupling constant basis set TZ2P-J, sizable differences were observed for the $^{2}J_{Hg,P}$ coupling constants. The calculated values of $^{2}J_{Hg,P}$ varied in the range of approximately 100 Hz when using different functionals, which represented approximately 80% of the experimental data. The B3LYP functional demonstrated the largest deviation from the experiment, while PBE0 gave the closest result. However, both functionals essentially overestimated the experimental value of $^{2}J_{Hg,P}$. Meanwhile, two GGA functionals, PBE and BP86, demonstrated almost the same performance, essentially underestimating the experimental result. In general, the hybrid functional PBE0 gave the most accurate results for the mercury chemical shifts as well as for the mercury–phosphorus spin–spin coupling constants.

Basis sets. As expected, the switch from the TZ2P to QZ4P basis set brought a sizable change in the ^{199}Hg NMR chemical shift of −544 ppm. Concerning the mercury–phosphorus geminal spin–spin coupling constant, a substantial change was observed when going from TZ2P to the specialized coupling constant basis set TZ2P-J, on which $^{2}J_{Hg,P}$ increased in absolute value (became more negative) by approximately 30 Hz. This implied that the QZ4P basis set included some of the functions that were important for the calculation of coupling constants and that were missing in the TZ2P basis set. When moving then from QZ4P to the corresponding coupling constant basis set QZ4P-J, the further change in $^{2}J_{Hg,P}$ was rather small, amounting to only 5.5 Hz. Summarizing these results, one can conclude

that the TZ2P-J basis set appeared to be the optimal choice for that type of coupling constant.

Solvent effects. In general, the addition of the solvent effects using the COSMO model in the ZORA-PBE0 calculations of the ^{199}Hg NMR parameters did not improve the agreement with the experimental results compared to the gas phase results. For the ^{199}Hg NMR chemical shift, the solvent effect correction was 16 ppm, which was only 1% of the experimental value. At that time, the solvent correction brought the PBE0 result further away from the experimental value. For the mercury – phosphorus spin – spin coupling constant, the solvent effect correction was 28 Hz, but again in the wrong direction, if compared to experiment.

2.8. ^{205}Tl NMR

Early experimental ^{205}Tl NMR results are well reviewed by Hinton,[141] while theoretical calculations of thallium NMR chemical shifts and spin – spin coupling constants are mostly presented in the papers by Autschbach and coworkers,[96, 98, 99, 142 – 145] Bagno and Saielli,[130] Wodyński *et al.*[34] together with a very recent contribution by Bashi and Aliabad,[146] which are briefly reviewed below.

Thus, in the pioneering paper of 2001 by Autschbach and Ziegler,[142] the $^1J_{Tl,X}$ spin – spin coupling constants were calculated at the sc-ZORA and so-ZORA levels in a classical series of TlX, X = ^{19}F, ^{35}Cl, ^{79}Br, and ^{127}I (Table 36), compared to experiment. It was found that spin – orbit effects were very important and necessary to obtain even qualitatively correct coupling constants in this series. Those calculations were carried out with double and triple zeta basis sets with one polarization function for Tl and I, while the double and triple zeta core all-electron Slater basis sets were assigned at H, C, F, Cl, and Br.

Table 36. Spin – spin coupling constants $^1J_{Tl,X}$ (SI units) calculated at different levels of theory in the series of TlX, X = ^{19}F, ^{35}Cl, ^{79}Br, and ^{127}I. Compiled from Autschbach and Ziegler.[142]

Compound	NR	sc-ZORA	so-ZORA	Experiment
TlF	−120.3	−138.8	−203.4	−202
TlCl	−133.2	−128.8	−218.5	−224
TlBr	−217.2	−131.6	−315.3	−361
TlI	−287.8	−114.9	−381.8	−474

Generally, the spin – orbit ZORA results were in fair agreement with the experimental data. It was demonstrated that only the inclusion of spin – orbit coupling, in particular, the large negative FC + SD + PSO cross term, brought calculated coupling constants in rather good agreement with the experimental data. At the nonrelativistic level, the PSO term strongly decreased when going from TlF to TlI, while the FC term remained almost unchanged. Scalar relativistic effects caused the FC term to become more positive with increasing nuclear charge, resulting in a wrong chemical trend for scalar relativistic couplings. The cancellation of terms played an important role in indirect nuclear spin – spin coupling in the examined TlX series.

Several years later, those results were reexamined by Autschbach alone[145] used three different functionals, VWN, PBE, and PBE0. Those data are compiled in Table 37. It was found that both the PBE and PBE0 functionals somewhat overestimated the large experimental values of $^1J_{Tl,X}$. The GGA functionals were expected to work rather well in the high-density region around heavy nuclei, which could serve as a premise for the similar performance of PBE and PBE0 in that case.

Table 37. Spin – spin coupling constants $^1J_{Tl,X}$ (SI units) calculated with different functionals in the series of TlX, X = F, Cl, Br, and I. Compiled from Autschbach.[145]

Compound	Functional	sc-ZORA	so-ZORA	Experiment
TlF	VVN	−120	−184	−202
	PBE	−138	−201	
	PBE0	−170	−232	
TlCl	VVN	−97	−187	−224
	PBE	−117	−201	
	PBE0	−157	−242	
TlBr	VVN	−105	−283	−361
	PBE	−128	−290	
	PBE0	−195	−361	
TlI	VVN	−101	−363	−474
	PBE	−126	−357	
	PBE0	−208	−449	

Much later, in 2020, Bashi and Aliabad[146] reexamined the same series of thallium halogenides TlX, X = F, Cl, Br, and I. It was demonstrated that including spin – orbit relativistic corrections improved the prediction of ^{205}Tl NMR chemical shifts by up to 11% in TlF and TlCl. On the other hand, taking into account spin – orbit coupling changed the shielding results by only 1%. The calculated ^{205}Tl isotropic shielding constants showed an inverse relationship between the fluorine and chlorine atoms due to the small ionic radius of fluorine, expanding the fluorine 2*s* orbital in the core region and decreasing the length of the thallium – fluorine chemical bond.

Wodyński *et al.*[34] performed two- and four-component DFT calculations of the thallium shielding constant together with the thallium – carbon and thallium – nitrogen spin – spin coupling constants in thallium tetracyanide anion, $Tl(CN)_4^-$. Those results are compiled in Table 38. The two-component ZORA calculations were carried out using two GGA functionals, BVP86 and KT2, together with two hybrid functionals, B3LYP and PBE0, in combination with standard Slater basis sets TZP and TZ2P together with a relatively new jcpl basis set suggested by Autschbach.[145] The four-component calculation of shielding constants was performed by employing three nonrelativistic exchange-correlation functionals: LSDA, BP86, and PBE. For light atoms (nitrogen and carbon), the uncontracted triple zeta Jensen's pc-2 basis set was used, while Dyall's relativistic triple zeta basis set was employed for thallium. The four-component calculations were carried out using the Gaussian

Table 38. Thallium shielding constant, (σ_{Tl}, ppm) and thallium – carbon and thallium – nitrogen spin – spin coupling constants ($^1J_{Tl,C}$ and $^1J_{Tl,N}$, Hz) of thallium tetracyanide anion, $Tl(CN)_4^-$, calculated at the so-ZORA level using different functionals, compared to the nonrelativistic level and available experiment. Compiled from Wodyński *et al.*[34]

NMR parameter	NR [a]	so-ZORA [a]				Experiment
		BVP86	B3LYP	PBE0	KT2	
σ_{Tl}	6755	9173	9457	9532	9318	
$^1J_{Tl,C}$	2944	2731	4548	4430	2376	5440
$^1J_{Tl,N}$	−25.4	225.4	157.2	132.4	235.9	

[a] TZP basis set was used throughout.

charge distribution nuclear model, while two-component ZORA calculations were performed with the point–nuclear model. In the four-component calculations of spin–spin coupling constants involving thallium, no magnetic balance was employed, so that the large and small components of the wave function were connected by the unrestricted kinetic balance. Further insight into this effect in terms of the orbital contributions to scalar and spin–orbit interactions can be gained from the most recent publication by Vicha *et al.*[147]

Interestingly, scalar effects were shown to work in the opposite direction (leading to deshielding of the thallium nucleus) compared to spin–orbit coupling effects, and the latter were found to be much larger. The choice of a functional had a smaller effect on the calculated σ_{Tl} than on the spin–spin coupling constants involving thallium. At the same time, the nonhybrid functional BVP86 systematically underestimated the shielding constant calculated using the B3LYP hybrid functional, while PBE0 somewhat overestimated it. Keal-Tozer's KT2 functional resulted in the calculated σ_{Tl} falling between the BVP86 and B3LYP values.

For the thallium–carbon spin–spin coupling constant, the largest spin–orbit effect of approximately 220 Hz (14% of relativistic contribution) was observed, which was of the opposite sign to that of the scalar effects. It has long been known[148] that for some thallium complexes, the spin–orbit effect is more significant than for other systems, which is in line with the results of the study under consideration.[34] For the thallium–nitrogen spin–spin coupling constant, the nonrelativistic result had an opposite sign to the relativistic values (both scalar and spin–orbit coupling), and the difference between the sc-ZORA and so-ZORA results was 13.9 Hz (which is 8% of the total relativistic contribution).

In a series of papers, Autschbach *et al.* performed a systematic study of thallium chemical shifts and spin–spin coupling constants in the thallium–platinum unbridged (bonded) complexes in a classical series of pure cyanide complexes[96,98,143] and their derivatives.[99,144,145]

Thus, in the very first basic paper[96] it was demonstrated that experimentally observed spin–spin coupling constants $^1J_{Tl,Pt}$, $^1J_{Tl,C}$, and $^2J_{Tl,C}$ in the thallium–platinum unbridged cyanide complex **153** shown in Figure 36 were semiquantitatively reproduced by the ZORA calculations if both relativistic and solvent effects were taken into account. Solvent effects were very substantial and increased the $^1J_{Tl,Pt}$ coupling constant by more than 100%. It was also demonstrated that a relativistic increase in the *s*-orbital density at thallium and platinum atoms, charge donation by the solvent, and specific features of the multicenter C–Pt–Tl–C moiety were responsible for the observed trends in the values of $^1J_{Tl,Pt}$, $^1J_{Tl,C}$, and $^2J_{Tl,C}$.

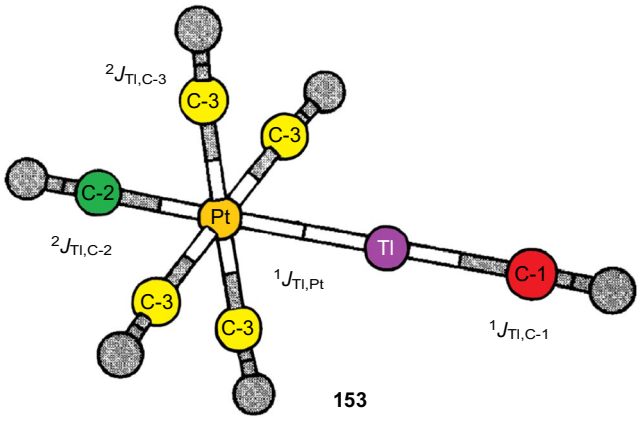


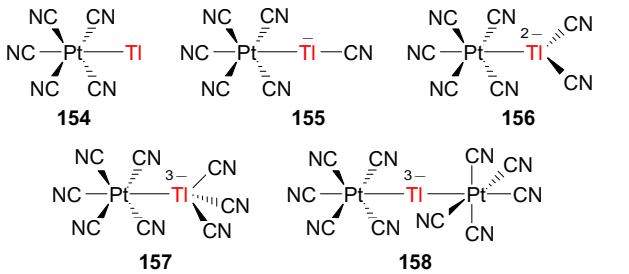
Figure 36. Scalar relativistically optimized structure of the thallium–platinum unbridged cyanide complex. Element colors: proton — gray, carbon — red, yellow and green (differed by symmetry), platinum — dark yellow, and thallium — purple. Reproduced with minor editing privilege from Autschbach and Ziegler[96] with the permission of the *American Chemical Society*.

It was demonstrated that the scalar relativistic increase of all three title couplings, especially that of $^1J_{Tl,Pt}$, was very substantial. The contributions to spin–spin couplings due to electronic orbital angular momentum (PSO and DSO) were shown to be fairly negligible. All coupling constants were strongly dominated by the Fermi-contact mechanism, which was very sensitive to the well-known relativistic increase in the valence *s*-orbital density at the heavy nuclei. However, no qualitative agreement with the experiment was achieved from the computations on the free (not solvated) molecule. Semiquantitatively correct values of spin–spin couplings were obtained by the explicit inclusion of up to four solvent molecules into computational space. The solvent (water) appeared to influence $^1J_{Tl,Pt}$ much more strongly than $^2J_{Tl,C}$. However, most coupling constants demonstrated rather large changes upon coordination of thallium by the solvent molecules of water, especially if the solvent-coordinated atom or its direct neighbors were involved in coordination.

It was also shown[96] that calculations at that level were able to reproduce the fact that $^2J_{Tl,C}$ was much larger than $^1J_{Tl,C}$, provided that relativity and solvent effects were taken into account. The increase in the computed $^1J_{Tl,Pt}$ coupling constant due to the solvent effect was remarkably large, so that solvation seemed to be reasonably well described by saturating the first coordination shell with solvent molecules of water.

In continuation of the previous study, Autschbach and Guennic[98] performed further investigation of $^1J_{Tl,Pt}$, $^1J_{Tl,C}$, and $^2J_{Tl,C}$ in the thallium–platinum unbridged cyanide complexes $[(NC)_5Pt-Tl(CN)_n]^{n-}$, $n = 0-3$ (**154**–**157**), and related thallium–diplatinum complex $[(NC)_5Pt-Tl-Pt(CN)_5]^{3-}$ (**158**). Optimized structures of **154**–**156** and **158** are presented in Figure 37. In view of the dominant role of solvent effects in the values of those couplings, that study was called by the authors 'a lesson on environmental effects'. It was generally shown that a computational model employing the statistical average of the orbital-dependent model potentials (SAOP)[149–152] in addition to the solvent effects, especially the latter, allowed the authors to accurately reproduce all experimental coupling constants. The main finding of the performed study

Structures 154–158



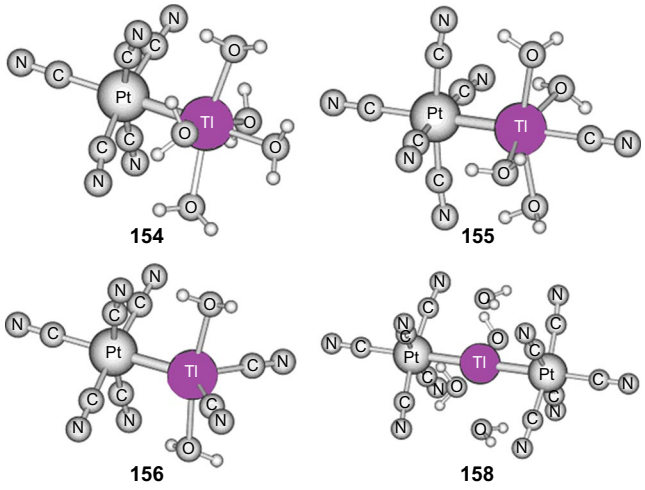


Figure 37. Comparison of calculated and experimental one-bond and geminal platinum – thallium (*a*), platinum – carbon (*b*), and thallium – carbon (*c*) spin – spin coupling constants in the series of **154** – **158** for different computational approaches: the unsolvated model (empty circles); explicit inclusion of solvent molecules (filled circles); the implicit addition of the bulk solvent (empty triangles); and the model based on the SAOP potential (filled squires). Reproduced with minor editing privilege from Autschbach and Guennic [98] with the permission of the *American Chemical Society*.

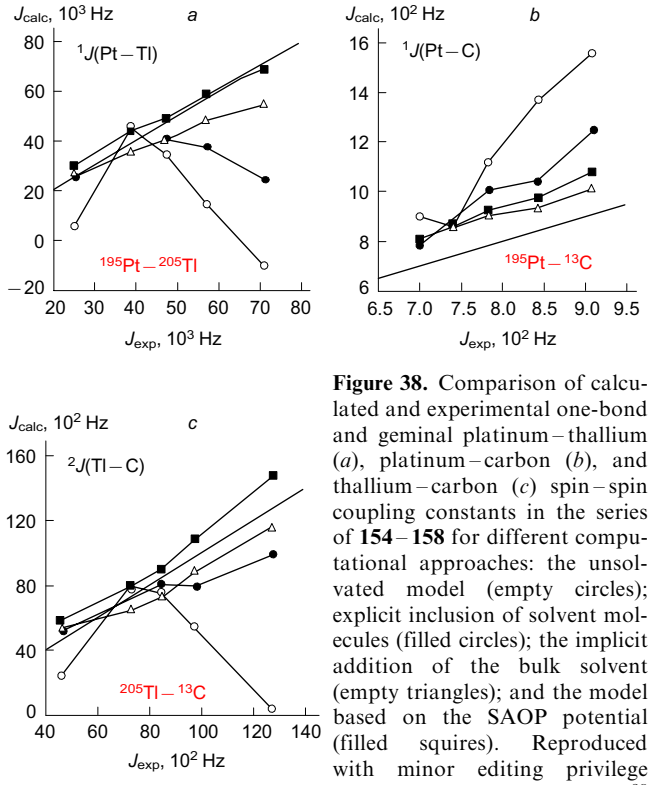


Figure 38. Comparison of calculated and experimental one-bond and geminal platinum – thallium (*a*), platinum – carbon (*b*), and thallium – carbon (*c*) spin – spin coupling constants in the series of **154** – **158** for different computational approaches: the unsolvated model (empty circles); explicit inclusion of solvent molecules (filled circles); the implicit addition of the bulk solvent (empty triangles); and the model based on the SAOP potential (filled squires). Reproduced with minor editing privilege from Autschbach and Guennic [98] with the permission of the *American Chemical Society*.

was that huge $^1J_{Tl,Pt}$ as well as other thallium couplings, $^1J_{Tl,C}$, and $^2J_{Tl,C}$, were almost entirely due to the presence of solvent molecules (H_2O) in the computational space, which was supported by the related NMR measurements.

All calculations were performed within the relativistic ZORA formalism using the Vosko – Wilk – Nusair local density functional, LDA, in combination with the triple zeta quality basis sets augmented with two polarization functions for thallium and platinum valence shells, triple zeta basis sets with one polarization function for carbon, nitrogen, and oxygen, and the double zeta quality basis sets for the core shells in the case of the all-electron computations. Solvent effects, which were shown to play a key role in the performed calculations of $^1J_{Tl,Pt}$, $^1J_{Tl,C}$, and $^2J_{Tl,C}$, were included both in an inexplicit way within the COSMO formalism and by explicitly adding up to five solvent molecules of water into computational space.

Earlier, it was shown [96] that the effects of Tl coordination by the solvent (H_2O) could be responsible for almost half of the huge 57 kHz magnitude of the Tl – Pt coupling constant. In a subsequent paper [98] it was demonstrated that this large coupling was entirely due to the presence of solvent water molecules. The increase in the computed Tl – Pt couplings due to the explicit inclusion of solvent molecules was remarkably large. For instance, the values of Tl – Pt couplings were shifted by approximately 30, 20, and 20 kHz for complexes **154**, **155**, and **158**, respectively. The higher was the coordination of thallium by the cyano ligands, the smaller was the effect of the coordination of additional solvent molecules on different coupling constants. The effect on the Tl – Pt coupling constant from the different number of solvent molecules coordinated to the thallium atom in complex **154** corroborated that conclusion, with a $^1J_{Tl,Pt}$ being approximately three times higher with five than with three surrounding water molecules. Thus, qualitative agreement with the experiment was observed for the different computed coupling constants, followed by the trends shown in Figure 38. However, there was still a considerable difference between the computed and experimental Tl – Pt couplings for the lower CN-coordinated complexes. For instance, this error was approximately 16.7, 9.1, and 7.5 kHz for complexes **154**, **155**, and **156**, respectively. Only the model including both solvent effects and the SAOP potential allowed the authors to reproduce the experimental Tl – Pt coupling constants within the 5 kHz range.[98] It was found that the model based on the inclusion of the polarization continuum model reaction field in combination with treating the solvating molecules in an explicit way was the most straightforward approach to account for solvent effects in these systems.

In the forthcoming paper [143] Autschbach and Guennic investigated at the so-ZORA level solvent effects on ^{205}Tl NMR chemical shifts of the discussed earlier thallium – platinum cyano complexes of a general formula $[(NC)_5Pt-Tl(CN)_n]^{n-}$, $n = 0-3$ (**154** – **157**), together with the related thallium – diplatinum complex $[(NC)_5Pt-Tl-Pt(CN)_5]^{3-}$ (**158**). The effects of electronic spin – orbit coupling, known to be of high importance for a correct description of heavy nucleus magnetic shieldings and chemical shifts, were included in those NMR computations. Taking into account the effects of various accuracy factors into consideration, the final results were interpreted as quite satisfactory when compared to the experimental data.

The same computational model that yielded the best agreement with experimental data for the thallium spin – spin coupling constants [96, 98] also performed quite well for the thallium chemical shifts. The effects of electronic spin – orbit coupling, known to be of high importance for a

Table 39. Calculated ^{205}Tl NMR chemical shifts (ppm) of the thallium–platinum cyano complexes referenced to $Tl(CN)_3$. Compiled from Autschbach and Guennic.[143]

Compound	Model	Method/functional			Experiment
		LDA	PW91	SAOP	
154	Unsolvated	−3890	−3777	−4079	−2056
	A (4 H_2O)	−2357	−2347	−2715	
	B	−6566	−6277	−6334	
	C (4 H_2O)	−1657	−1657	−2027	
155	Unsolvated	−663	−685	−513	−1471
	A (4 H_2O)	−1650	−1615	−1851	
	B	−1064	−1069	−923	
	C (4 H_2O)	−1244	−1222	−1520	
156	Unsolvated	−109	−139	−78	−867
	A (2 H_2O)	−1745	−1659	−1678	
	C (2 H_2O)	−790	−716	−850	
157	Unsolvated	−1624	−1518	−1599	−618
	B	−727	−615	−723	
158	Unsolvated	931	910	1235	−1605
	A (4 H_2O)	−2319	−2251	−2379	
	B	1045	995	1202	
	C (4 H_2O)	−1664	−1597	−1754	

correct description of thallium coupling constants, were included in all computations of thallium chemical shifts. Taking into consideration the large effects from various accuracy factors (relativistic and solvent effects, the quality of the description of electronic structure, geometries, functionals and basis sets), the final results were regarded as quite satisfactory when compared to experimental data.

As was usual for those authors, the Vosko–Wilk–Nusair local density approximation LDA functional was used in all geometry optimizations and subsequent NMR computations of thallium chemical shifts, providing reasonable accuracy for the considered structures **154**–**158**. The ^{205}Tl NMR chemical shifts were also computed by using the Perdew–Wang generalized gradient correction functional PW91. Additionally, the SAOP Kohn–Sham potential,

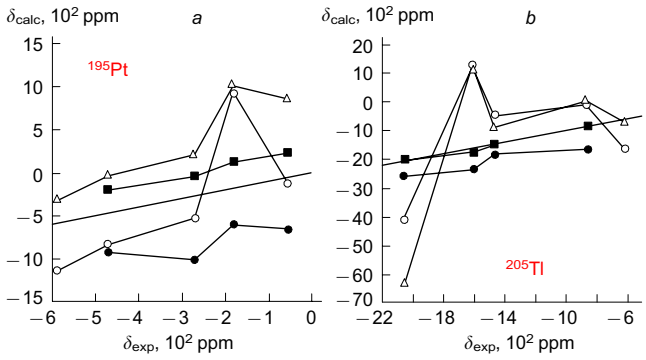


Figure 39. Comparison of calculated and experimental platinum (*a*) and thallium (*b*) chemical shifts for different computational approaches: the unsolvated model (empty circles); explicit inclusion of solvent molecules (filled circles); the implicit addition of the bulk solvent (empty triangles); and the model based on the SAOP potential (filled squires). Reproduced with minor editing privilege from Autschbach and Guennic[143] with the permission of *John Wiley and Sons*.

previously used for the calculation of thallium spin–spin coupling constants,[96,98] was employed in that study[143] for the computation of thallium chemical shifts. The manifestation of those three methods compared to the experiment is shown in Table 39 and graphically displayed in Figure 39. The performance of LDA, PW91, and SAOP functionals was tested for the four different models: (a) no solvent effects considered in any way (unsolvated); (b) scalar relativistically optimized geometry including explicit first solvation shell consisting of either 2 or 4 solvent molecules (model A); (c) scalar relativistically optimized geometry using the COSMO model for the solvent effects with no explicit first solvation shell (model B); (d) model A + COSMO for the bulk solvent effects (model C).

The basic conclusion of the performed study[143] was that the SAOP method in combination with the explicit first solvation shell consisting of several solvent molecules in COSMO medium behaved best of all compared to experiment, while unsolvated model provided the worst result for all tested methods and functionals. As a consequence of that result, it became obvious that the main factor governing the beheviour of thallium chemical shifts was the solvation effect. The same conclusion was valid for thallium spin–spin coupling constants, as followed from the studies by the same principal authors.[96,98]

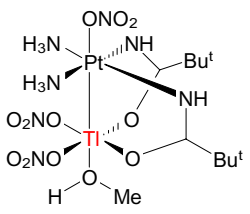
In the next two papers on thallium computational NMR of thallium–platinum complexes, Guennic and coworkers[99,144] continued investigation of solvent effects on ^{205}Tl NMR chemical shifts and ^{205}Tl–^{195}Pt spin–spin coupling constants in thallium–platinum complex **159** and derivatives at the same level of theory as in related publications.[96,98,143,145]

The decomposition of thallium shielding constants into paramagnetic, diamagnetic and spin–orbit terms showed the nonnegligible contribution of the relativistic spin–orbit mechanism. A noticeable spin–orbit effect on the ^{205}Tl NMR shielding constant was found, the latter being approximately 1500 ppm.

For the ^{205}Tl NMR chemical shifts in complex **159**, the application of the COSMO model and the SAOP potential resulted in the best agreement between the computed and experimental values, with −3415 against −3716 ppm. However, despite this rather convincing agreement, the experimental trends were not reproduced.

As expected, $^1J_{Pt,Tl}$ was strongly governed by scalar relativistic effects in the Fermi-contact mechanism. The computed $^1J_{Pt,Tl}$ of the unsolvated experimental complex **159** (*i.e.* no solvent effects were taken into account both at the stage of geometry optimization and during the computation of the $^1J_{Pt,Tl}$ coupling constant) underestimated the experimental value by approximately 30 kHz. The addition of electronic spin–orbit coupling to the computed spin–spin coupling constant only partially reduced the difference between the calculated and experimental values but resulted in an increase in that coupling by 10 kHz. This could be

Structure 159



159

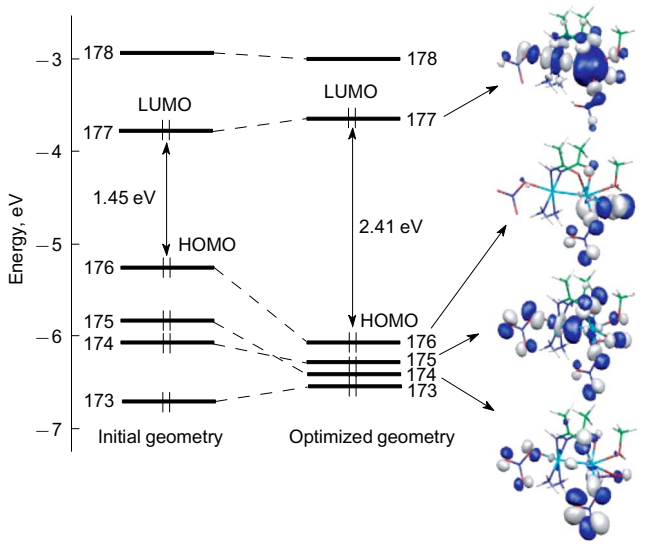


Figure 40. Influence of the geometry optimization on the molecular orbital levels of **159**. Figures given near the energy levels are the numbers of molecular orbitals. Reproduced with minor editing privilege from Guennic *et al.*[99] with the permission of *John Wiley and Sons*.

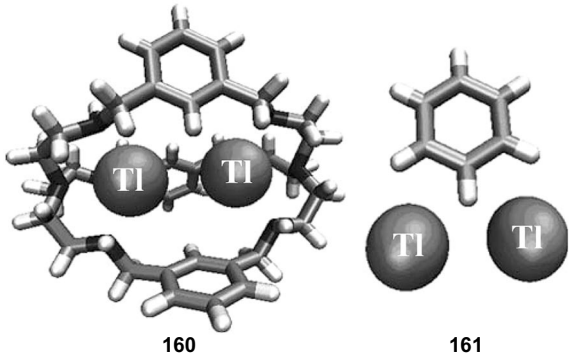


Figure 41. 3D structures of the original dithallium(I) cryptate (**160**) and the reduced model system used in the ZORA calculations (**161**). Reproduced with minor editing privilege from Bagno and Saielly [130] with the permission of *Springer Nature*.

ascribed to the HOMO shrinkage in the optimized structure, as illustrated in Figure 40.

The last paper discussed in this Section is that by Bagno and Saielli [130] dealing with the ZORA computation of the through-space $^{TS}J_{Tl,Tl}$ coupling constant in dithallium(I) cryptate (**160**) shown in Figure 41. Model system **161** (which was used in all ZORA calculations due to the enormously large original complex) was composed of two thallium(I) cations and one benzene molecule in the same relative position as in the original dithallium(I) cryptate.

Calculations of the through-space $^{TS}J_{Tl,Tl}$ coupling constant in the model dithallium(I) benzene dication **161** were performed at both the sc-ZORA and so-ZORA levels with TZP and TZ2P basis sets. The 'widely' (as termed in the original publication [130]) different results were obtained with respect to the basis set and the relativistic level. For example, at the so-ZORA level, the PSO contribution was the dominant term, but other contributions were also strongly affected in contrast to sc-ZORA results. Based on the data presented in Table 40, the through-space $^{TS}J_{Tl,Tl}$ coupling constant was roughly estimated to be approximately −(2 – 3) kHz.

Table 40. Calculated through-space thallium – thallium spin – spin coupling constants and their contributions (Hz) in the model $Tl_2(C_6H_6)^{2+}$ dication. Compiled from Bagno and Saielly.[130]

Basis set theory	Level of	DSO	PSO	FC + SD	Total
TZP	sc-ZORA	0.0	350.2	6513.8	6844.1
	so-ZORA	0.0	−5041.5	1844.9	−3197.4
TZ2P	sc-ZORA	0.0	318.0	6370.7	6688.7
	so-ZORA	0.0	−4223.0	2478.6	−1744.4

2.9. ^{207}Pb NMR

Computational NMR of ^{207}Pb isotope is much less developed than that of other nuclei considered in that review. This is especially because only simple inorganic derivatives of plumbane, PbH_4, together with the simplest organometallic plumbanes, the derivatives of ethynylplumbane, $PbH_3C{\equiv}CH$, were involved in those studies.

The story of modern computational ^{207}Pb NMR begins with the most essential publications dealing with the calculation of lead spin – spin coupling constants in plumbane and derivatives, which appeared some 20 years ago: those of Autschbach and Ziegler,[94] Kirpekar and Sauer,[153] Enevoldsen *et al.*,[51] and Khandogin and Ziegler.[52] It should be emphasized that early calculations by Enevoldsen *et al.*[51] were performed at the four-component DKS level, while the rest were carried out within the two-component quasirelativistic ZORA formalism. Within the next decade, a number of more related publications [52, 56, 58, 137, 145, 148] appeared dealing with the calculation of ^{207}Pb NMR parameters (lead shieldings, chemical shifts, and spin – spin coupling constants) in simple inorganic plumbanes.

Thus, in the most known paper of that period, by Autschbach and Ziegler,[94] a relativistic formulation of the spin – spin coupling hyperfine terms based on the two component zeroth-order regular approximate Hamiltonian was presented. The scalar relativistic parts of the resulting operators were used for the calculation of the reduced one-bond lead couplings, $^1K_{Pb,H}$, $^1K_{Pb,C}$, and $^1K_{Pb,Cl}$ of PbH_4, $PbMe_2H_2$, $PbMe_3H$, $PbMe_4$, and $PbCl_4$, which are collected in Table 41. It was found that scalar relativistic calculations were able to reproduce major parts of the relativistic effects on the coupling constants of that type. Most calculations were carried out within the VWN local density approximation with Becke88 and Perdew86 nonlocal gradient corrections in combination with the all-

Table 41. Calculated reduced spin – spin coupling constants (K) involving lead (SI units) of simple plumbanes compiled from Autschbach and Ziegler.[94]

Compound	Coupling constant	NR	ZORA-GGA	ZORA-VWN	Experiment [a]
PbH_4	$^1K_{Pb,H}$	599	1318	1208	1115
$PbMe_2H_2$	$^1K_{Pb,H}$	578	1073	1038	987
$PbMe_3H$	$^1K_{Pb,H}$	566	978	974	923
$PbMe_4$	$^1K_{Pb,C}$	104	−198	−234	(−)394
$PbCl_4$	$^1K_{Pb,Cl}$	−2116	−3215	−3281	(−)2889

[a] The sign in parentheses was not experimentally determined.

electron triple zeta Slater basis set with one polarization core function.

It was generally found that the nonrelativistic approach was not at all able to predict spin–spin coupling constants involving lead. The relativistic corrections to ^{207}Pb spin–spin coupling constants turned out to be substantially large, in some cases even larger than total nonrelativistic values. The performed ZORA scalar relativistic computations were able to recover major parts of the relativistic effects, thereby gaining an acceptable mean relative accuracy with respect to experimental data.

The $^{1}J_{Pb,H}$ coupling constant in the molecule of plumbane, PbH_4, was subjected to a thorough scrutiny by means of two dedicated perturbation theory-based methods, SOPPA(MP2) and SOPPA(CCSD), together with the valence complete active space and restricted active space methods (CAS and RAS).[153] The most important part of the spin–orbit correction was evaluated at the level of the random phase approximation, RPA. Electron correlation correction to that coupling constant was calculated with the multiconfigurational linear-response method using the extended complete and restricted active space wavefunctions, as well as with the second-order polarization propagator approximation, SOPPA(MP2), and the second-order polarization propagator approximation with coupled-cluster singles and doubles amplitudes, SOPPA(CCSD). The relativistic spin–orbit correction was estimated from the one-electron part of the FC-OP cross term amounting to approximately 10% of the FC contribution at the RPA level. All those data are compiled in Table 42.

The general result of the performed study [153] was that the FC term was the 'all-dominating contribution' (as termed in the original publication) to the value of $^{1}J_{Pb,H}$ of plumbane. Electron correlation did not change the importance of the individual contributions, although the FC term was reduced by approximately 20%, and the SD term changed its sign. The relativistic spin–orbit correction, approximated by the one-electron part of the FC-OP cross term, was the second most important contribution to the $^{1}J_{Pb,H}$ coupling constant; at the RPA level, it amounted to approximately 10% of the FC term.

In another early fundamental publication [51] dealing with the ^{207}Pb–^{1}H coupling constant in plumbane, relativistic four-component random phase approximation calculations based on the Dirac–Coulomb Hamiltonian were performed, and a relativistic increase in that coupling constant of as much as 156% was found. The substantial relativistic effect on the title coupling constant was explained as being mainly due to scalar relativistic factors rather than spin–orbit corrections. Complementarily, it was shown that there was a similar dependence and a need for tight *s*-functions in the basis sets in the relativistic case to obtain the basis set converged results.

Table 42. Coupling contributions of the $^{1}J_{Pb,H}$ coupling constant (Hz) of plumbane. Compiled from Kirpekar and Sauer.[153]

Method	FC	SD	OP	OD	FC-OP	Total
RPA	1806.94	−0.36	−6.22	0.02	−198.60	1601.78
SOPPA	1449.96		−5.93	0.02		1444.05
SOPPA (CCSD)	1374.20		−6.11	0.02		1368.11
CAS	1424.00	0.14	−5.75	0.03		1418.42
RAS	1448.65	0.12	−5.84	0.02		1442.95

In the paper by Khandogin and Ziegler,[52] on the basis of the nonrelativistic hyperfine operators, two approximate frozen-core scalar relativistic corrections were derived to account for the major relativistic effects on the $^{1}J_{Pb,H}$ in plumbane. In the first scheme, the quasirelativistic approach was incorporated into the nonrelativistic coupling calculation. In the second scheme, a refined version of the hyperfine correction was used, which involved the correction of the *s*-orbital value at lead in the evaluation of the Fermi-contact contribution of $^{1}J_{Pb,H}$ in plumbane. Performed calculations revealed that the second method gave significant improvement over the first one.

Several levels of theory (DFT, HF, and post-HF) in combination with the all-electron triple zeta plus double polarization basis set for protons and the frozen-core triple zeta plus single polarization basis set for lead were employed in that study.[52] The fact that the BP86 functional resulted in a better agreement with experimental values was considered to be a direct proof that nonlocal corrections were important for describing magnetic molecular properties such as $^{1}J_{Pb,H}$.

We will not concentrate on the most papers like those [56, 137, 145] appeared in the interim of 2001–2010 devoted to the same simple inorganic derivatives of plumbane including plumbane itself, PbH_4, together with $PbMeH_3$, $PbMe_2H_2$, $PbMe_3H$, and $PbMe_4$ except for the two most interesting publications — that by Lantto *et al.*[58] and a generalizing paper by Moncho and Autschbach.[148]

In the first paper,[58] the principal relativistic heavy-atom lead effect on the NMR shielding tensor of lead itself (HAHA effect) was calculated in the series of Pb^{2+}, Pb^{4+}, PbH_2, and PbH_3^- using *ab initio* methods at the level of Breit–Pauli Hamiltonian, implying the second-order cross-term of the Fermi contact hyperfine interaction and the electronic spin-Zeeman interaction with kinetic energy correction. Fully relativistic four-component DHF calculations of $^{1}J_{Pb,H}$ of those systems were carried out with a fully uncontracted quadruple zeta basis set with extra valence correlation functions on lead. Those results are compiled in Table 43.

An interesting finding of that study [58] was that while the nonrelativistic shielding terms were sensitive to both electron correlation and chemical surroundings of lead, the dependence of the relativistic terms on those factors was much smaller. This was interpreted as reflecting the predominantly core nature of the relativistic terms, as on the one hand it was the Coulomb interaction with lead nucleus and not the electron–electron interaction that dominated the energetics of the core electrons, and on the other hand, that the core orbitals were quite invariant to the chemical

Table 43. Calculated nonrelativistic and main relativistic contributions to the lead shielding constant (ppm). Compiled from Lantto *et al.*[58]

System	Wave function	NR	Total relativistic correction	4-component DHF
Pb^{2+}	SCF	10049	16216	17523
Pb^{4+}	SCF	10034	16201	17534
PbH_2	SCF	2886	7294	−6987
	CAS	3278	7933	
PbH_3^-	SCF	7374	13393	13612
	CAS	7468	13502	

surroundings of lead, implying only small chemical shift effects arising from those contributions.

In the second paper,[148] a comprehensive study of different nonrelativistic and relativistic DFT protocols for the calculations of lead coupling constants in the extended series of inorganic plumbanes was performed, as presented in Table 44. As a result of that survey, the highest-level computational model (hybrid density functional computations including scalar plus spin – orbit relativistic effects, the COSMO solvent model, and a Gaussian finite-nucleus model) was recommended as performing best of all, as exemplified in Figure 42 for a series of heavy isotopes including ^{207}Pb. Again, a very good performance of the hybrid functional PBE0 (compared to other functionals) in the computations of lead spin – spin coupling constants was established.

Table 44. Calculated and experimental reduced spin – spin coupling constants (K) involving lead (SI units) of plumbanes, compiled from Moncho and Autschbach.[148]

Compound	Coupling constant	sc-ZORA		so-ZORA		Experiment [a]
		PBE	PBE0	PBE	PBE0	
PbH_4	$^1K_{Pb,H}$	1090.7	1242.9	1007.9	1157.7	1115.0
$PbMe_2H_2$	$^1K_{Pb,H}$	814.0	959.1	736.2	879.6	979.4
	$^2K_{Pb,H}$	−10.1	−29.0	−5.9	−23.9	−30.3
$PbMe_3H$	$^1K_{Pb,H}$	692.5	835.0	616.9	758.2	915.9
	$^2K_{Pb,H}$	−6.4	−24.5	−2.6	−19.4	−27.1
$PbMe_4$	$^1K_{Pb,C}$	−84.6	229.5	−104.7	219.5	396.7
	$^2K_{Pb,H}$	−2.3	−18.5	1.8	−13.9	24.5
$PbMe_3CF_3$	$^2K_{Pb,H}$	−4.9	−24.1	−0.5	−19.0	28.7
	$^2K_{Pb,F}$	17.1	−0.2	31.1	19.1	102.0
$PbMe_2(CF_3)_2$	$^2K_{Pb,H}$	−6.8	−30.8	−2.5	−25.5	33.9
	$^2K_{Pb,F}$	70.4	52.5	90.0	78.7	160.7
$PbCl_4$	$^1K_{Pb,Cl}$	−3014.1	−3658.3	−2573.6	−3103.5	(−)2868.3
Pb_2Me_6	$^1K_{Pb,C}$	−416.5	−166.7	−448.7	−184.0	44.4
	$^2K_{Pb,H}$	5.0	−9.0	9.8	−3.5	−16.8
	$^2K_{Pb,C}$	121.7	182.1	108.9	163.3	146.0
	$^3K_{Pb,H}$	10.5	8.3	10.2	8.2	9.1

[a] The sign in parentheses was not experimentally determined.

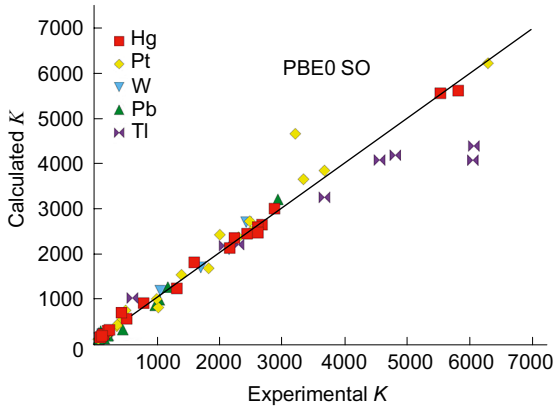


Figure 42. A plot of calculated reduced coupling constants involving Hg, Pt, W, Pb, and Tl against the experiment. All couplings are in SI units. Reproduced with minor editing privilege from Moncho and Autschbach [148] with the permission of the *American Chemical Society*.

In a more recent publication by Kristkova *et al.*,[61] the 'primordial' plumbane, PbH_4, was revisited at the fully relativistic 4-component DKS level in the framework of the four-component matrix Dirac – Kohn – Sham approach termed 'matrix Dirac – Kohn – Sham Restricted Magnetic Balance' (mDKS-RMB). The authors used either the local density approximation with Slater exchange and VWN correlation (SVWN) or the GGA functionals of Becke exchange with Perdew correlation functional (BP86) and Perdew – Burke – Ernzerhof exchange-correlation functional (PBE) in combination with Dyall's triple zeta basis set. The performed mDKS-RMB calculations resulted in $^1J_{Pb,H}$ in plumbane of 2495 Hz, in very good agreement with the experimental 2594 Hz (estimated on the basis of experimental values for methylsubstituted plumbanes).

A year earlier, Maldonado and Aucar[59] calculated ^{207}Pb NMR shielding constants (converted to δ-scale) in the series of halogenoplumbanes together with a parent plumbane. For the reference $PbMe_4$, σ_{Pb} was evaluated to be 14475.1 ± 500.7 ppm. This value corresponded to the calculations using the four-component relativistic polarization propagator method at the RPA level of approximation, which was found to be closer to the experimental values than those obtained at the DFT level with a few different functionals, PBE0, B3LYP, BLYP, BP86, KT2, and KT3. The finite-size nucleus model of Gaussian-type and uncontracted basis sets were used in that study.

Among the findings of the later publication,[59] for the series of PbX_4 (X = H, F, Cl, Br, and I), the diamagnetic component was shown to be increased only by 8.4% when going from PbH_4 to PbI_4, being quite independent of the electron correlation, even for the heaviest molecular systems PBr_4 and PI_4. However, the paramagnetic component significantly increased when the substituents of the molecular models became heavier. Thus, for PbH_4, the shielding constant σ^p(Pb) was found to be 4644.85 ppm, while it was as large as 9654.45 ppm for PbI4, corresponding to an increase of 107% from the lightest to the heaviest molecular system. Finally, the HAVHA effect of Pb was shown to be mostly due to the paramagnetic-like contributions providing a quadratic dependence on the number of iodine atoms in the PbH_nI_{4-n} model series.

Finally, very recently, two related publications by Demissie[62] and Jakubowska *et al.*[63] appeared dealing with the calculation of lead chemical shifts and spin – spin coupling constants in the acetylenic derivatives of lead.

In the first paper,[62] four-component relativistic DFT together with two-component ZORA calculations at both scalar and spin – orbit levels of ^{207}Pb NMR chemical shifts and spin – spin coupling constants in three acetylenic derivatives of lead, $Pb(C{\equiv}C-Me)_4$, $PbMe_2(C{\equiv}C-Me)_4$, and $PbMe_3(C{\equiv}C-H)$, were performed in good agreement with experimental values. The molecular geometries of those compounds were optimized at the so-ZORA level using the hybrid PBE0 exchange-correlation functional and the all-electron triple zeta doubly polarized Slater-type basis set, TZ2P. The ^{207}Pb NMR chemical shifts and spin – spin coupling constants were calculated using the four-component Dirac – Kohn – Sham relativistic Hamiltonian in combination with the PBE and PBE0 exchange-correlation functionals together with Dyall's relativistic all-electron core-valence triple zeta (dyall-cvtz) basis set.

As follows from the data presented in Table 45, the spin – orbit contributions to the ^{207}Pb NMR chemical shifts of $Pb(C{\equiv}C-Me)_4$ are small compared to their scalar

Table 45. ^{207}Pb NMR chemical shifts (ppm) and spin – spin coupling constants (Hz) and their relativistic corrections evaluated at the two- and four-component relativistic levels. Compiled from Demissie.[62]

Compound	NMR parameter	NR	so-ZORA	sc-ZORA	4c-DKS	Δ_{sc} (see [a])	Δ_{so} (see [a])	Δ_{rel} (see [b])
$Pb(C{\equiv}C-Me)_4$	δ_{Pb}	−621.6	−1108.0	−778.6	−788.7	−156.9	−1.8	−158.7
	$^1J_{Pb,C\equiv}$	906.6	1505.3	1855.0	1776.9 (1624.5) [c]	948.4	−90.3	858.1
	$^4J_{Pb,H}$	−18.1	−32.8	−46.3	−43.7 (−28.0)	−28.2	12.2	−16.1
	$^2J_{Pb,C\equiv}$	200.0	380.4	429.8	429.7 (347.4)	229.8	−4.5	225.3
	$^3J_{Pb,C}$	17.6	28.9	40.9	40.2 (30.5)	23.3	−0.9	22.4
$PbMe_2(C{\equiv}C-Me)_2$	δ_{Pb}	−314.5	−556.1	−413.0	−343.6	−98.5	78.4	−20.1
	$^1J_{Pb,C}$	320.1	373.7	490.0	498.2 (574.3)	169.7	1.5	171.2
	$^1J_{Pb,C\equiv}$	467.5	55.9	66.9	−5.7 (208.0)	−400.6	−70.3	−470.9
	$^2J_{Pb,H}$	−65.4	−62.1	−129.3	−120.3 (−100.9)	−63.9	10.1	−53.8
	$^4J_{Pb,H}$	−13.2	−12.7	−17.8	−15.1 (−13.5)	−4.6	2.8	−1.8
	$^2J_{Pb,C\equiv}$	112.2	70.0	65.6	60.0 (70.3)	−46.6	−5.5	−52.2
	$^3J_{Pb,C}$	11.5	7.3	11.5	10.6 (9.2)	0.0	−0.8	−0.9
$PbMe_3(C{\equiv}C-H)$	δ_{Pb}	−176.2	−298.8	−219.4	−184.5	−43.2	24.2	−19.0
	$^1J_{Pb,C}$	255.6	199.9	259.6	266.8	4.0	5.2	9.2
	$^1J_{Pb,C\equiv}$	279.5	−321.5	−368.0	−445.8	−647.5	−72.9	−720.4
	$^2J_{Pb,H}$	−51.9	−44.7	−73.3	−53.3	−21.5	9.8	−11.6
	$^3J_{Pb,H}$	23.8	16.3	23.3	18.6	−0.5	−4.8	−5.4
	$^2J_{Pb,C\equiv}$	69.3	−24.3	−38.9	−47.2	−108.3	−7.5	−115.8

[a] Both scalar and spin – orbit relativistic corrections were evaluated at the fully relativistic 4c-DKS level. [b] Total 4c-DKS relativistic correction. [c] Given in parentheses are experimental values.

contributions. However, in the other two molecules they almost canceled each other. For example, Δ_{sc} of lead in $PbMe_2(C{\equiv}C-Me)_2$ was found to be −98.50 ppm, whereas Δ_{so} was 78.4 ppm, making a net Δ_{rel} of −20.12 ppm. In most cases, the net relativistic correction and the scalar contribution were found to be close to each other.

For the spin – spin coupling constants involving lead, the relativistic corrections were mostly of the same order of magnitude as the nonrelativistically calculated values. Overall, the scalar contributions to lead couplings were dominant over the spin – orbit contributions, which could be due to the low *s*-character of the Pb−C bonds. It was also found that the net relativistic corrections to lead spin – spin couplings in most of the molecules were negative. Even though the Δ_{so} contributions were small, it was important to consider both the scalar and spin – orbit contributions to obtain accurate results. The relativistic corrections to lead geminal coupling constants were found to be larger than those through three bonds. In some cases, the relativistic corrections were close to the experimental spin – spin coupling constants.

The general result of the performed study [62] was that the full four-component relativistic approach together with the hybrid PBE0 exchange-correlation functional gave the best agreement between the calculated and experimental ^{207}Pb NMR chemical shifts and spin – spin coupling constants. The analysis of the scalar and spin – orbit contributions of those NMR parameters showed that the main relativistic effect was due to the scalar relativistic contraction of the *s*-shells and not due to spin – orbit coupling. However, the inclusion of both contributions was important for the quality of the results. The relativistic correction to both lead chemical shifts and spin – spin coupling constants was considerable, indicating the importance of using the four-component relativistic approach for the calculation of ^{207}Pb NMR parameters.

A very similar study was performed recently by Jakubowska *et al.*[63] on $PbH_3C{\equiv}CH$ and $PbEt_3C{\equiv}CH$ molecules, where $^1J_{Pb,C}$ and $^2J_{Pb,C\equiv}$ were calculated at the four-component DFT level using the BLYP, B3LYP, and BHLYP functionals and compared to the nonrelativistic CCSD results. The general conclusion of the performed investigation was that the use of the B3LYP functional was the most satisfactory. The BLYP values differed only slightly (up to 4%) from those calculated using the B3LYP functional, whereas the differences between the values calculated using the BHLYP and B3LYP functionals were larger by up to 15%. The use of the ATZP basis set provided results in better agreement with the experiment as compared to the aug-cc-pVTZ-J basis set. The difference between the relativistic and nonrelativistic values reached almost 50%. In general, for those systems, a proper description of the electron correlation was found to provide a larger effect on the calculated ^{207}Pb NMR coupling constants than total relativistic corrections.

2.10. Other isotopes

Papers dealing with the calculations of the NMR parameters (chemical shifts and spin – spin coupling constants) of heavy nuclei have now also become available for a number of more exotic and less popular, mainly quadruple isotopes such as ^{63}Cu (see Refs 154 – 156), ^{67}Zn (see Refs 38, 52), ^{73}Ge (see Refs 51, 52, 58, 61 – 63, 157), ^{99}Ru (see Ref. 158), ^{129}Xe (see Refs 159, 160 – 167), ^{183}W (see Refs 94, 148), ^{193}Ir (see Ref. 168), ^{235}U (see Refs 169, 170), and many others (see, for example, Refs 58, 72, 171, 172), which were, however, beyond the scope of the present review. Interested readers are most welcome to read some of the cited key papers together with references given therein dealing with each particular isotope.

3. Note added in proof

Very recently, a comprehensive review by Rusakova and Rusakov [173] on quantum chemical calculations of ^{77}Se and ^{125}Te NMR chemical shifts and spin – spin coupling constants has appeared. In that publication, different computational protocols that had been used in recent decade to simulate NMR spectra of selenium and tellurium compounds were discussed with a strong emphasis on their accuracy. A special attention was placed on the relativistic calculations in view of the fact that taking into account relativistic effects appreciably influences the precision of NMR calculations of selenium and, especially, tellurium NMR parameters. Stereochemical applications of quantum chemical calculations of ^{77}Se and ^{125}Te NMR chemical shifts and spin – spin coupling constants were discussed to exemplify the importance of integrated approach of experimental and computational NMR techniques. That review seems to be a smart supplement to what had been discussed in Section 2.5.

4. Conclusion

At present, we are witnessing marked progress in the field of theoretical calculations of the NMR parameters of heavy nuclei, represented in the present review by the most common 1/2 spin isotopes of ^{109}Ag, ^{113}Cd, ^{119}Sn, ^{125}Te, ^{195}Pt, ^{199}Hg, ^{205}Tl, and ^{207}Pb. These calculations are rapidly developing and becoming of increasing practical interest on the cutting edge of modern computational chemistry. Vivid progress is also observed in the theoretical interpretation of stereoelectronic effects involving the nuclei studied based on the calculations of their NMR parameters.

Computational NMR has become an efficient tool for the structural elucidation of organic and biological molecules. Theoretical prediction of NMR parameters provided a new guide into molecular structure. In particular, recent advances in computational NMR of heavy nuclei at the relativistic level provided a profound impact on the calculation of chemical shifts and spin – spin coupling constants of heavy nuclei, two basic NMR parameters that could be derived from experimental NMR spectra. At present, the development of relativistic approaches to the calculation of NMR parameters is of utmost importance, as outlined in a number of 'relativistic' reviews involving those of Rusakova and Krivdin [69] and Autschbach.[11 – 13]

Formally speaking, relativistic effects are pure theoretical phenomena that arise from the difference between the levels of physical theory used for their evaluation in particular cases. This means that there is actually no way to measure relativistic effects experimentally. Generally, relativistic effects in the values of NMR parameters could be estimated only from the difference between those calculated within relativistic theory and those calculated at the nonrelativistic level. It should also be recalled that the four-component relativistic methods are extremely computationally demanding compared to the one- and two-component relativistic calculations.

Provided in this review is also a general insight into relativistic HAHA and HALA effects of heavy isotopes, ^{109}Ag, ^{113}Cd, ^{119}Sn, ^{125}Te, ^{195}Pt, ^{199}Hg, ^{205}Tl, and ^{207}Pb, on their NMR chemical shifts and spin – spin coupling constants with concentrating mainly on practical computational aspects and paying not too much attention to pure theoretical issues. In particular, for the studied series of heavy isotopes, the principle results were achieved, as described below.

For the ^{109}Ag NMR, the 'Cinderella nucleus' silver is extremely difficult to observe experimentally; however, this situation was slightly improved in recent years, while theoretical calculations of the NMR parameters of heavy nuclei at the modern levels of theory are still in a cradle. Only recently did two pioneering papers by Alkorta and coworkers appeared reporting the calculations and experimental measurements of ^{109}Ag NMR chemical shifts in the series of trinuclear Ag(I) complexes with pyrazolate ligands and dinuclear silver pyrazolates. In the earlier study by Kauch and Pecul, the one-bond silver-nitrogen spin – spin coupling constants of Ag^+ cations intercalated between imidazole rings in DNA chains with nitrogens-15 of neighboring silver-bound imidazole pairs were calculated within the DFT framework with relativistic effects taken into account at the two-component relativistic level both with and without accounting for spin – orbit coupling effects. Wodyński and co-workers performed two-component ZORA calculations of $^1J_{Ag,C}$ and $^1J_{Ag,N}$ coupling constants of the silver cyanide dimer AgCN···AgCN with different nonrelativistic exchange-correlation functionals and triple zeta relativistic Dyall's basis set.

^{113}Cd NMR chemical shifts spread over a large range of almost 1000 ppm, which is very attractive for structural studies of cadmium complexes by means of theoretical calculations. One of the most representative examples dealing with the calculation of ^{113}Cd NMR chemical shifts is that by Casella and coworkers who tested several DFT protocols at the nonrelativistic and two-component relativistic scalar and spin – orbit ZORA levels for the calculation of cadmium chemical shifts for a number of cadmium complexes. In an earlier publication by Kauch and Pecul, the indirect isotropic ^{113}Cd – ^{1}H spin – spin coupling constants separated formally by as many as five chemical bonds were calculated in the model rubredoxin complex. At approximately the same period of time, Roukala and coworkers investigated the performance of the Breit – Pauli perturbation theory against the fully relativistic four-component method in computing ^{113}Cd NMR chemical shifts of dimethyl cadmium. Some a decade earlier, Krauss and collaborators performed calculations of ^{113}Cd NMR chemical shifts of the cadmium ion binding sites of dicadmium phosphotriesterase, including full amino acid side chains, representing the protein environment surrounding the cadmium active sites. In that study, one to three water molecules were included in the cadmium active site in addition to the bridging hydroxide. It should also be mentioned that a number of early papers appeared in the previous decade (*i.e.* those published in the interim of 2000 – 2010) dealing with different aspects of the computation of ^{113}Cd NMR chemical shifts and spin – spin coupling constants involving ^{113}Cd isotopes.

A number of early calculations of ^{119}Sn NMR chemical shifts were performed mainly at the one-component nonrelativistic and/or the two-component relativistic levels. As an illustrative example, Bagno, Casella, and Saiell calculated at two-component ZORA level ^{119}Sn NMR shielding constants and spin – spin coupling constants involving tin in stannane, tetramethylstannane, and tin halides. Lantto and coworkers investigated a principal relativistic heavy-atom effect on the NMR shielding tensor of the heavy atom itself (known as the 'HAHA effect') for tin in a series of closed-shell Sn^{2+}, Sn^{4+}, SnH_2, and SnH_3^- systems. It was found

that the second-order spin–orbit mechanism, *i.e.* the second-order spin orbital mechanism arising from the cross-term contribution of the Fermi contact interaction and spin-Zeeman interaction, was isotropic and practically independent of the electron correlation effects, as well as of the chemical environment of heavy atoms. In a more recent study by Křístková and colleagues, relativistic four-component calculations of $^{1}J_{Sn,H}$ in stannane were performed using an efficient evaluation of the exchange-correlation response kernel. The authors reported the development and implementation of a new scheme for the efficient calculation of indirect nuclear spin–spin coupling constants involving tin in the framework of the four-component matrix Dirac-Kohn–Sham approach. Demissie reported manifestation of scalar and spin–orbit relativistic effects in the ^{119}Sn NMR chemical shifts and spin–spin coupling constants derived from the nonrelativistic as well as from the two- and four-component relativistic DFT calculations. The main relativistic effect was shown to arise not due to spin–orbit coupling (as might be expected) but rather due to the scalar relativistic contraction of *s*-shells. Jakubowska and co-workers reported calculations of the one-bond and geminal tin-carbon coupling constants in ethynylstannane performed at both nonrelativistic CCSD and DFT levels, the latter in the nonrelativistic and relativistic four-component approach with different exchange-correlation functionals and basis sets to estimate the effects of the electron correlation and relativity. In two related papers by Bagno and co-workers, the structures of the complex of D-ribonic acid with dimethyltin together with a series of organotin *erythro* and *threo* derivatives were evaluated based on the experimental and theoretical ^{119}Sn NMR study, which allowed the determination of its stable conformation in solution as well as the detection of a dimerization process involving tin atoms. In two related papers, Casella and co-workers derived the dihedral angle beheviour of $^{3}J_{Sn,H}$ and $^{3}J_{Sn,C}$ to verify their Karplus-type dependences together with the manifestation of the effect of heteroatom in the coupling path at both nonrelativistic and relativistic scalar ZORA levels.

^{125}Te NMR chemical shifts and spin–spin coupling constants were thoroughly investigated by Hada and co-workers, who evaluated a quasirelativistic Hamiltonian including the spin-free relativistic, one- and two-electron spin–orbit, and relativistic magnetic interaction terms in a series of the simplest tellurides, TeH_2, TeF_6, $Te(CH_3)_2$, $Te(CH_3)_4$, and $Te(CH_3)_2Cl_2$. The main result of the performed calculations was that relativistic effects amounting to as much as 1300 ppm were very important for reproducing the absolute values of ^{125}Te NMR shielding constants obtained experimentally. On the other hand, for ^{125}Te NMR chemical shifts, relativistic effects were less important because they cancelled each other between a sample and a reference. Jaszuński and Olejniczak performed an extensive nonrelativistic HF, CCSD, and CCSD(T) study together with four-component Hartree–Fock, DFT, and spin-density functional theory relativistic calculations of $^{1}J_{Te,H}$ in TeH_2 with relativistic effects described within the Dirac–Coulomb Hamiltonian. In that study, the role of the level of theory, basis sets, electron correlation, relativistic and rovibrational effects was thoroughly investigated. In a number of papers, Rusakova and co-workers calculated ^{125}Te NMR chemical shifts at the four-component relativistic level by taking into account solvent and vibrational corrections in a wide series of organotellurium compounds. It was found that relativistic corrections varied in a wide range of several dozens of parts per million, which gave on average a quarter of the total relativistic values of tellurium chemical shifts. On the other hand, Rusakov and co-workers performed a high-level correlated calculation of spin–spin coupling constants involving tellurium, $^{2}J_{Te,H}$ and $^{3}J_{Te,H}$, of divinyl telluride and tellurophene while taking into account relativistic effects, vibrational corrections, and solvent effects. At the nonrelativistic level, a very well approved Sauer's polarization propagator methods, SOPPA(MP2), SOPPA(CC2), and SOPPA(CCSD), were applied at the two-component ZORA level together with the B3LYP and PBE0 functionals within the DFT framework. A full-electron basis set av3z-J derived in that paper was employed for tellurium, while Sauer's contracted basis set, aug-cc-pVTZ-J, was used for the hydrogens involved in spin–spin coupling with tellurium. A marked stereospecificity of geminal and vicinal ^{125}Te-^{1}H spin–spin coupling constants originated in the orientational lone pair effect of tellurium was also found in that study which provided a new guide in the stereochemistry of the organic derivatives of tellurium. Among a number of very interesting studies by different authors (see Section 2.5 for details), dos Reis Lino and co-workers calculated ^{125}Te NMR chemical shifts and spin–spin coupling constants involving tellurium using spin–orbit ZORA and four-component Dirac–Kohn–Sham relativistic methods in a series of tellurium-containing complexes. The influence of different conformers, basis sets, functionals, and methods to treat relativistic and solvent effects was examined. In general, the authors of that research performed a deep study of the accuracy factors involving the influence of different functionals and basis sets, solvent effects, and, most essentially, relativistic effects contributing to the tellurium chemical shifts and spin–spin coupling constants.

The main results dealing with the computational aspects of ^{195}Pt NMR are based on a series of fundamental contributions from Autschbach and collaborators, who performed a systematic study of different types of spin–spin coupling constants involving platinum in platinum complexes, namely, those of platinum–carbon platinum–phosphorus platinum–platinum and platinum–thallium, $^{n}J_{Pt,X}$ (X = C, P, Pt, and Tl). The basic conclusion derived from those studies, performed at the two-component ZORA level, was that the scalar and spin–orbit mechanisms together with solvent effects were of prime importance in the values of those coupling constants. Krykunov, Ziegler, and van Lenthe applied the so-ZORA formalism to the calculation of ^{195}Pt NMR chemical shifts in the series of platinum square-planar complexes. Those calculations were performed using a ZORA Hamiltonian with spin–orbit coupling and polarized double and triple basis sets in combination with B3LYP, BP86, and BLYP functionals. Roukala and co-workers conducted interesting scrutiny of ^{195}Pt NMR chemical shifts and ^{195}Pt–^{31}P spin–spin coupling constants in a series of bis(dialkyldithiophosphato) platinum complexes. Interestingly, the anisotropic platinum chemical shifts and spin–spin coupling constants afforded more detailed structural information than the isotropic data. Very recently, ^{195}Pt NMR chemical shifts were evaluated at the DFT level in a series of simple square-planar platinum complexes — cisplatin and transplatin together with a number of their derivatives, which was reported by Semenov and co-workers. In this study, ^{195}Pt NMR chemical shifts were evaluated at the nonrelativistic and fully

relativistic four-component levels. The most essential result of the performed calculations was that relativistic corrections to ^{195}Pt NMR chemical shifts were very important, being on average as much as approximately 1500 – 2000 parts per million. These results provided an unambiguous indication of marked relativistic effects in the ^{195}Pt NMR chemical shifts of the square-planar platinum complexes. Very recently, Marek, Kaupp, and co-workers performed a systematic study of the accuracy factors involving stereoelectronic, solvent, and relativistic effects in the values of the NMR chemical shifts of square-planar 4*d* and 5*d* transition metal complexes. For platinum complexes, it was found that there was an essential σ-donation from the occupied ligand's HOMO to unoccupied LUMO together with a π-back-donation from the occupied metal *d*-orbitals to the antibonding orbitals of ligands. The groups of Mastrorilli and Todisco performed a detailed investigation of the phosphanido bridged platinum complexes by means of the extensive DFT calculations of their ^{195}Pt NMR chemical shifts. Those calculations were carried out at the so-ZORA level with a BP86 functional and triple zeta singly and/or doubly polarized Slater basis sets, TZP and TZ2P. It was found that paramagnetic and spin – orbit terms were the most important contributions to the calculated ^{195}Pt NMR chemical shifts.

The perspectives of computational ^{199}Hg NMR mostly stem from the results for the simplest system studied very recently by Jakubowska and Pecul, which is a molecular complex Hg···H_2O consisting of one atom of mercury and one molecule of water, being a classical molecular van der Waals complex of mercury. A detailed computational investigation of ^{199}Hg NMR chemical shifts and ^{199}Hg – ^{1}H spin – spin coupling constants in this system was carried out at the four-component relativistic level. It was found that for the mercury shielding constant, spin – orbit effects did not play an important role and that the through-space mercury – proton intermolecular spin – spin coupling constants depended on the distance between oxygen and mercury atoms, not monotonously, with at least one extremum. Much earlier, Autschbach and co-workers performed a detailed computational study of the mercury – mercury spin – spin coupling constants in $[Hg-Hg]^{2+}$ and $[Hg-Hg-Hg]^{2+}$ dications at the two-component scalar and spin – orbit ZORA levels. It was found that the calculated one-bond couplings in the gas phase were dramatically overestimated compared to the experimental values. However, taking into account the solvent effect by an explicit inclusion of solvent molecules into the calculation space brought calculated values of $^{1}J_{Hg,Hg}$ in almost ideal agreement with the experimental values. In continuation of those studies, Bagno and Saielli calculated $^{n}J_{Hg,Hg}$ (n = 1, 2, and 3) coupling constants in Hg_4^{2+} dication at the so-ZORA level and by Lehn and co-workers using the so-called 'grid compounds', which self-assemble to form extended networks containing mercury at the regular positions of a grid. Performed calculations highlighted the extremely strong through-space spin – spin coupling that mercury nuclei could exhibit even when separated by large distances of up to 7 – 8 Å. A huge amount of the published papers deals with two- and four-component relativistic calculations of ^{199}Hg NMR chemical shifts and spin – spin coupling constants involving mercury in simple inorganic compounds provided by several independent groups led by Autschbach and Ziegler, Kristkova, Gütz, and Wodinski. The general result of those studies was that scalar effects on shielding constants of mercury were on average somewhat smaller than for spin – spin coupling constants. At the same time, scalar effects worked in the opposite direction (leading to deshielding of the mercury nucleus) compared to spin – orbit coupling effects. Regarding organic derivatives of mercury, it should be recalled that some a decade ago, Gryff-Keller and co-workers calculated all $^{n}J_{Hg,C}$ (n = 1 – 6) spin – spin coupling constants, both isotropic and anisotropic, of bis(phenylethynyl)mercury at the scalar and spin – orbit ZORA levels. It was found that the performed theoretical calculations reproduced the experimental values of both isotropic and anisotropic NMR coupling constants quite well, especially when taking into account solvent effects. Bryce and co-workers performed scalar and spin – orbit ZORA calculations of ^{199}Hg – ^{31}P isotropic and anisotropic spin – spin coupling constants in a series of mercury phosphine dimer derivatives. The basic result of that study was that isotropic coupling constants and coupling anisotropies were dominated by the ZORA Fermi-contact-spin-dipolar cross term and that ZORA spin – orbit relativistic corrections to coupling constants and coupling anisotropies were relatively small as compared to the remaining discrepancies between experiment and theory. Bagno and Saielli performed sc-ZORA calculations of δ_{Hg} together with $^{1}J_{Hg,N}$ and $^{2}J_{Hg,N}$ in the mercury thymine adducts of Hg^{2+} and Hg^{22+} dications. An interesting result of that study was that coordination of thymine with Hg^{22+} resulted in $^{2}J_{Hg,N}$ being essentially larger than $^{1}J_{Hg,N}$. Kauch and Pecul performed ZORA calculations of the formal five-bond ^{199}Hg – ^{1}H spin – spin coupling constants in the model system of mercury-substituted rubredoxin. It was found that the calculated ^{199}Hg – ^{1}H coupling constants matched well with their experimental values provided that relativistic effects were taken into account. At the same time, relativistic effects dominated the total values of the mercury – proton coupling constants. The nonrelativistic absolute values were up to one order of magnitude times smaller than the values obtained using relativistic methods. As a whole, relativistic effects were by far dominated by the scalar terms. Very recently, dos Reis Lino and co-workers calculated at the quasirelativistic two-component ZORA and fully relativistic four-component 4c-DKS levels mercury chemical shifts and geminal mercury – phosphorus spin – spin coupling constants in tellurium-containing mercury complexes. The influence of different accuracy factors (level of theory, DFT functional, basis set, and solvent effects) on the values of computed δ_{Hg} and $^{2}J_{Hg,P}$ was evaluated.

Computational ^{205}Tl NMR results stem mostly from the early pioneering paper by Autschbach and Ziegler, where $^{1}J_{Tl,X}$ spin – spin coupling constants were calculated at the sc-ZORA and so-ZORA levels in a classical series of thallium halides, TlX with X = ^{19}F, ^{35}Cl, ^{79}Br, and ^{127}I. It was found that spin – orbit effects were very important and necessary to obtain even qualitatively correct coupling constants in this series. Much later, Bashi and Aliabad reexamined the same series of compounds. It was demonstrated that including spin – orbit relativistic corrections improved the prediction of ^{205}Tl NMR chemical shifts by up to 11% in TlF and TlCl. On the other hand, taking into account spin – orbit coupling changed the shielding results by only 1%. Wodyński and co-workers performed two- and four-component DFT calculations of the thallium shielding constant together with the thallium – carbon and thallium – nitrogen spin – spin coupling constants in thallium

tetracyanide anion, $Tl(CN)_4^-$. Further insight into thallium NMR parameters was recently obtained by Vicha and co-workers in terms of the orbital contributions to scalar and spin–orbit interactions. Interestingly, for thallium shielding constants, scalar effects were shown to work in the opposite direction (leading to deshielding of the thallium nucleus) compared to spin–orbit coupling effects, and the latter were found to be much larger. For the thallium–carbon spin–spin coupling constant, the largest spin–orbit effect of approximately 220 Hz was observed, which was of the opposite sign to that of the scalar effects. In a series of papers, Autschbach and coworkers performed a systematic study of thallium chemical shifts and spin–spin coupling constants in thallium–platinum unbridged (bonded) cyanide complexes. It was demonstrated that experimentally observed spin–spin coupling constants $^1J_{Tl,Pt}$, $^1J_{Tl,C}$, and $^2J_{Tl,C}$ in thallium–platinum unbridged cyanide complexes were reproduced by ZORA calculations if both relativistic and solvent effects were taken into account. Solvent effects were found to be very substantial, increasing the $^1J_{Tl,Pt}$ coupling constant by more than 100%! In this line, it was demonstrated that a relativistic increase in the *s*-orbital density at thallium and platinum atoms and charge donation by the solvent were responsible for the observed trends in the values of $^1J_{Tl,Pt}$, $^1J_{Tl,C}$, and $^2J_{Tl,C}$. It was demonstrated that the $^1J_{Tl,Pt}$ coupling constants were strongly governed by scalar relativistic effects in the Fermi-contact mechanism. The computed $^1J_{Tl,Pt}$ of unsolvated thallium–platinum complexes underestimated their experimental values by approximately 30 kHz. The addition of electronic spin–orbit coupling to the computed spin–spin coupling constants only partially reduced the difference between the calculated and experimental values but resulted in an increase in those couplings by approximately 10 kHz. Bagno and Saiell performed ZORA computation of the through-space $^{TS}J_{Tl,Tl}$ coupling constant in dithallium cryptate. At the so-ZORA level, the PSO contribution appeared to be the dominant term, but other contributions were also essential in contrast to the sc-ZORA results.

The story of modern computational ^{207}Pb NMR begins with the most essential publications dealing with the calculation of lead spin–spin coupling constants in plumbane and derivatives that appeared 20 years ago — those of Autschbach and Ziegler, Kirpekar and Sauer, Enevoldsen and co-workers, and Khandogin and Ziegler. Within the next decade, a number of more related publications appeared dealing with the calculation of ^{207}Pb NMR parameters (lead shieldings, chemical shifts, and spin–spin coupling constants) in simple inorganic plumbanes. It was generally found that the nonrelativistic approach was not at all able to predict spin–spin coupling constants involving lead. The relativistic corrections to ^{207}Pb spin–spin coupling constants turned out to be substantially large, in some cases even larger than total nonrelativistic values. The performed ZORA scalar relativistic computations were able to recover major parts of the relativistic effects, thereby gaining an acceptable mean relative accuracy with respect to experimental data. In a more recent publication by Kristkova and co-workers, the parent plumbane, PbH_4, was revisited at the fully relativistic four-component level in the framework of the four-component matrix Dirac-Kohn–Sham approach termed 'matrix Dirac-Kohn–Sham Restricted Magnetic Balance'. The performed calculations resulted in a value of $^1J_{Pb,H}$ in plumbane of 2495 Hz, which was in very good agreement with the experimental 2594 Hz. Maldonado and Aucar calculated ^{207}Pb NMR shielding constants in the series of halogenoplumbanes together with a parent plumbane. For reference $PbMe_4$, the lead shielding constant was evaluated to be 14475.1 ± 500.7 ppm. This value was evaluated at the four-component relativistic polarization propagator method at the RPA level of approximation, which was found to be much closer to the experiment than that obtained at the DFT level. In the series of halogenoplumbanes, the diamagnetic component was shown to be increased only by 8.4% when going from PbH_4 to PbI_4, being quite independent of the electron correlation, even for the heaviest molecular systems PBr_4 and PI_4. Very recently, Demissi and, on the other hand, Jakubowska and co-workers calculated lead chemical shifts and spin–spin coupling constants in acetylenic derivatives of lead. In those studies, the four-component relativistic DFT calculations of ^{207}Pb chemical shifts and spin–spin coupling constants in the acetylenic derivatives of lead were performed in good agreement with the experimental results. In most cases, the net relativistic correction and the scalar contribution were found to be close to each other. The general result of those studies was that the full four-component relativistic approach gave the best agreement between the calculated and experimental ^{207}Pb chemical shifts and spin–spin coupling constants. The analysis of the scalar and spin–orbit contributions of those NMR parameters showed that the main relativistic effect was due to the scalar relativistic contraction of the *s*-shells and not due to the spin–orbit coupling.

5. List of acronyms

BPPT — Breit–Pauli Perturbation Theory,
CC3 — coupled Cluster singles, doubles, and triples model,
CCSD — coupled cluster single and double excitation model,
CCSD(T) — coupled cluster single and double excitation model with perturbative triple corrections,
COSMO — conductor-like screening model,
DCS — Dirac–Kohn–Sham,
DFT — density functional theory,
DHF — Dirac–Hartree–Fock,
DSO — diamagnetic spin–orbit (contribution),
FC — Fermi contact (contribution),
FC/SZ-KE — Fermi contact hyperfine interaction and the relativistically modified spin-Zeeman interaction,
GGA — generalized gradient approximation,
GIAO — Gauge-including atomic orbitals,
HAHA — heavy atom on heavy atom (effect),
HAVHA — heavy atom on vicinal heavy atom (effect),
HOMO — highest occupied molecular orbital,
HF — Hartree–Fock,
IEF-PCM — integral equation formalism polarizable continuum model,
LDA — local density approximation,
LDBS — locally dense basis set,
LMO — localized molecular orbital,
LP — lone pair,
LUMO — lowest unoccupied molecular orbital,
MAE — mean absolute error,
MAS — magic angle spinning,
mDKS-RMB — matrix Dirac–Kohn–Sham restricted magnetic balance,
MO — molecular obital,

MP2 — second-order Møller – Plesset perturbation theory,
NBO — natural bond orbital,
NMR — nuclear magnetic resonance,
NR — nonrelativistic,
PBE — Perdew – Burke – Ernzerhof (functional),
PCM — polarizable continuum model,
PSO — paramagnetic spin – orbit (contribution),
RelPPA — relativistic polarization propagator approach,
RHF — restricted Hartree – Fock,
RKB — restricted kinetic balance,
RMS — root mean square,
RMSD — root mean square deviation,
RPA — random phase approximation,
SAOP — statistical average of orbital-dependent model potentials,
SCF — self-consistent field,
sc-ZORA — scalar zeroth order regular approximation,
SD — spin dipolar (contribution),
SO — spin – orbit,
so-ZORA — spin – orbit zeroth order regular approximation,
SOPPA — second-order polarization propagator approach,
SOPPA(MP2) — second-order polarization propagator approach in combination with Møller – Plesset perturbation theory,
SOPPA (CC2) — second-order polarization propagator approach in combination with a second-order approximate coupled cluster model,
SOPPA (CCSD) — second-order polarization propagator approach in combination with coupled cluster single and double excitation model,
SZ-KE — spin-zeeman interaction with kinetic energy correction,
TD-DHF — time-dependent dirac-hartree-fock (method),
TD-DKS — time-dependent dirac-Kohn – Sham (method),
TD-RDFT — time-dependent relativistic four-component density functional theory,
TO — total (sum of all coupling contributions),
RRPA — relativistic random phase approximation,
UKB — unrestricted kinetic balance,
VWN — Vosko – Wilk – Nusair (functional),
ZORA — zeroth-order regular approximation,
ZPVC — zero-point vibrational correction.

References

1. S.P.A.Sauer, *Molecular Electromagnetism. A Computational Chemistry Approach*. (Oxford: University Press, 2012); ISBN: 9780199575398
2. T.Helgaker, M.Jaszuński, K.Ruud. *Chem. Rev.*, **99**, 293 (1999); https://doi.org/10.1021/cr960017t
3. T.Helgaker, M.Jaszuński, M.Pecul. *Prog. NMR Spectrosc.*, **53**, 249 (2008); https://doi.org/10.1016/j.pnmrs.2008.02.002
4. G.A.Aucar, R.H.Romero, A.F.Maldonado. *Int. Rev. Phys. Chem.*, **29**, 1 (2010); https://doi.org/10.1080/01442350903432865
5. *High Resolution NMR Spectroscopy: Understanding Molecules and their Electronic Structures*. (Ed. R.H.Contreras). (The Netherland: Elsevier, 2013). ISBN: 978-0444594112
6. Yu.Yu.Rusakov, L.B.Krivdin. *Russ. Chem. Rev.*, **82**, 99 (2013); https://doi.org/10.1070/RC2013v082n02ABEH004350
7. F.A.A.Mulder, M.Filatov. *Chem. Soc. Rev.*, **39**, 578 (2010); https://doi.org/10.1039/B811366C
8. L.B.Krivdin, R.H.Contreras. *Ann. Rep. NMR Spectrosc.*, **61**, 133 (2007); ISBN: 9780123739186
9. L.B.Casabianca. *Magn. Reson. Chem.*, **58**, 611 (2020); https://doi.org/10.1002/mrc.4994
10. Y.Xiao, W.Liu, J.Autschbach. In *Handbook of Relativistic Quantum Chemistry*. (Ed. W.Liu). (Berlin: Springer, 2017); https://doi.org/10.1007/978-3-642-41611-8_17-1
11. J.Autschbach, T.Ziegler. In *Calculation of NMR and EPR Parameters: Theory and Applications*. (Eds M.Kaupp, M.Bühl, V.G.Malkin). (Weinheim, Wiley-VCH Verlag GmbH & Co. KGaA, 2004). P. 249
12. J.Autschbach. In *Structure and Bonding*. (Eds N.Kaltsoyannis, J.E.McGrady). (Berlin: Springer, 2004). Vol. 112. P. 1; https://doi.org/10.1007/978-3-540-78634-4
13. J.Autschbach. *Phyl. Trans. Royal Soc. A*, **372**, 1 (2014); https://doi.org/10.1098/rsta.2012.0489
14. M.Repisky, S.Komorovsky, R.Bast, K.Ruud. In *Gas Phase NMR*. (Eds K.Jackowski, M.Jaszunski). (Cambridge: The Royal Society of Chemistry, 2016); https://doi.org/10.1039/9781782623816
15. I. L.Rusakova, Yu.Yu.Rusakov, L.B.Krivdin. *Russ. Chem. Rev.*, **85**, 356 (2016); https://doi.org/10.1070/RCR4561
16. L.B.Krivdin. *Magn. Reson. Chem.*, **57**, 897 (2019); https://doi.org/10.1002/mrc.4873
17. L.B.Krivdin. *Magn. Reson. Chem.*, **58**, 5 (2020); https://doi.org/10.1002/mrc.4896
18. L.B.Krivdin. *Magn. Reson. Chem.*, **58**, 15 (2020); https://doi.org/10.1002/mrc.4895
19. L.B.Krivdin. *Prog. NMR Spectrosc.*, **108**, 17 (2018); https://doi.org/10.1016/j.pnmrs.2018.10.002
20. L.B.Krivdin. *Prog. NMR Spectrosc.*, **112 – 113**, 103 (2019); https://doi.org/10.1016/j.pnmrs.2019.05.004
21. L.B.Krivdin. *Prog. NMR Spectrosc.*, **102 – 103**, 98 (2017); https://doi.org/10.1016/j.pnmrs.2017.08.001
22. L.B.Krivdin. *Prog. NMR Spectrosc.*, **105**, 54 (2018); https://doi.org/10.1016/j.pnmrs.2018.03.001
23. L.B.Krivdin. *Russ. Chem. Rev.*, **89** 1040 (2020); https://doi.org/10.1070/RCR4948
24. L.B.Krivdin. *Russ. Chem. Rev.*, **89**, 449 (2020); https://doi.org/10.1070/RCR4927
25. L.B.Krivdin. *Magn. Reson. Chem.*, **58**, 478 (2020); https://doi.org/10.1002/mrc.4965
26. L.B.Krivdin. *Magn. Reson. Chem.*, **58**, 500 (2020); https://doi.org/10.1002/mrc.4973
27. L.B.Krivdin. *Russ. Chem. Rev.*, **90**, 265 (2021); https://doi.org/10.1070/RCR4960
28. J.Vícha, J.Novotný, S.Komorovsky, M.Straka, M.Kaupp, R.Marek. *Chem. Rev.*, **120**, 7065 (2020); https://doi.org/10.1021/acs,chemrev.9b00785
29. B.E.Mann. *Ann. Rep. NMR Spectrosc.*, **23**, 141 (1991); ISBN: 9780128120859
30. I.Alkorta, J.Elguero, H.V.R.Dias, D. Parasar, M.Martín-Pastor. *Magn. Reson. Chem.*, **58**, 319 (2020); https://doi.org/10.1002/mrc.5002
31. I.Alkorta, C.Trujillo, G.Sánchez-Sanz, J.Elguero. *Crystals*, **10**, 137 (2020); https://doi.org/10.3390/cryst10020137
32. M.Kauch, M.Pecul. *ChemPhysChem*, **13**, 1332 (2012); https://doi.org/10.1002/cphc.201100846
33. S.Johannsen, N.Megger, D.Bçhme, R.K.O.Sigel, J.Müller. *Nat. Chem.*, **2**, 229 (2010); https://doi.org/10.1038/nchem.512
34. A.Wodyński, M.Repiský, M.Pecul. *J. Chem. Phys.*, **137**, 014311 (2012); https://doi.org/10.1063/1.4730944
35. D.L.Bryce, R.E.Wasylishen. *Inorg. Chem.*, **41**, 4131 (2002); https://doi.org/10.1021/ic0201553
36. G.Casella, F.Ferrante, G.Saielli. *Polyhedron*, **117**, 48 (2016); https://doi.org/10.1016/j.poly.2016.05.038

37. M.Kauch, M.Pecul. *J. Phys. Chem. A*, **118**, 4471 (2014); https://doi.org/10.1021/jp501888c
38. J.Roukala, A.F.Maldonado, J.Vaara, G.A.Aucar, P.Lantto. *Phys. Chem. Chem. Phys.*, **13**, 21016 (2011); https://doi.org/10.1039/C1CP22043H
39. M.Krauss, L.Olsen, J.Antony, L.Hemmingsen. *J. Phys. Chem. B*, **106**, 9446 (2002); https://doi.org/10.1021/jp025870c
40. V.Kellö, A.J.Sadlej. *Theor. Chim. Acta*, **91**, 353 (1995); https://doi.org/10.1007/978-94-017-0105-1_9
41. P.D.Ellis, J.D.Odom, A.S.Lipton, J.M.Gulick. *J. Am. Chem. Soc.*, **115**, 755 (1993); https://doi.org/10.1021/ja00055a055
42. T.Higashioji, M.Hada, M.Sugimoto, H.Nakatsuji. *Chem. Phys.*, **203**, 159 (1996); https://doi.org/10.1016/0301-0104(95)00398-3
43. S.S.Kidambi, A.Ramamoorthy. *J. Phys. Chem. A*, **106**, 10363 (2002); https://doi.org/10.1021/jp0265891
44. S.Kidambi, A.Ramamoorthy. *Inorg. Chem.*, **42**, 2200 (2003); https://doi.org/10.1021/ic026165l
45. S.S.Kidambi, D.-K.Lee, A.Ramamoorthy. *Inorg. Chem.*, **42**, 3142 (2003); https://doi.org/10.1021/ic026287d
46. L.Hemmingsen, L.Olsen, J.Antony, S.P.A.Sauer. *J. Biol. Inorg. Chem.*, **9**, 591 (2004); https://doi.org/10.1007/s00775-004-0553-0
47. X.Li, Z. Rinkevicius, Y.Tu, H.Tian, H.Ågren. *J. Phys. Chem. B*, **112**, 11347 (2008); https://doi.org/10.1021/jp802238f
48. H.Nakatsuji, T.Inoue, T.Nakao. *J. Phys. Chem.*, **96**, 7953 (1992); https://doi.org/10.1021/j100199a025
49. H.Kaneko, M.Hada, T.Nakajima, H.Nakatsuji. *Chem. Phys. Lett.*, **261**, 1 (1996); https://doi.org/10.1016/0009-2614(96)00906-2
50. S.Kirpekar, H.J.A.Jensen, J.Oddershede. *Theor. Chim. Acta*, **95**, 35 (1997); https://doi.org/10.1007/BF02329240
51. T.Enevoldsen, L.Visscher, T.Saue, H.J.A.Jensen, J.Oddershede. *J. Chem. Phys.*, **112**, 3493 (2000); https://doi.org/10.1063/1.480504
52. J.Khandogin, T.Ziegler. *J. Phys. Chem. A*, **104**, 113 (2000); https://doi.org/10.1021/jp992571n
53. R.Vivas-Reyes, F.De Proft, M.Biesemans, R.Willem, P.Geerlings. *J. Phys. Chem. A*, **106**, 2753 (2002); https://doi.org/10.1021/jp0145917
54. P.Avalle, R.K.Harris, R.D.Fischer. *Phys. Chem. Chem. Phys.*, **4**, 3558 (2002); https://doi.org/10.1039/B202909J
55. P.Avalle, R.K.Harris, P.B.Kardakov, P.J.Wilson. *Phys. Chem. Chem. Phys.*, **4**, 5925 (2002); https://doi.org/10.1039/B208435J
56. M.Filatov, D.Cremer. *J. Chem. Phys.*, **120**, 11407 (2004); https://doi.org/10.1063/1.1752876
57. A.Bagno, G.Casella, G.Saielli. *J. Chem. Theory Comput.*, **2**, 37 (2006); https://doi.org/10.1021/ct050173k
58. P.Lantto, R.H.Romero, S.S.Gómez, G.A.Aucar. *J. Chem. Phys.*, **125**, 184113 (2006); https://doi.org/10.1063/1.2378737
59. A.F.Maldonado, G.A.Aucar. *J. Phys. Chem. A*, **118**, 7863 (2014); https://doi.org/10.1021/jp502543m
60. A.F.Maldonado, G.A.Aucar, J.I.Melo. *J. Mol. Model.*, **20**, 2417 (2014); https://doi.org/10.1007/s00894-014-2417-z
61. A.Křstková, S.Komorovsky, M.Repisky, V.G.Malkin, O.L.Malkina. *J. Chem. Phys.*, **142**, 114102 (2015); https://doi.org/10.1063/1.4913639
62. T.B.Demissie. *J. Chem. Phys.*, **147**, 174301 (2017); https://doi.org/10.1063/1.4996712
63. K.Jakubowska, M.Pecul, M.Jaszuński. *Theor. Chem. Acc.*, **137**, 41 (2018); https://doi.org/10.1007/s00214-018-2215-2
64. A.Bagno, N.Bertazzi, G.Casella, L.Pellerito, G.Saielli, I.D.Sciacca. *J. Phys. Org. Chem.*, **19**, 874 (2006); https://doi.org/10.1002/poc.1041
65. G.Casella, F.Ferrante, G.Saielli. *Inorg. Chem.*, **47**, 4796 (2008); https://doi.org/10.1021/ic8000976
66. G.Casella, F.Ferrante, G.Saielli. *Eur. J. Org. Chem.*, 3526 (2009); https://doi.org/10.1002/ejoc.200900197
67. G.Casella, F.Ferrante, G.Saielli. *Org. Biomol. Chem.*, **8**, 2711 (2010); https://doi.org/10.1039/C000679C
68. A.Bagno, G.Casella, F.Ferrante, G.Saielli. *J. Organometal. Chem.*, **724**, 139 (2013); https://doi.org/10.1016/j.jorganchem.2012.10.041
69. I.L.Rusakova, L.B.Krivdin. *Mendeleev Commun.*, **28**, 1 (2018); https://doi.org/10.1016/j.mencom.2018.01.001
70. J.Vaara, K.Ruud, O.Vahras. *J. Comp. Chem.*, **20**, 1314 (1999); https://doi.org/10.1002/(SICI)1096-987X(199909)20 : 12<1314:-:AID-JCC12>3.0.CO;2-0
71. M.Hada, J.Van, R.Fukuda, H.Nakatsuji. *J. Comp. Chem.*, **22**, 1502 (2001); https://doi.org/10.1002/jcc.1103
72. S.S.Gomez, R.H.Romero, G.A.Aucar. *J. Chem. Phys.*, **117**, 7942 (2002); https://doi.org/10.1063/1.1510731
73. M.Jaszuński, M.Olejniczak. *Mol. Phys.*, **111**, 1355 (2013); https://doi.org/10.1080/00268976.2013.793839
74. I.L.Rusakova, Yu.Yu.Rusakov, L.B.Krivdin. *J. Phys. Chem. A*, **121**, 4793 (2017); https://doi.org/10.1021/acs.jpca.7b03198
75. Yu.Yu.Rusakov, L.B.Krivdin, F.F.Østerstrøm, S.P.A.Sauer, V.A.Potapov, S.V.Amosova. *Phys. Chem. Chem. Phys.*, **15**, 13101 (2013); https://doi.org/10.1039/c3cp51462e
76. T.Enevoldsen, J.Oddershede, S.P.A.Sauer. *Theor. Chem. Acc.*, **100**, 275 (1998); https://doi.org/10.1007/s002140050388
77. P.F.Provasi, G.A.Aucar, S.P.A.Sauer. *J. Chem. Phys.*, **115**, 1324 (2001); https://doi.org/10.1063/1.1379331
78. Yu.Yu.Rusakov, I.L.Rusakova. *Int. J. Quant. Chem.*, **119**, e25809 (2019); https://doi.org/10.1002/qua.25809
79. S.V.Zinchenko, L.B.Krivdin. *Current Org. Chem.*, **2**, 173 (1998); ISBN: 1385-2728/98
80. I.L.Rusakova, Yu.Yu.Rusakov, L.B.Krivdin. *J. Comp. Chem.*, **37**, 1367 (2016); https://doi.org/10.1002/jcc.24345
81. Yu.Yu.Rusakov, I.L.Rusakova. *J.Phys. Chem. A*, **123**, 6564 (2019); https://doi.org/10.1021/acs.jpca.9b05276
82. Yu.Yu.Rusakov, I.L.Rusakova. *Magn. Reson. Chem.*, **58**, 929 (2020); https://doi.org/10.1002/mrc.5058
83. M.Bortoli, M.D.Tiezza, C.Muraro, G.Saielli, L.Orian. *Molecules*, **24**, 1250 (2019); https://doi.org/10.3390/molecules24071250
84. P.Granger, S.Chapelle, W.R.McWhinnie, A.Al-Rubaie. *J. Organometal. Chem.*, **220**, 149 (1981); https://doi.org/10.1016/S0022-328X(00)90102-5
85. M.Bühl, F.R.Knight, A.Křístková, I.Malkin Ondík, O.L.Malkina, R.A.M.Randall, A.M.Z. Slawin, J.D.Woollins. *Angew. Chem., Int. Ed.*, **52**, 2495 (2013); https://doi.org/10.1002/anie.201205998
86. F.R.Knight, L.M.Diamond, K.S.A.Arachchige, P.S.Camacho, R.A.M.Randall, S.E.Ashbrook, M.Bühl, A.M.Z. Slawin, J.D.Woollins. *Chem. – Eur. J.*, **21**, 3613 (2015); https://doi.org/10.1002/chem.201405599
87. J.B.dos Reis Lino, S.P.A.Sauer, T.C.Ramalho. *J. Phys. Chem. A*, **124**, 4946 (2020); https://doi.org/10.1021/acs.jpca.0c01607
88. Yu.Yu.Rusakov, I.L.Rusakova. *J. Chem. Phys. A*, **124**, 6714 (2020); https://doi.org/10.1021/acs.jpca.0c05780
89. P.A.B.Haase, R.Faber, P.F.Provasi, S.P.A.Sauer. *J. Comp. Chem.*, **41**, 43 (2020); https://doi.org/10.1002/jcc.26074
90. M.W.Jørgensen, S.P.A.Sauer. *J. Chem. Phys.*, **152**, 234101 (2020); https://doi.org/10.1063/5.0011195
91. M.W.Jørgensen, R.Faber, A.Ligabue, S.P.A.Sauer. *J. Chem. Theory Comput.*, **16**, 3006 (2020); https://doi.org/10.1021/acs.jctc.9b01300
92. M.Jaszunski, S.P.A.Sauer, R.Faber, D.J.D.Wilson. *Phys. Chem. Chem. Phys.*, **22**, 21350 (2020); https://doi.org/10.1039/D0CP02730H
93. A.K.Schnack-Petersen, M.Simmermacher, E.Faßhauer, H.J.A.Jensen, S.P.A.Sauer. *J. Chem. Phys.*, **152**, 134113 (2020); https://doi.org/10.1063/5.0002389
94. J.Autschbach, T.Ziegler. *J. Chem. Phys.*, **113**, 936 (2000); https://doi.org/10.1063/1.481874

95. J.Autschbach, T.Ziegler. *J. Am. Chem. Soc.*, **123**, 3341 (2001); https://doi.org/10.1021/ja003481v
96. J.Autschbach, T.Ziegler. *J. Am. Chem. Soc.*, **123**, 5320 (2001); https://doi.org/10.1021/ja003866d
97. J.Autschbach, C.D.Igna, T.Ziegler. *J. Am. Chem. Soc.*, **125**, 1028 (2003); https://doi.org/10.1021/ja027931q
98. J.Autschbach, B.Le Guennic. *J. Am. Chem. Soc.*, **125**, 13585 (2003); https://doi.org/10.1021/ja0368047
99. B.Le Guennic, K.Matsumoto, J.Autschbach. *Magn. Reson. Chem.*, **42**, S99 (2004); https://doi.org/10.1002/mrc.1450
100. M.Krykunov, T.Ziegler, E.van Lenthe. *J. Phys. Chem. A*, **113**, 11495 (2009); https://doi.org/10.1021/jp901991s
101. A.V.Ivanov, T.A.Rodina, M.A.Ivanov, A.V.Gerasimenko, O.N.Antzutkin. *Dokl. Phys. Chem.*, **423**, 311 (2008); https://doi.org/10.1134/S0012501608110067
102. T.A.Rodina, I.A.Lutsenko, A.V.Gerasimenko, A.V.Ivanov. *Russ. J. Coord. Chem.*, **35**, 534 (2009); https://doi.org/10.1134/S1070328409070112
103. T.A.Rodina, A.V.Ivanov, A.V.Gerasimenko, I.A.Lutsenko, M.A.Ivanov, J.V.Hanna, O.N.Antzutkin, V.I.Sergienko. *Polyhedron*, **30**, 2210 (2011); https://doi.org/10.1016/j.poly.2011.05.050
104. A.V.Ivanov, V.I.Palazhchenko, V.E.Strikha, O.N.Antzutkin, W.Forsling. *Dokl. Earth. Sci.*, **410**, 1141 (2006); https://doi.org/10.1134/S1028334X06070312
105. V.I.Rozhdestvina, A.V.Ivanov, M.A.Zaremba, O.N.Antzutkin, W.Forsling. *Crystallogr. Reports*, **53**, 391 (2008); https://doi.org/10.1134/S106377450803005X
106. J.Roukala, S.Orr, J.V.Hanna, J.Vaara, A.V.Ivanov, O.N.Antzutkin, P.Lantto. *J. Chem. Phys. A*, **120**, 8326 (2016); https://doi.org/10.1021/acs.jpca.6b09586
107. V.A.Semenov, Yu.Yu.Rusakov, D.O.Samultsev, L.B.Krivdin. *Mendeleev Commun.*, **29**, 315 (2019); https://doi.org/10.1016/j.mencom.2019.05.025
108. V.A.Semenov, D.O.Samultsev, I.L.Rusakova, L.B.Krivdin. *J. Phys. Chem. A*, **123**, 4908 (2019); https://doi.org/10.1021/acs.jpca.9b02867
109. J.Vicha, J.Novotny, M.Straka, M.Repisky, K.Ruud, S.Komorovsky, R.Marek. *Phys. Chem. Chem. Phys.*, **17**, 24944 (2015); https://doi.org/10.1039/C5CP04214C
110. J.Vicha, C.Foroutan-Nejad, T.Pawlak, M.Munzarova, M.Straka, R.Marek. *J. Chem. Theory Comput.*, **11**, 1509 (2015); https://doi.org/10.1021/ct501089z
111. T.Pawlak, M.L.Munzarova, L.Pazderski, R.Marek. *J. Chem. Theory Comput.*, **7**, 3909 (2011); https://doi.org/10.1021/ct200366n
112. A.H.Greif, P.Hrobarik, V.Hrobarikova, A.V.Arbuznikov, J.Autschbach, M.Kaupp. *Inorg. Chem.*, **54**, 7199 (2015); https://doi.org/10.1021/acs.inorgchem.5b00446
113. C.Fortuño, A.Martín, P.Mastrorilli, V.Gallo, S.Todisco. *Organometallics*, **36**, 4325 (2017); https://doi.org/10.1021/acs.organomet.7b00746
114. D.Giardina-Papa, I.Ara, S.Ibáñez, P.Mastrorilli, V.Gallo, J.Fornies. *Polyhedron*, **120**, 44 (2016); https://doi.org/10.1016/j.poly.2016.05.040
115. P.Mastrorilli, V.Gallo, S.Todisco, M.Latronico, G.Saielli. *Chem. – Eur. J.*, **22**, 7964 (2016); https://doi.org/10.1002/chem.201600078
116. P.Mastrorilli. *Eur. J. Inorg. Chem.*, **31**, 4835 (2008); https://doi.org/10.1002/ejic.200800530
117. I.Ara, J.Forniés, S.Ibáñez, P.Mastrorilli, S.Todisco, V.Gallo. *Dalton Trans.*, **45**, 2156 (2016); https://doi.org/10.1039/C5DT02593A
118. A.Arias, J.Fornies, C.Fortuño, A.Martín, P.Mastrorilli, V.Gallo, S.Todisco. *Eur. J. Inorg. Chem.*, **10**, 1679 (2014); https://doi.org/10.1002/ejic.201300808
119. A.Arias, J.Fornies, C.Fortuño, S.Ibanez, A.Martín, P.Mastrorilli, V.Gallo, S.Todisco. *Inorg. Chem.*, **52**, 11398 (2013); https://doi.org/10.1021/ic401689c
120. A.Arias, J.Fornies, C.Fortuño, A.Martín, P.Mastrorilli, S.Todisco, M.Latronico, V.Gallo. *Inorg. Chem.*, **52**, 5493 (2013); https://doi.org/10.1021/ic4004005
121. A.Arias, J.Fornies, C.Fortuño, A.Martín, M.Latronico, P.Mastrorilli, S.Todisco, V.Gallo. *Inorg. Chem.*, **51**, 12682 (2012); https://doi.org/10.1021/ic301298p
122. P.Mastrorilli, S.Todisco, A.Bagno, V.Gallo, M.Latronico, C.Fortuño, D.Gudat. *Inorg. Chem.*, **54**, 5855 (2015); https://doi.org/10.1021/acs.inorgchem.5b00627
123. S.Todisco, G.Saielli, V.Gallo, M.Latronico, A.Rizzuti, P.Mastrorilli. *Dalton Trans.*, **47**, 8884 (2018); https://doi.org/10.1039/C8DT01561A
124. K.Jakubowska, M.Pecul. *Chem. Phys. Lett.*, **736**, 136775 (2019); https://doi.org/10.1016/j.cplett.2019.136775
125. M.C.Duval, B.Soep. *J. Phys. Chem.*, **95**, 9075 (1991); https://doi.org/10.1021/j100176a012
126. J.Autschbach, C.D.Igna, T.Ziegler. *J. Am. Chem. Soc.*, **125**, 4937 (2003); https://doi.org/10.1021/ja028721g
127. J.Autschbach, M.Sterzel. *J. Am. Chem. Soc.*, **129**, 11093 (2007); https://doi.org/10.1021/ja073166+
128. R.Malleier, H.Kopacka, W.Schuh, K.Wurst, P.Peringer. *Chem. Commun.*, 51 (2001); https://doi.org/10.1039/B007581G
129. R.J.Gillespie, P.Granger, K.R.Morgan, G.J.Schrobilgen. *Inorg. Chem.*, **23**, 887 (1984); https://doi.org/10.1021/ic00175a019
130. A.Bagno, G.Saielli. *Theor. Chem. Acc.*, **117**, 603 (2007); https://doi.org/10.1007/s00214-006-0196-z
131. E.Breuning, G.S.Hanan, F.J.Romero-Salguero, A.M.Garcia, P.N.W.Baxter, J.M.Lehn, E.Wegelius, K.Rissanen, H.Nierengarten, A.van Dorsselaer. *Chem. – Eur. J.*, **8**, 3458 (2002); https://doi.org/10.1002/1521-3765(20020802)8 : 15<3458::AID-CHEM3458>3.0.CO;2-Y
132. R.Fukuda, M.Hada, H.Nakatsuji. *J. Chem. Phys.*, **118**, 1027 (2003); https://doi.org/10.1063/1.1528934
133. J.Autschbach, A.M.Kantola, J.Jokisaari. *J. Phys. Chem. A*, **111**, 5343 (2007); https://doi.org/10.1021/jp0713817
134. V.Arcisauskaite, J.I.Melo, L.Hemmingsen, S.P.A.Sauer. *J. Chem. Phys.*, **135**, 044306 (2011); https://doi.org/10.1063/1.3608153
135. S.Zheng, J.Autschbach. *Chem. – Eur. J.*, **17**, 161 (2011); https://doi.org/10.1002/chem.201001343
136. A.W.Götz, J.Autschbach, L.Visscher. *J. Chem. Phys.*, **140**, 104107 (2014); https://doi.org/10.1063/1.4864053
137. J.Autschbach, T.Ziegler. *Enc. Nucl. Magn. Reson.*, **9**, 306 (2002); ISBN: 10.1063/1.4864053
138. A.Gryff-Keller, A.Kraska-Dziadecka, S.Molchanov, A.Wodyński. *J. Phys. Chem. A*, **116**, 10615 (2012); https://doi.org/10.1021/jp307828e
139. D.L.Bryce, N.M.D.Courchesne, F.A.Perras. *Solid State NMR*, **36**, 182 (2009); https://doi.org/10.1016/j.ssnmr.2009.11.004
140. A.Bagno, G.Saielli. *J. Am. Chem. Soc.*, **129**, 11360 (2007); https://doi.org/10.1021/ja0746417
141. J.F.Hinton. *Bull. Magn. Reson.*, **13**, 90 (1992); ISSN: 0163-559X
142. J.Autschbach, T.Ziegler. *J. Chem. Phys.*, **113**, 9410 (2000); ISSN: 0079-6565
143. J.Autschbach, B.Le Guennic. *Chem. – Eur. J.*, **10**, 2581 (2004); https://doi.org/10.1002/chem.200305513
144. W.Chen, F.Liu, K.Matsumoto, J.Autschbach, B.Le Guennic, T.Ziegler, M.Maliarik, J.Glaser. *Inorg. Chem.*, **45**, 4526 (2006); https://doi.org/10.1021/ic051678o
145. J.Autschbach. *J. Chem. Phys.*, **129**, 094105 (2008); https://doi.org/10.1063/1.2969100
146. M.Bashi, H.A.Rahnamaye Aliabad. *Magn. Reson. Chem.*, **58**, 223 (2020); https://doi.org/10.1002/mrc.4970
147. J.Vícha, R.Marek, M.Straka. *Inorg. Chem.*, **55**, 10302 (2016); https://doi.org/10.1021/acs.inorgchem.6b01575
148. S.Moncho, J.Autschbach. *J. Chem. Theory Comput.*, **6**, 223 (2010); https://doi.org/10.1021/ct900535d

149. P.R.T.Schipper, O.V.Gritsenko, S.J.A.van Gisbergen, E.J.Baerends. *J. Chem. Phys.*, **112**, 1344 (2000); https://doi.org/10.1063/1.480688
150. O.V.Gritsenko, P.R.T.Schipper, E.J.Baerends. *Int. J. Quantum Chem.*, **76**, 407 (2000); https://doi.org/10.1002/(SICI)1097-461X(2000)76 : 3<407::AID-QUA9>3.0.CO;2-A
151. D.P.Chong, O.V.Gritsenko, E.J.Baerends. *J. Chem. Phys.*, **116**, 1760 (2002); https://doi.org/10.1063/1.1430255
152. M.Grüning, O.V.Gritsenko, S.J.A.van Gisbergen, E.J.Baerends. *J. Chem. Phys.*, **116**, 9591 (2002); https://doi.org/10.1063/1.1476007
153. S.Kirpekar, S.P.A.Sauer. *Theor. Chem. Acc.*, **103**, 146 (1999); https://doi.org/10.1007/s002149900027
154. H.R.Zhekova, M.Seth, T.Ziegler. *J. Chem. Phys.*, **135**, 184105 (2011); https://doi.org/10.1063/1.3658643
155. H.Zhekova, M.Seth, T.Ziegler. *J. Chem. Theory Comput.*, **7**, 1858 (2011); https://doi.org/10.1021/ct200141v
156. I.Seidu, H.R.Zhekova, M.Seth, T.Ziegler. *J. Phys. Chem. A*, **116**, 2268 (2012); https://doi.org/10.1021/jp209507n
157. C.I.Oprea, Z.Rinkevicius, O.Vahtras, H.Ågren. *J. Chem. Phys.*, **123**, 014101 (2005); https://doi.org/10.1063/1.1947190
158. A.Bagno, M.Bonchio. *Magn. Reson. Chem.*, **42**, S79 (2004); https://doi.org/10.1002/mrc.1412
159. M.Hanni, P.Lantto, N.Runeberg, J.Jokisaari, J.Vaara. *J. Chem. Phys.*, **121**, 5908 (2004); https://doi.org/10.1063/1.1785146
160. M.Hanni, P.Lantto, M.Iliaš, H.J.A.Jensen, J.Vaara. *J. Chem. Phys.*, **127**, 164313 (2007); https://doi.org/10.1063/1.2777143
161. P.Lantto, J.Vaara. *J. Chem. Phys.*, **127**, 084312 (2007); https://doi.org/10.1063/1.2759205
162. M.Straka, P.Lantto, M.Räsänen, J.Vaara. *J. Chem. Phys.*, **127**, 234314 (2007); https://doi.org/10.1063/1.2805389
163. M.Straka, P.Lantto, J.Vaara. *J. Phys. Chem. A*, **112**, 2658 (2008); https://doi.org/10.1021/jp711674y
164. S.Standara, P.Kulhánek, R.Marek, J.Horníček, P.Bouř, M.Straka. *Theor. Chem. Acc.*, **129**, 677 (2011); https://doi.org/10.1007/s00214-011-0930-z
165. P.Lantto, S.Kangasvieri, J.Vaara. *J. Chem. Phys.*, **137**, 214309 (2012); https://doi.org/10.1063/1.4768471
166. P.Lantto, S.Standara, S.Riedel, J.Vaara, M.Straka. *Phys. Chem. Chem. Phys.*, **14**, 10944 (2012); https://doi.org/10.1039/c2cp41240c
167. M.Selent, J.Nyman, J.Roukala, M.Ilczyszyn, R.Oilunkaniemi, P.J.Bygrave, R.Laitinen, J.Jokisaari, G.M.Day, P.Lantto. *Chem. – Eur. J.*, **23**, 5258 (2017); https://doi.org/10.1002/chem.201604797
168. M.Olejniczak, M.Pecul. *ChemPhysChem*, **10**, 1247 (2009); https://doi.org/10.1002/cphc.200800817
169. G.Schreckenbach, S.K.Wolff, T.Ziegler. *J. Phys. Chem. A*, **104**, 8244 (2000); https://doi.org/10.1021/jp001143a
170. G.Schreckenbach. *Inorg. Chem.*, **41**, 6560 (2002); https://doi.org/10.1021/ic020370j
171. J.Khandogin, T.Ziegler. *Spectrochim. Acta A*, **55**, 607 (1999); https://doi.org/10.1016/S1386-1425(98)00265-0
172. G.B.Hall, A.Andersen, N.M.Washton, S.Chatterjee, T.G.Levitskaia. *Inorg. Chem.*, **55**, 8341 (2016); https://doi.org/10.1021/acs.inorgchem.6b00458
173. I. L. Rusakova, Y. Y. Rusakov. *Magn. Reson. Chem.*, **59**, 359 (2021); https://doi.org/10.1002/mrc.5111